UNIVERSITY OF NAPLES "FEDERICO II"

Facoltà di ingegneria

Dipartimento di Ingegneria Idraulica, Geotecnica ed Ambientale

Dottorato di ricerca in Ingegneria dei sistemi idraulici, di trasporto e territoriali

PH. D. THESIS

Mathematical modelling of anaerobic suspended and attached growth bioreactors

Luigi Frunzo

Promoters

Prof. Berardino D'Acunto

Prof. Eng. Francesco Pirozzi

Coordinator

Prof. Eng. Guelfo Pulci Doria

Naples, November 2011

Il sapere e la saggezza sono la vera forza

Acknowledgments

First of all I would like to express my sincere gratitude to my promoters Prof. Berardino D'Acunto and Prof. Francesco Pirozzi for introducing me to the interesting field of mathematical model of environmental engineering and for giving me the possibility to work in this area as Ph.D. Student.

Particular acknowledgement goes to Prof. Giovanni Esposito for guiding me in world of research, for giving me always the best suggestions for my problems and for being there for me in the bad periods.

I would like to thank the Committee of the Ph.D. Programme of the department of Hydraulics, Geotechnical and Environmental Engineering - DIGA of the University of Naples *Federico II* and, in a special way, the Coordinator of the Ph. D. Programme Prof. Guelfo Pulci Doria, for approving my partecipations in numerous national and international courses and conferences.

Many thanks to Ludovico for introducing me to the laboratories and analitycal apparatus of *LARA* (Laboratory of Environmental analysis and research) of DIGA.

I am also grateful to my collegue Antonio, Flavia, Rosita, Raffaele, Luca, and Maria Rosaria for helping me in all circumstancies I need.

My deepest gratefulness to my parents Pasquale (father) and Nevina (mother), not only for the infinite love and incentive during all steps of my life, but also for making me the man that I am. Thanks to my sister Angela for all motivation and companionship.

If I may add just one more line, I would like to acknowledge how the companionship and love of Maria Giuseppa Rosa d'Ambrosio are important for me. Your will to live and afection makes me realize how fortunate I was to have across you. I am persuaded to believe that togheter we are stronger than ever.

Luigi Frunzo

Naples, Italy, November, 2011.

Contents

List of Figures

List of Tables

Sintesi

Negli ultimi anni con sempre maggiore interesse è stata considerata la possibilità di far ricorso a processi biologici anaerobici per la degradazione dei substrati organici ed inorganici. Tale indirizzo è stato certamente favorito dal limitato impegno economico all'uopo richiesto, potendo al contrario, talvolta addirittura contare sulla produzione di una miscela gassosa ad elevata valenza energetica (e quindi economica), qual'è il biogas. Ne sono conseguiti: da un lato, applicazioni a substrati sempre più complessi, comunque diversi da quello tradizionale, costituito dai fanghi della depurazione; dall'altro, il ricorso a nuove configurazioni impiantistiche, classificabili sia tra quelle a colture sospese che nell'ambito dei sistemi a colture adese. A tale ampia casistica di applicazioni fa da contraltare la mancata disponibilità di modelli matematici idonei a simulare le complesse reazioni che hanno luogo all'interno delle unità di processo anaerobiche, che possano costituire adeguati strumenti sia di dimensionamento che di verifica delle relative prestazioni. In tale contesto, obiettivi precipui del lavoro svolto durante il dottorato di ricerca sono stati:

1 - l'analisi dei fenomeni che si succedono nel corso dei processi di trasformazione per via biologica anaerobica di substrati complessi, anche diversi dai fanghi della depurazione; 2 - la messa a punto di una serie di modelli matematici, riferiti a substrati e a sistemi diversi, i cui codici di calcolo sono stati implemetati in ambiente MATLAB®.

In particolare, relativamente a questo secondo obiettivo si è provveduto alla messa a punto sia di due diversi codici di calcolo applicabili a sistemi biologici a colture sospese per la degradazione di composti organici comunque complessi e/o di composti inorganici che di un terzo codice di calcolo idoneo a simulare la degradazione anaerobica di substrati disciolti in sistemi biologici a colture adese. Per la calibrazione e la validazione del primo codice di calcolo sono stati anche eseguiti numerosi test di biometanazione, sia su substrati puri di diversa natura che su loro miscele.

La descrizione dei modelli matematici e dei relativi codici di calcolo per i sistemi a colture sospese è riportata nel **Capitolo IV** . Il primo di tali

due modelli riguarda la degradazione anaerobica in sistemi CSTR di miscele di diversi substrati (co-digestione). Esso è basato sulle equazioni differenziali di bilancio di massa relative ai substrati, ai prodotti intermedi ed ai prodotti finali, nonché alle specie batteriche coinvolte, prendendo in considerazione le reazioni chimiche e biochimiche di trasformazione dei substrati biodegradabili e le cinetiche di crescita e decadimento dei gruppi microbici che si sviluppano all'interno del reattore biologico. Nel dettaglio, sono stati considerati 5 processi fondamentali (Figura 1.1), vale a dire disintegrazione del substrato organico complesso, idrolisi extracellulare, acidogenesi, acetogenesi e metanogenesi, descritti seguendo un approccio analogo a quello proposto dall'Anaerobic Digestion Model n°1 ([4]) dell'International Water Association (IWA), che è stato assunto come base di partenza per lo sviluppo del modello di co-digestione. L'approccio proposto dall'IWA è stato seguito anche nella scelta della rappresentazione matriciale (Tabelle 1a e 1b Appendix) che, insieme alla verifica dei bilanci di massa, racchiude le espressioni cinetiche e la stechiometria del modello. Il modello proposto si differenzia dall'ADM1 per vari aspetti: i) la descrizione degli equilibri acido-base; ii) le equazioni di bilancio sul carbonio e sull'azoto per le quali è stato usato l'approccio proposto da [5]; iii) la cinetica del processo di disintegrazione, che gioca un ruolo fondamentale nel caso di substrati comunque complessi; iv) il frazionamento dei prodotti della disintegrazione in una componente rapidamente biodegradabile e una componente lentamente biodegradabile.

Il secondo modello relativo a sistemi CSTR a colture sospese è applicato ai processi di riduzione dei solfati, ed è stato finalizzato alla simulazione in condizioni dinamiche dei processi fisici, chimici e biologici che hanno luogo nei reattori gas-lift. Il modello, basato su equazioni differenziali di bilancio di massa su substrati, famiglie microbiche e prodotti delle reazioni biologiche, è in grado di simulare la competizione tra le varie specie batteriche presenti, e di modellare il rendimento del reattore. Il modello è costituito da due moduli fondamentali. Un modulo cinetico in cui è inclusa la crescita, il metabolismo, la crescita microbica nonchè l'andamento dei substrati considerati; un secondo modulo termodinamico volto alla modellazione dei trasferimenti di massa tra la fase gassosa e la fase liquida e viceversa.

La sperimentazione utilizzata per la calibrazione e la validazione del primo dei modelli appena citati è descritta nel **Capitolo II**. All'uopo sono stati eseguiti 57 test di biometanazione, che hanno richiesto l'avvio di 171 reattori. Le matrici utilizzate sono state: fanghi della depurazione di reflui urbani, frazione organica del rifiuto solido urbano (FORSU), liquami zootecnici (bovini, suinicoli, avicoli e soprattutto bufalini), scarti ortofrutticoli, matrici sintetiche atte a simulare particolari substrati organici. Tali matrici sono state degradate singolarmente o dopo loro opportune miscelazioni. Il con-

fronto dei dati sperimentali con quelli numerici è stato effettuato attraverso l'utilizzo di un algoritmo di calibrazione appositamente messo a punto, ricorrendo a tre differenti indici: lo scarto quadratico medio (Root Mean Square Error - RMSE); il grado di efficienza di modellazione (Modelling Efficiency - ME); l'indice di accuratezza (Index of Agreement - IoA).

La descrizione del modello matematico e del codice di calcolo riferiti a sistemi a colture adese è riportata nel **Capitolo V**. Tale modello presenta un'elevata flessibilità in quanto consente di trattare qualsiasi cinetica microbica, qualsiasi configurazione del reattore e tutti i meccanismi di distacco della biomassa. Esso può essere utilizzato per avere risposte a breve termine sulle performance del biofilm a seguito di variazioni dei substrati all'interno del bulk liquido così come informazioni a lungo termine relative allo spessore del biofilm ed alla distribuzione spaziale della biomassa.

Il modello matematico proposto è basato fondamentalmente sulla seconda legge di Fick per quanto riguarda i substrati e su una nuova equazione di bilancio di massa per quanto riguarda le specie microbiche adese al supporto inerte. Entrambe le equazioni rivestono particolare rilevanza nell'ambito della modellazione dei *multispecies biofilm*, in quanto descrivono fondamentalmente i due processi che sono alla base dello sviluppo di una pellicola biologica: la diffusione dei substrati e la crescita della biomassa intesa come un flusso convettivo. l'output principale del modello è costituito dall'indi viduazione della distribuione spaziale della biomassa e dei profili di concentrazione dei substrati all'interno del biofilm. Le procedure numeriche sono state testate e implementate nel caso di un biofilm microbico solfato riduttore e sono stati presentati i risultati delle simulazioni effettuate al variare dei parametri che governano il processo. Nello specifico, sono state investigate le performance del biofilm in termini di dinamiche dei substrati e distribuzione della biomassa al variare del rapporto di alimentazione COD/SO_4^{2-}.

Introduction

On the last decades the recourse to the anaerobic degradation processes as system to treat organic solid wastes became more and more frequent. The reason of this new tendency in treatments of solid wastes can be explained considering mainly three factors [6, 7, 8]: i) the need of applying a process to dispose of organic solid wastes more environmental friendly than landfills as requested by the latest rules concerning the environmental protection in many countries in the world; ii) the opportunity to obtain from this process a renewable fuel called biogas alternative to fossil ones; iii) the advantage of relatively low costs in starting up and managing this process. The anaerobic process is a multi-step biological process thank to which the originally complex and big sized organic solid wastes are progressively transformed in simpler and smaller sized organic compounds by different bacteria strains up to have a final energetically worthwhile gaseous product, called biogas, and a semi-solid material, called digestate, rich in nutrients and thus suitable for its utilization in agricultural contexts [9]. Despite the linearity according to which the anaerobic processes of organic solid wastes evolves, these systems are commonly prone to drops in performance due to the occurrence of dysfunctions or failures that make it strongly dependable on the choice of the substrates as well as on the environmental and operating conditions [10]. This last aspect can be reasonably considered the only drawback of these processes in treating solid organic wastes. Anaerobic degradation processes are easily performed in biological reactors where mixers and heater exchangers could be the only technological and power consuming equipments needed. Moreover these processes can gain money by disposing of organic solid wastes as well as selling the biogas or the power generated by its combustion and, when possible, the digestate as fertilizer in agriculture.

These processes have therefore opened up interesting perspectives not only for the treatment of the organic solid wastes, but also for the production of a renewable source of power, that is cheap and easy to obtain. Nevertheless the anaerobic processes are still affected by sceptical judges about their utilization as processes to treat organic solid wastes because of not comforting

past experiences mainly due to a lack of knowledge about this topic.

Mathematical models enable the representation of the main aspects of a biological system. They improve the understanding of the system, the formulation and validation of some hypothesis, the prediction of the system's behavior under different conditions, reducing, consequently, the experimental information requirements, costs, risk and time ([11]). Mathematical models must be a useful tool able to improve the understanding of biological processes and to predict the behaviour of the system.

This thesis has two main purposes. The first objective is to conduct an experimental work in order to understand the dynamic of anaerobic processes and to determine the biomethane potential of new substrates. The second objective is the development of mathematical models able to simulate under dynamic conditions the physical, chemical and biological processes prevailing in a anaerobic degradation processes. The application of mathematical models can help to develop, and improve, the design and the management of these technologies.

Structure of this thesis

Chapter I of this thesis reports a general introduction on anaerobic biological processes and a general description of environmental factors influencing these processes; Laboratory experiments are presented in **Chapter II** of this thesis. In particular several anaerobic biomethanation tests are carried out in order to: i) evaluate the anaerobic bio-degradation of different substrates; ii) obtain experimental results for calibration and validation of mathematical models presented in **Chapter IV**. A briefly literature review of existing mathematical models of biological anaerobic processes, focused in particular, on anaerobic digestion and anaerobic codigestion is reported in **Chapter III**. In **Chapter IV** a mathematical model, based on ADM1 approach [4], for suspended-growth bio-reactor are described. In particular the proposed model consider a new approach, based on surface based kinetics, for disintegration process. Numerical results are also presented in the chapter.

In **Chapter V** two Mathematical model for anaerobic attached-growth system are presented. The first model is a 1D multispecies biofilm model applied on sulfate reducing biofilm. The second one is a multispecies biofilm describing formation of Initial cell layer. The existence and uniqueness of solution are proved for both models.

Chapter 1

Biological anaerobic processes

1.1 Biokinetic of anaerobic degradation processes

The anaerobic anaerobic degradation processes are biochemical processes, where in anaerobic condition, is possible to degrade complex organic matter, with the production of a biological gas mixture, named "biogas" composed mostly by methane and carbon dioxide.

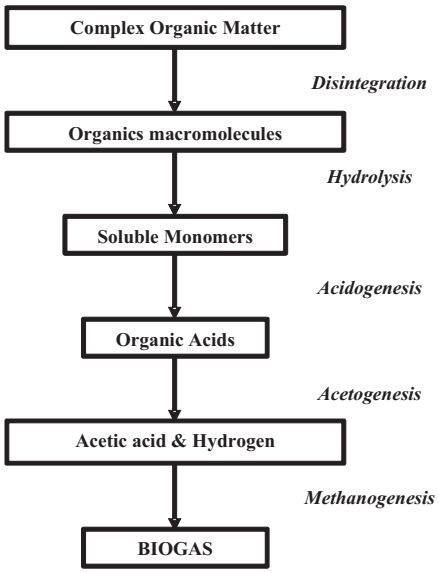

Figure 1.1: Main Steps anaerobic degradation of organic matter

The biogas shows an interesting calorific value $20000 \div 24000\ KJ\ Nm^3$; for this reason, it could be considered as an important renewable energy resource.

The different types of substrate and the different biochemical process conditions bring to complex organic matter degradation rate and consequently biogas production rate included in 40% to 90% range. These processes are carried out by a bacterial consortium and involve a more intricate series of metabolic reactions before final conversion to methane [12]. The Slowest among this processes determines the overall anaerobic digestion process velocity. Nutrients (i.e Nitrogen and Phosphorus) are not removed during anaerobic processes. Anaerobic processes are strongly dependable on the operational conditions, such as temperature, pH, carbon-to-nitrogen ratio (C/N) and inhibitors content. The substrates most commonly used to feed the anaerobic digesters are livestock manure, organic fraction of the municipal solid waste (OFMSW), wastes generated from food factories and farming [13]. The anaerobic degradation process can be divided into five main steps (Figure 1.1). The first two steps, disintegration and enzymatic hydrolysis, are extracellular (partly non biological) as well as the other three steps, acidogenesis acetogenesis and methanogenesis are cellular (biochemical). In the disintegration step the complex organic matter is degraded to macromolecular substrates that can be successively hydrolyzed. During the hydrolysis, hydrolytic bacteria degrade macromolecular substrates to their respective soluble monomers (in particular monosaccharides, aminoacids and fatty acids). During the acidogenesis (fermentation), fermentative bacteria convert monomeric organic substance to hydrogen or formate, carbon dioxide, pyruvate, volatile fatty acids, and other organic products. From the achieved products of acidogenesis step, the acetogens bacteria give acetic acids, carbon dioxide, and hydrogen. The production of Methane is the final step of anaerobic metabolism. The methane formation can be obtained by two main pathways: conversion of acetic acid by acetoclastic methanogenic bacteria, known as acetoclastic methanogenesis, and methanogenic respiration of carbon dioxide by hydrogenofil methanogenic bacteria, known as hydrogenitrofic methanogenesis.

1.2 Environmental factors affecting anaerobic degradation processes

Achievement optimal and stable reaction conditions is the goal of a correct control strategy. For the anaerobic digestion this fact is very important because methanogenesis is particularly sensitive on the environmental change of reaction conditions. The most important parameters are: Temperature, pH, Nutrients concentration, Alkalinity, Gas Production and Toxic Substances.

Temperature

The anaerobic degradation processes are governed by several microbial species, since the variation of process temperature is very important. A variation of process temperature does not bring only a simple acceleration or slow-down of metabolic processes, but determines the replacement of microbial species present into reactor. In particular, methanogenesis is strongly influenced by this temperature, in general there are three optimal ranges of anaerobic digestion operation: i) psycrophilic condition less than 20 C°, ii) mesophilic condition $25 \div 40$C°, iii) thermophilic condition $45 \div 60$C°. It is also possible to obtain anaerobic digestion process at ultra-thermophilic condition with temperature major than 60 C°. While there aren't many applications of psycrophilic anaerobic digesters, mesophilic and thermophilic anaerobic digesters are widely used. Mesophilic temperatures are preferable because the process is more stable and manageable than thermophilic temperatures. Thermophilic temperatures offer better yields, faster kinetics, and consequently, higher biogas production. Therefore, it can be said that although biogas production yields and bioreactor kinetics can be more favourable at thermophilic temperatures, optimal conditions depend on the type of substrates – concentration and biodegradability – and the type of system used.

pH

The pH gives an indication of process stability, because a pH change suggests equilibria variations of microbial species involved into anaerobic digestion process. The pH value in a digester depends mainly on dioxide carbon in liquid phase, hence on her partial pressure into biogas, and on organic acid and ammonia concentration. It's important to note that, pH can give informations about process instability, but with delay respect to the effective trends of process, because pH trends depend on alkalinity of the system. Furthermore, the pH response has low sensitivity in a well-buffered system[14]. The overall anaerobic process occurs at maximum rate in the pH range 6–8. For a pH below 6, the activity of the methane–forming bacteria drops rapidly so that at a pH of 5.5 they have largely stopped their activity [15].

Biogas composition

Monitoring biogas composition (in terms of methane and dioxide carbon concentration) is a traditional parameter since high carbon dioxide content indicates inadequate process performance. However, the carbon dioxide content is dependent on pH and, consequently, fluctuation of pH can affect the gas composition without decreasing methane production [16].

Alkalinity, buffering effect

The anaerobic processes influence the alkalinity. The acid step reduces the alkalinity and the methane step increases it. The overall result is a small reduction in alkalinity [15]. Alkalinity of $3000 \div 5000\ mgCaCO_3$ per liter is typical for a stable digestion process.

VFA

During acid step there is the formation of volatile fatty acids (VFAs) that are fatty acids with a carbon chain of six carbons or fewer, named also short chain fatty acids (i.e. acetic acid; propanoic acid; butyric acid; valeric acid and caproic acid). The concentration of VFA, expressed as mg of Acetic acid per liter $[mgAc/l]$, depends on the type of substrate. VFA concentration $200 \div 2000\ mgAc/l$ is typical for a stable digestion process. Monitoring the trends of VFAs concentration is more important than of absolute VFAs concentration. Faster change of VFA concentration suggests an increase of acidogenic activity and a decrease of methanogenic activity.

Ratio of VFAs to Alcalinity

VFA concentration and Alkalinity are the parameters that show a faster change when there are imbalances into anaerobic digester: VFAs increase while alkalinity decreases. The ratio of VFAs to Alkalinity is a good indicator of impeding failure. Value of VFAs to Alkalinity ratio near to 0,3 suggests good process performances.

Chapter 2

Experiments

2.1 Materials and methods

2.1.1 BMP tests methodology

The Bio-Methane test (BMP) can be used as an index of the anaerobic biodegradation potential as it is the experimental value of the maximum quantity of methane produced per gram of VS. The BMP is measured with the BMP test, which consists in measuring the bio-methane or biogas produced by a known quantity of waste in batch and anaerobic conditions. The approach of the BMP test is simple, an organic substrate is mixed with an anaerobic inoculum in defined operational conditions, and the gas evolved is quantified by a specific measurement method. In literature there are different attempts to define a standard protocol in order to gain comparable results but so far such standardization has not been reached.

One of the last attempts to define a common protocol for BMP testing with some basic guidelines for a common procedure was given in [17]. Some studies are also published in literature, aimed at collecting data and methods that are commonly used by different international laboratories [18]. The last collection of data, from 19 laboratories, was done in [19], with the aim of providing an extensive database for BMP results in terms of specific methane yield and degradation rates as a function of the experimental conditions selected.

Protocols for BMP tests should be provided for a clear setting of all those parameters that can affect significantly the experiments results, such as temperature, pH, stirring intensity, physical and chemical characteristics of substrates, substrate/inoculum (S/I) ratio. Temperature affects the biomethanation rate and usually higher temperatures imply greater methane yields in a shorter digestion time. Nevertheless sharp increases of temper-

ature should be avoided because they can cause a decrease in bio-methane production due to the death of specific bacteria strains, particularly sensitive to temperature changes [20]. To keep constant the temperature during BMP tests it is needed to submerge the reactors in a water bath kept at the selected temperature [21] or to incubate them in a thermostatically controlled room [22].

BMP tests have to be carried out keeping the pH around the neutrality (values ranging between 7.0 to 7.8). pH values below 6.0-6.5 inhibit the methane bacteria activity. To avoid drops in pH chemicals are added to the organic substrate to supply a buffer capacity. Sodium bicarbonate, sodium hydroxide, sodium carbonate and sodium sulphide are the most used chemicals [23]. Stirring intensity guarantees an uniform moisture content and maximizes the contact between substrates and microorganisms. Mixing can be provided by several ways: turning manually up to down the reactors once a day [17], using stirring magnet bar, using an external agitation systems [24] Substrate particles size affects significantly the BMP tests [[25], [26], [27], [28], [29]] as it influences the ratio between surface and volume for each organic particle. This ratio is relevant since microorganisms can degrade only the substances present on the organic solids surface. Substrate/inoculum (S/I) ratio influences the performance of BMP tests. According to [30] a S/I ratio ranging between 0.5 and 2.3 gVS/gVS can prevent acidification phenomena. Instability in the anaerobic process, such as high COD content in the effluent and volatile fatty acids (VFAs) accumulation, occurs with S/I ratio lower than 0.5 [31]. Further studies [32] showed that the biogas yield is in an inverse proportion to the S/I ratio in the range 1.6-5.0. In literature different methods to measure the biogas produced are used. The most common are the manometric and volumetric methods. The manometric method measures the biogas production by the overpressure generated by biogas inside the reactor where volume and temperature are kept constant. The overpressure can be measured using a common differential manometer or a more sophisticated pressure transducer [33] The volumetric method measures the biogas produced when pressure and temperature are kept constant. One of simplest volumetric methods connects the reactor with a graduated piston [25]. Another equipment that uses the liquid displacement to measure the biogas produced is the Eudiometer described in detail in [34]. Systems similar to Eudiometer can be built using graduated reverse cylinder filled with a barrier solution inside [35]. Volumetric methods permit to know the biogas composition as percentages of CH_4 and CO_2 by using a gas chromatograph or measuring directly the CH_4 flow after removing CO_2 from biogas by bubbling it through a $NaOH2N$ solution.

2.1.2 BMP tests set up and operation

The experimental tests represent the most powerful tool to remove all those doubts that still hamper the full establishment of the anaerobic digestion as the environmentally and economically most convenient and helpful process to treat organic solids. Among all available experimental methods, the bio-methane potential (BMP) tests are those that have been most successful, mainly thanks to their easy set up and conduction as well as the useful information obtainable from them.

Figure 2.1: Biomethanation test

The BMP tests are conducted in batch conditions and in bench scale, measuring the maximum amount of biogas or bio-methane produced per gram of volatile solids (VS) contained in the organics used as substrate in the anaerobic digestion process [36]. Furthermore relevant elements coming from the conduction of such tests are mainly the environmental and operating conditions that could lead the process to failure, the time needed to have a complete substrate degradation, the average rate of bio-methanation for each substrate investigated, the evaluation of the digestion kinetics by coupling the BMP tests results to a mathematical model simulating the anaerobic digestion.

The relevance of the BMP tests as useful tool to improve the knowledge on the anaerobic digestion process to treat organic wastes. BMP test allow to improve our knowledge about the biodegradability of the substrate investigated, the relative specific rate of bio-methanation, the theoretical production of bio-methane and the disintegration process kinetics.

These tests were conducted using either pure substrates or a mixture of two substrates in order to investigate also the effect that the combination of

different organic wastes has on the digestion process (co-digestion). Indeed according to recent studies [37, 38, 39, 40, 41, 42], the concurrent presence in the same anaerobic reactor of different organic wastes can improve the performance of the digestion process. The co-digestion of different organic substrates has been studied during the last 10-15 years and the results have showed a synergic effect of the combined treatment as the biodegradability of the resulting mixture was higher than the biodegradability of the single substrates when investigated separately. In particular, the combination of different substrates with proper percentages of each fraction can result in the production of a mixture with a Carbon:Nitrogen (C:N) ratio included in the optimal range $20:1 \div 30:1$ [43].

Analogous results were obtained with regard to the Carbon:Phosphorous (C:P) ratio. Therefore the above-cited improvement of the biodegradability characteristics of the solid mixture is substantially due to the C:N:P ratio adjustment. Further benefits of the co-digestion are higher biogas and energy production [44] and the decrease of the amount of solid waste to be disposed due to the gasification of a higher percentage of the substrate.

Each BMP test, reported in this work, was performed under controlled and reproducible conditions in a 1000 mL glass bottle GL 45 (Schott Duran, Germany) 2.1. Each bottle was partially filled with inoculum and a substrate, according to a ratio equal to 2 between their VS content; tap water was added up to a 500 mL total volume. Small amounts of Na_2CO_3 powder, ranging from 0.10 to 0.60 g, were also added (Table 2.2 and 2.4) to prevent critical drops in pH. Each bottle was sealed with a 5 mm thick silicone disc that was held tightly to the bottle head by a plastic screw cap punched in the middle (Schott Duran, Germany). All bottles were shaken for 30 min at 80 rpm speed by bottle shakers KL-2 (Edmund Bühler, Germany) and were immersed up to half of their height in hot water, kept at a constant temperature of $35 \pm 1C$ by 200W A-763 submersible heaters (Hagen, Germany). Once a day, each bottle was connected by a capillary tube to an inverted 1000 mL glass bottle containing an alkaline solution (2% NaOH) and sealed in the same way as done for the BMP bottle. To enable gas transfer through the two connected bottles, the capillary tube was equipped on both ends with a needle, sharp enough to pierce the silicone disc.

2.1.3 Analytical measurements

Sludge and synthetic solid waste characterization

The weight, Total Solids (TS) and Volatile Solids (VS) concentration of the granular anaerobic sludge as well as the dry matter, moist organic matter and

ash content of pasta, cheese and dewatered sludge were determined according to Standard Methods [45]. The composition of both pasta and cheese, in terms of carbohydrates, proteins and lipids, was taken from the respective packaging labels and was experimentally verified according to the procedures described in the Handbook of Food Analysis [46].

Methane production

Daily methane production was monitored using an inverted 1000 mL glass bottle filled with a 2% NaOH solution and connected to the digester by a capillary tube.

Figure 2.2: Biomethanation test

The volume of alkaline solution displaced from the 1000-mL bottle, which was collected and measured using a graduated cylinder, was assumed to be equivalent to the volume of the daily methane production. The CO_2 contained in the biogas did not affect the volumetric methane measurements as the CO_2 was dissolved in the alkaline solution.

pH and temperature monitoring

Temperature and pH of all mixtures investigated were monitored for at least once a day with a TFK 325 thermometer (WTW, Germany) and a pH meter (Carlo Erba, Italy), respectively.

Measurements

TS and VS contents as well as F_{li} of each substrate were measured according to Standard Methods [45]. F_{pr} was obtained by multiplying by 6.25 the organic nitrogen content of each substrate (TKN minus NH4-N) measured according to Standard Methods [45], whereas F_{ch} was evaluated by subtracting the sum of proteins and lipids from VS content [47]. Daily methane production was monitored measuring the volume of alkaline solution displaced from the measure bottle and collected in a graduated cylinder. The CO_2 contained in the biogas did not affect the volumetric methane measurements as it was dissolved in the alkaline solution. Temperature and pH in each BMP bottle were also monitored for at least once a day with a TFK 325 thermometer (WTW, Germany) and a pH meter (Carlo Erba, Italy), respectively.

2.2 Anaerobic Digestion of pure substrates

2.2.1 Manure Waste anaerobic digestion

Experimental design

BMP tests were conducted using three different livestock manure (i.e. Buffalo manure(BM), Poultry manure (PM) and Swine manure (SM)), whose main characteristics in terms of Total Solids (TS), VS, Carbohydrates Fraction (F_{ch}), Proteins Fraction (F_{pr}) and Lipids Fraction (F_{li}) are shown in Table2.1. In particular, BMP tests were conducted on each manure (identified by the test indexes T1, T2 and T3). A further BMP test (identified by the test index T4) was conducted on the inoculum, to estimate the volume of methane resulting by the fermentation of the organic matter contained in the anaerobic sludge. In total, 4 BMP tests were conducted, each of them in triplicate (Table2.2).

Parameter	Units	BM	PM	SM	Inoculum
TS	$g/kg, wet$	102.7 ± 0.8	867.1 ± 2.0	101.5	140.9 ± 0.8
VS	$g/kg, wet$	81.4 ± 0.6	365.2 ± 1.4	83.06	85.4 ± 0.5
F_{ch}	$g/g, dry$	0.18	0.30	0.35	-
F_{pr}	$g/g, dry$	0.31	0.20	0.28	-
F_{li}	$g/g, dry$	0.017	0.015	0.012	-

Table 2.1: Main characteristics of the organic solid wastes used in BMP tests T_1, T_2 and T_3.

Test	BM Mass[g]	PM Mass[g]	SM Mass[g]	Inoculum Mass[g]	Na_2CO_3 Mass[g]
T_1	77.61 ± 0.64	-	-	150.22 ± 0.62	0.35 ± 0.04
T_2	-	17.61 ± 0.51	-	150.15 ± 0.89	0.55 ± 0.06
T_3	-	-	76.87 ± 0.37	150.22 ± 0.62	0.30 ± 0.01
T_4	-	-	-	150.16 ± 0.77	0.45 ± 0.05

Table 2.2: Mass composition of organic matrix for BMP tests $T_1 - T_4$

Substrates collection and preparation

PM, SM and BM were collected from a farm in Albanella, near Salerno, in the southern Italy and stored in 10 L buckets at 4^0C. Granular anaerobic sludge, used as inoculum, was taken from an Upflow Anaerobic Sludge Blanket (UASB) reactor treating the wastewater produced by a potatoes factory.

Methane production from manure

Figure 2.3 shows the cumulative methane production from the BMP tests conducted using pure substrates: T_1 and T_3 gave the highest and lowest methane production, respectively; intermediate values were obtained from T_2.

T_3 gave the fastest bio-methane production. After twenty days the production of the three BMT are approximatly the 80% 70% 60% of total biomethane potential. For all the substrates, after 80 days the methane produced was close to the maximum obtainable, indicated by the achievement of the plateau.

2.2.2 Organic solid Waste anaerobic digestion

Experimental design

BMP tests were conducted using two different organic wastes (i.e. Organic fraction of municipal solid waste (OFMSW) and greengrocery waste (GW)), whose main characteristics in terms of Total Solids (TS), VS, Carbohydrates Fraction (F_{ch}), Proteins Fraction (F_{pr}) and Lipids Fraction (F_{li}) are shown in Table2.3. In particular, BMP tests were conducted on each pure substrate (identified by the test indexes T_5, T_6) A further BMP test (identified by the test index E3) was conducted on the inoculum, to estimate the volume of methane resulting by the fermentation of the organic solids contained in the

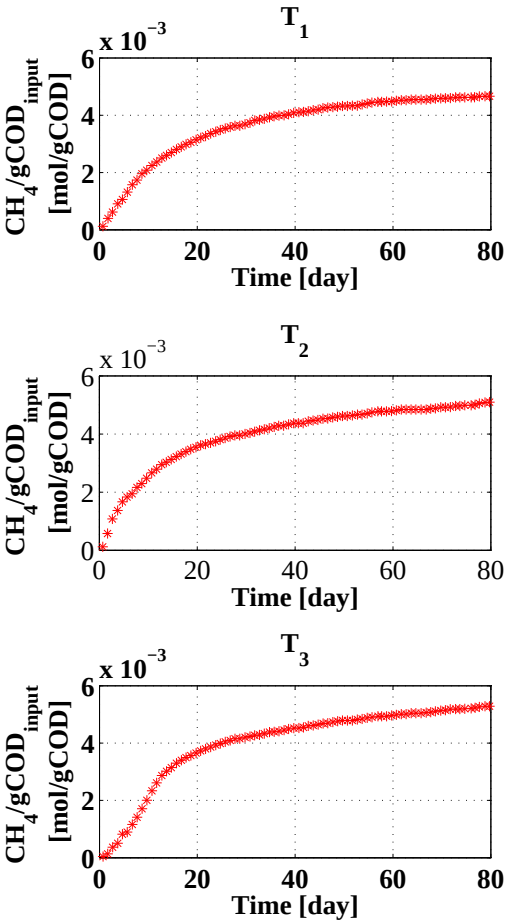

Figure 2.3: Cumulative bio-methane production from BMP tests $T_1 - T_3$

anaerobic sludge. In total, three BMP tests were conducted, each of them in triplicate Table2.2.

Substrates collection and preparation

Representative samples of OFMSW and GW were collected according to the waste sampling methodology [48] from the household source-separated wastes and the fruit and vegetable market of Naples respectively. Both samples of OFMSW and GW were ground and sieved as far as to have an homogeneous material composed of particles with size ranging between 1 and 2 cm.

Par	Units	OFMSW	GW	Inoculum
TS	$g/kg, wet$	334.7 ± 0.9	151.8 ± 0.5	140.9 ± 0.8
VS	$g/kg, wet$	251.4 ± 0.7	140.9 ± 0.3	85.4 ± 0.5
F_{ch}	$g/g, dry$	0.28	0.32	-
F_{pr}	$g/g, dry$	0.18	0.17	-
F_{li}	$g/g, dry$	0.25	0.02	-

Table 2.3: Main characteristics of the organic solid wastes used in BMP tests T_5 and T_6.

Test	OFMSW Mass[g]	GW Mass[g]	Inoculum Mass[g]	Na_2CO_3 Mass[g]
T_5	24.43 ± 0.38	-	150.22 ± 0.62	0.35 ± 0.04
T_6	-	56.45 ± 0.72	150.32 ± 0.65	0.60 ± 0.04
T_7	-	-	150.27 ± 1.05	0.30 ± 0.04

Table 2.4: Mass composition of organic matrix for BMP tests $T_5 - T_7$

Methane production from organic solid wastes

Tests T_5 and T_6 were conducted on the two pure substrates OFMSW and GW.

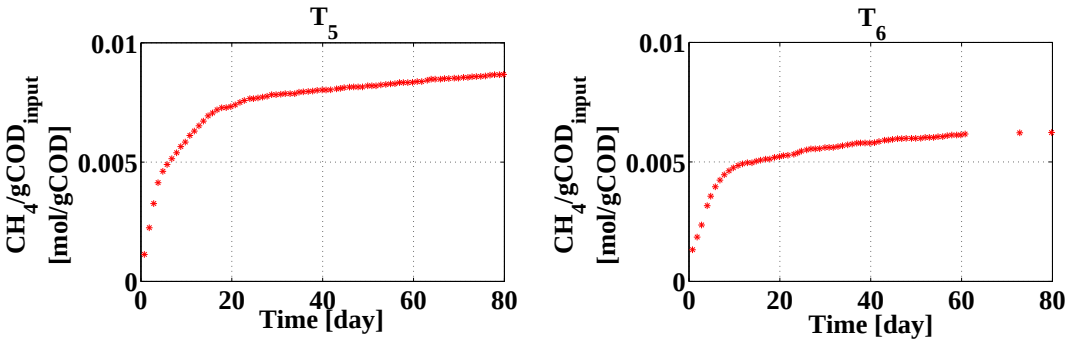

Figure 2.4: Cumulative bio-methane production from BMP tests T_5 and T_6

2.3 Anaerobic co-digestion

2.3.1 Buffalo manure and Organic solid waste co-digestion

Experimental design

Figures 2.3 and 2.4 show the cumulative methane production from the BMP tests conducted using pure substrates. The methanization process was faster when OFMSW (T_5) and GW (T_6) were used as substrate rather than livestock manure, as shown by the initial slope of the cumulative curves (Figure 2.4). For all the pure substrates, after 80 days the methane produced was close to the maximum obtainable, indicated by the achievement of the plateau. After 30 days the methane obtained by T_5, T_6, T_1, T_2 and T_3 were respectively, corresponding to 90%, 89%, 79% and 78% of the relating total methane produced after 80 days. These differences in the amount of methane produced as well as in the production rate between organic solid wastes and livestock manure are explainable considering that the first substrates are more biodegradable than the second ones since they were not preliminary passed through the digestive system of animals. On the other hand a high biodegradable substrate, such as OFMSW, can cause problems in the progress of the digestion process since the production of VFAs can be faster than their conversion into methane. When this event happens a sharp drop in pH occurs and consequently the digestion process becomes slower or can even fail. The occurrence of these failures can be avoided if the organic substrate has a sufficient buffer capacity. From this point of view, the ammonia contained in livestock manure could turn from a cause of inhibition [49] into a positive element for the biological process, supplying the requested buffer capacity [50]. Moreover livestock manure contains enzymes and a high number of microorganisms that can make faster and also more efficient the biological process, as enzymes can help to consume the less biodegradable components of the municipal organic solid wastes such as cellulose. On the basis of the previous considerations, it was decided to mix organic solid wastes and livestock manure and assess their synergistic effect by means of further BMP tests. BMP tests were conducted using two mixtures obtained mixing BM and OFMSW in VS percentages of 50 and 50% and 70 and 30%, VS,respectively (identified by the test indexes T_7 and T_8). A further BMP test (identified by the test index T_9) was conducted on the inoculum, to estimate the volume of methane resulting by the fermentation of the organic solids contained in the anaerobic sludge. In total, 3 BMP tests were conducted, each of them in triplicate Table2.6.

Par	Units	BM	OFMSW	GW	Inoculum
TS	$g/kg, wet$	102.7 ± 0.8	334.7 ± 0.9	151.8 ± 0.5	140.9 ± 0.8
VS	$g/kg, wet$	81.4 ± 0.6	251.4 ± 0.7	140.9 ± 0.3	85.4 ± 0.5
F_{ch}	$g/g, dry$	0.18	0.28	0.32	
F_{pr}	$g/g, dry$	0.31	0.18	0.17	
F_{li}	$g/g, dry$	0.017	0.25	0.02	

Table 2.5: Main characteristics of the organic solid wastes used in BMP tests.

Substrates collection and preparation

Tests T_7 and T_8 were conducted on mixtures composed of the two pure substrates chosen between livestock manure and organic solid wastes, i.e. BM and OFMSW.

Test	BM Mass[g]	PM Mass[g]	OFMSW Mass[g]	GW Mass[g]	Inoculum Mass[g]	Na_2CO_3 Mass[g]
T_7	49.05 ± 0.51	-	11.19 ± 0.22	-	150.08 ± 0.93	0.35 ± 0.05
T_8	68.68 ± 0.62	-	6.71 ± 0.18	-	150.34 ± 0.89	0.25 ± 0.02
T_9	-	-	-	-	150.22 ± 0.62	0.35 ± 0.04

Table 2.6: Mass composition of organic matrix for BMP tests $T_7 - T_8$

Methane production from mixtures of organic substrates

These tests focused on the effect of mixing different substrates on methane production (Figure 2.5). The highest methane production was achieved in test T5, corresponding to the mixture characterized by the higher percentage of OFMSW. However it is interesting to notice that the co-digestion of two substrates was completed in almost 60 days, which is faster if compared with the digestion of the pure substrates, completed in a time longer than 80 days. This is due to the following main characteristics of the mixtures of BM and OFMSW: i) higher buffer capacity if compared with pure OFMSW; ii) natural presence of anaerobic-methanogenic biomass in livestock manure and iii) better balance in carbon and nutrients content. Moreover, Figure 2.5 shows that the methane volume obtained at any day from the mixture of organic wastes is higher than the sum of the amounts produced when the same organic wastes were separately digested. For instance, after 15 and 30 days the mixture of test T_5 gave a 30% and 12% higher methane production, respectively (Fig. 3a), whereas the same volume of methane produced in test

T6 at day 30 is obtainable by summing the amounts produced individually by the single pure substrates after almost 75 days. This means that the co-digestion of different substrates reduces the time needed to complete the digestion process, making possible to realize smaller size digesters.

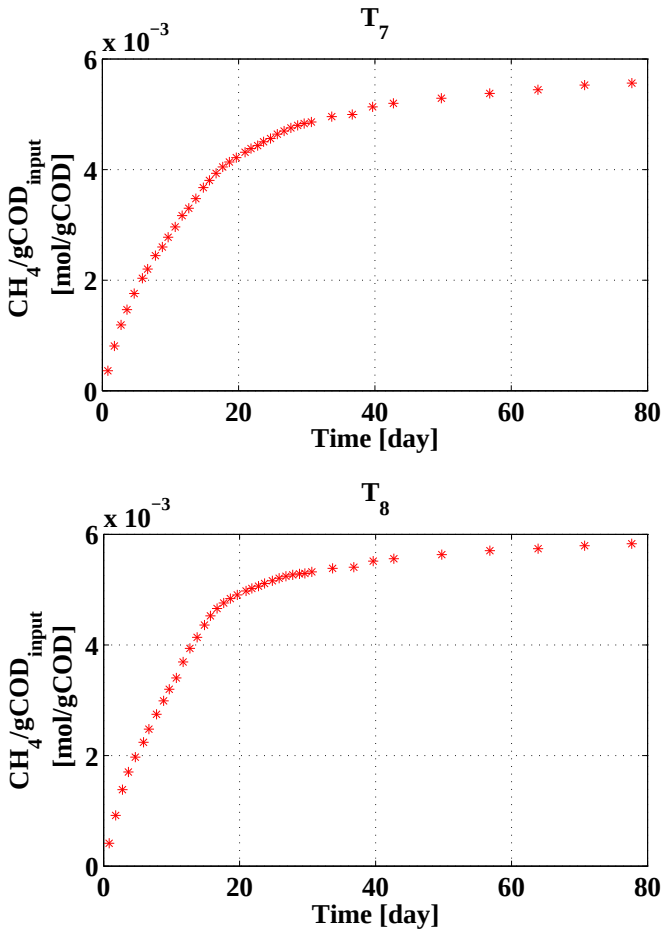

Figure 2.5: Cumulative bio-methane production from BMP tests T_7 and T_8

2.3.2 OFMSW and sewage sludge co-digestion

Experimental design

BMP experiments were performed using synthetic organic waste substrates with known concentrations of carbohydrates, proteins and lipids. The choice

of the substrates was determined by the need for the knowledge of carbohydrates, proteins and lipids in the digester influent, which are not easy to measure in OFMSW samples. Cumulative methane production from nine different mixtures of synthetic organic waste and anaerobic sludge was investigated. The composition of the organic mixtures in terms of the ratio between organic matter and anaerobic sludge, solid particle size and percentage of carbohydrates, lipids and proteins on a dry basis are reported in Tables 2.7. In addition to the tests conducted in triplicate with the three solid organic mixtures, a further test was conducted using only anaerobic sludge as the organic substrate to estimate the volume of methane resulting from the fermentation of the organics contained in the anaerobic sludge. Thirty tests were performed.

TEST	$\frac{VS_{OM}}{VS_{IB}}$ $[dimensionless]$	**Initial Radius** $[mm]$	**Carbohydrates** [%]	**Lipids** [%]	**Proteins** [%]
A_1	1	0.5	70	12	18
B_1	1	1.5	70	10	20
C_1	1	2.5	70	12	18
A_2	1	0.5	12	50	38
B_2	1	1.5	11	50	39
C_2	1	2.5	12	50	38
A_3	1	0.5	35	35	30
B_3	1	1.5	35	34	31
C_3	1	2.5	35	35	30
D	0	-	-	-	-

Table 2.7: Composition of the organic mixtures in terms of the ratio between organic matter and anaerobic sludge, solid particle size and percentage of carbohydrates, lipids and proteins on a dry basis.

Anaerobic digestion was performed on a small scale under controlled and reproducible conditions as reported in section 2.1.2

Substrates collection and preparation

Three different criteria were used to select the composition of the synthetic organic waste used for biomethanation tests: (i) the ratio between anaerobic sludge and synthetic organic waste expressed in terms of Volatile Solids (VS) content; (ii) the synthetic organic waste particle size; (iii) the synthetic organic waste in terms of the content of carbohydrates, lipids and proteins.

TEST	Hard wheat pasta [g]	Cow cheese [g]	Anaerobic sludge [%]	Na_2CO_3 [%]
A_1	15.0	4.4	150.0	0.20
B_1	15.0	4.2	173.0	0.20
C_1	15.0	4.4	150.0	0.20
A_2	2.4	22.6	196.0	0.40
B_2	2.2	22.0	193.0	0.30
C_2	2.4	22.6	196.0	0.40
A_3	4.6	10.0	114.0	0.20
B_3	4.6	10.0	121.0	0.30
C_3	4.6	10.0	114.0	0.30
D		-	100	-

Table 2.8: Mass composition of the organic mixtures (on a wet basis).

Figure 2.6: Synthetic organic waste

The thirty solid organic mixtures described in Tables 2.7 and 2.8 were made up using three types of pasta with different sizes, i.e., radius of 0.5 mm (Tempestina by pasta factory Rummo, Italy), 1.5 mm (Spaghetti alla chitarra by pasta factory Garofalo, Italy) and 2.5 mm(Fregola by pasta factory Quisardegna, Italy), and cow cheese (Provolone dolce by Soresina creamery, Italy), which was properly ground and sieved to achieve the same size as the pasta samples. Granular anaerobic sludge taken from an Upflow Anaerobic Sludge Blanket (UASB) reactor treating the wastewater produced by a potato processing factory was added to the three solid organic mixtures to reach a ratio between the VS contents of the anaerobic sludge and the synthetic solid waste equal to 1 (Tables 2.7 and 2.8).

Methane production from co-digestion of OFMSW and sewage sludge

Figures 2.7, 2.8 and 2.9 shows the cumulative methane production from the BMP tests.

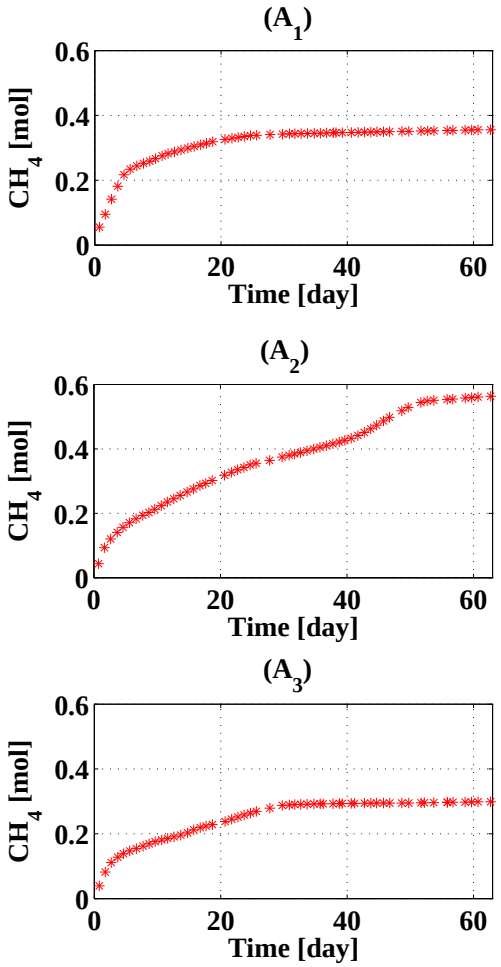

Figure 2.7: Cumulative bio-methane production from BMP tests $A_1; A_2; A_3$

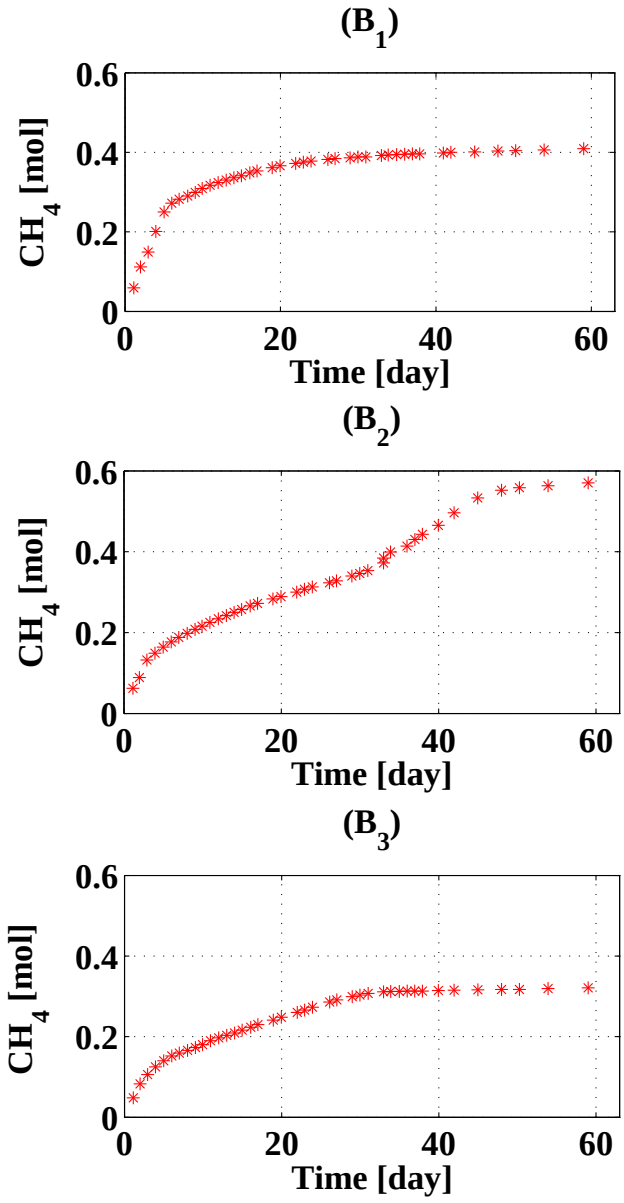

Figure 2.8: Cumulative bio-methane production from BMP tests $B_1; B_2; B_3$

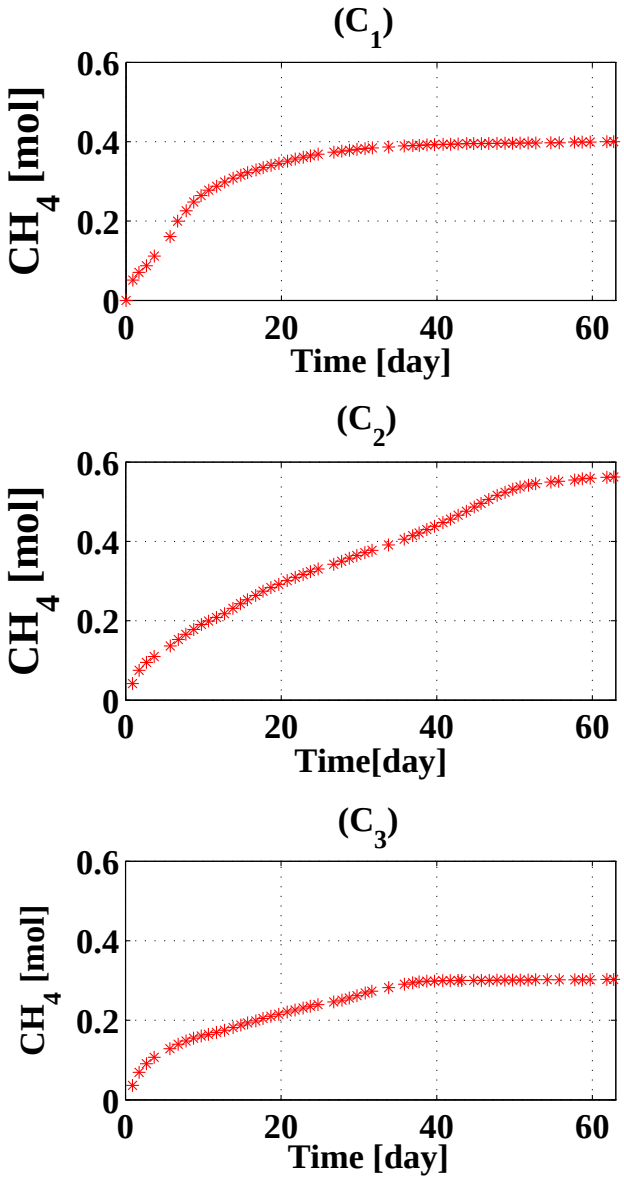

Figure 2.9: Cumulative bio-methane production from BMP tests $C_1; C_2; C_3$

Chapter 3

Mathematical modelling of biological anaerobic processes

3.1 Introduction

Anaerobic processes have been employed for over 150 years for the digestion and stabilization of sewage sludge, generated in wastewater treatment. They constitute a mature technology that can be adapted to most forms of residual biomass. The cost of methane production is still relatively high compared to the cost of natural-gas from fossil-fuel deposits, but this situation should change as natural-gas costs rise and anaerobic process technologies improve ([51]). Anaerobic processes have the advantage of producing small amounts of sludge, requiring less nutrients and energy than aerobic treatment processes and obviously the producted biogas can be used as a renewable source of energy. In particular anaerobic digestion is now considered as a consolidated technology with more than 2200 high-rate reactors implemented worldwide ([52]). Mathematical models enable the representation of the main aspects of a biological system. They improve the understanding of the system, the formulation and validation of some hypothesis, the prediction of the system's behavior under different conditions, reducing, consequently, the experimental information requirements, costs, risk and time ([11]). Mathematical models must be a useful tool able to improve the understanding of biological processes and to predict the behaviour of the system. Several mathematical models of anaerobic processes, in particular anaerobic digestion, have been proposed in the last decades. In the following sections an overview of the main dynamic models of anaerobic degradation is presented; a classification has been attempted according to different modelling approach. Thus two major categories are distinguished: anaerobic digestion models and anaerobic

co-digestion models.

3.2 Mathematical modelling of anaerobic digestion

3.2.1 Mathematical models proposed before the ADM1

During the last 45 years, many researchers have developed and proposed several models of anaerobic digestion. The first models focused the attention on the description of the limiting step of the anaerobic processes;i.e. the slowest step controls the global rate [53]. This series of models, consisted of a limited number of equations, were very simple and easy to use but were not able to adequately describe the process performance.

An example of this first generation of models [53] describes the animal waste digestion. In their study the autors consider two bacterial groups, the acidogens and acetoclastic methanogens. VFA inibitions for both microbial species and Ammonia inibitions for methanogens are also taken into account. [54] proposed a mathematical model of anaerobic digestion of soluble compounds, fats/lipids, carbohidrates and proteins. The model considers three microbial groups, fermentative bacteria, acetogenic bacteria and acetoclastic methanogens bacteria.

A model considering the concentration of volatile fatty acid as the key parameter of the process and incorporating acidogenesis and acetogenesis separately came later. This model considers two or more bacterial groups, include inhibition kinetics, pH calculation and gas-phase dinamics. In 1982 [55] developed a model in order to simulate anaerobic digestion of animal waste. This model take into account five microbial groups and considers four foundamental steps. In the first step of hydrolysis, complex organic material is converted in soluble biodegradable material by extracellular enzymes. In the second step (acetogenesis) the soluble organic material is converted to VFA (i.e. propionate, butyrate and acetate). During the third step, acetogenesis, acetogenic bacteria convert propionate and butyrate to acetate.

A new generation of models considering anaerobic degradation of real and complex wastewater or organic matter came later. The first model [56] considers the conversion of the complex organic matter to carbohidrates, proteins and lipids. Thanks to this approach it is possible to take into account the different composition of wastes. After carbohidrates proteins and lipids are converted to simple sugars, amino acids and fatty acids respectively. A mathematical model for co-digesting piggery, olive-mill and dairy wastewaters based on batch kinetic experiments was developed by [57] in 1996. This

model considers a four step process (hydrolysis, acidogenesis, acetogenesis, and methanogenesis). The model cannot predict the methane concentration, and does not consider the inhibitory effect by high ammonia concentration, VFA, LCFA, and hydrogen.

Several models describing the anaerobic digestion of synthetic substrates as glucose are present in literature. In particular, the model described in [58] applies to anaerobic digestion of glucose. In this model five steps are taken into account, and five bacterial groups are considered. Another model of anaerobic digestion of glucose [59] uses H_2 as the key parameter that regulates the production of VFA from glucose. Thereafter many models were based on the Mosey's model ([60, 61, 62, 63, 64]).

In 2000 [65] proposed a more detailed model of anaerobic degradation of complex wastewaters. This model incorporates additional processes and species and more detailed kinetics with inibition. In this model the authors consider three enzimatic groups and nine bacterial groups. Lipids, Carbohidrates and proteins are degraded to long chain fatty acids (LCFA), simple sugars, and soluble proteins during enzimatic hydrolysis. Acetate and other VFA are producted during acidogenesis. Successively, all the volatic acid are degraded to acetate (acetogenesis). Finally acetoclastic and hydrogenotrophic bacteria produce methane. In 1993 [50] proposed a complex matematical model for anaerobic digestion of particulate carbohydrates. This is the first model that takes into account the ammonia inhibition and considers the effect of self-regulation pH and self-resistance of un-ionized ammonia toxicity ([66]). The model considers four microbial groups, glucose fermenting acidogens, propionate and butyrate acetogens and acetoclastic methanogens. In 1997 the authors proposed an extende version of above-mentioned model for simulate the co-digestion of cattle manure and olive mill wastewater. Finally, in 1999, the model was extended in order to be able to simulate the anaerobic degradation of complex organic matter to biogas [67]. In particular in this model the substrate is characterized by its organic composition in terms of carbohydrates, proteins and lipids; and by inorganic composition in terms of ammonia, phosphate, carbonate, hydrogen sulfide, anions and cations.

In 1994 ([68]) proposed a mathematical model of anaerobic digestion of complex organic matter named "methane". In this model complex organic matter is degrated by extracellular hydrolytic enzimes, produced by acidogenic bacteria, to soluble organic matter which is characterized in terms of carbohydrates, proteins and lipids. Two groups of acidogenic bacteria (i.e. acetate-producing bacteria and propionate-producing bacteria) produce acetate and propionate by soluble organic matter, during this phase there is the release of hydrogen, ammonia and carbon dioxide. After the degradation

of propionate by acetogens bacteria the producted acetate is used in acetoclastic methanogenesis. Methane is also producted by hydrogenotrophic bacteria. Sulfate-reducing bacteria which oxydise propionate and lactate to CO_2 are also considered in the model. Inibition of free ammonia, sulfide and propionate is also considered in the model.

3.2.2 Mathematical models based on the ADM1 approach

In 2002 the International Water Association (IWA) Task Group for Mathematical Modelling of Anaerobic Digestion Processes developed a comprehensive mathematical model known as ADM1 [4], which was based on the knowledge of modelling and simulation of anaerobic digestion systems emerged over the previous years. The ADM1 gives a common framework for further model development, calibration and validation studies whith comparable results. However this model neglects some processes involved in the anaerobic digestion such as sulphate reduction, acetate oxidation, homoacetogenesis, solids precipitation and inhibition due to sulphide, nitrate, long chain fatty acid (LCFA), weak acid and base [69]. Some of the previous aspects have been studied and modelled afterwards; for instance further extensions were published in recent years. [70] in 2002 proposed an extension of ADM1 in order to simulate the effect of acid addiction in terms of pH decrease, and reduction of calcium carbonate ($CaCO_3$) precipitation. For this aim a specific calcium carbonate precipitation equation was added to the ADM1. In addition, in the same study, the authors apply the ADM1 to an anaerobic digester at a gelatine production facility in order to assess the effect of thermophilic condition for reduced ammonia inibition. In 2004 Batstone at al.[70] in order to describe anaerobic winery wastewater degradation proposed a further extension of ADM1 considering ethanol degradation. In 2003 an other extension of ADM1 was proposed by [71]. In their work the authors extended the ADM1 to the sulphate reductio processn. Modified version of ADM1 for degradation of agro-waste application and for sewage sludge termally pretreated was proposed, rispectively by [47] and [72]. A further extension aimed at removing the ADM1 discrepancies in both carbon and nitrogen balances was published in 2005 [5].

3.3 Mathematical modelling of biological anaerobic co-digestion

During the last decades many researchers have studied the Anaerobic co-digestion technology with the aim to establish the effect of mixing two or more substrates in an anaerobic digester. To achieve a correct combination of different substrates many experiments are needed as often the substrate mixture leads to process disturbance and biogas production. An accurate modelling can help to define a correct ratio between different organic substrates fed to the digester.

3.3.1 Mathematical models proposed before the ADM1

The first co-digestion model was proposed by [73]. It is a steady state mathematical model which simulates the degradation of the major component groups (i.e. lipids, hydrocarbons and proteins).

Author	Steady state model	Dynamic model	Calibration	Validation	Substrates used in calibration validation
[73]	x	-	-	-	-
[57]	-	x	-	x	OMW; PM; DW
[74]	-	x	-	x	OFMSW and PM
[75]	-	x	-	-	-
[67]	-	x	-	x	M> M&G; M&P
[76]	-	-	x	x	WAS; GW

Table 3.1: Mathematical models proposed before the ADM1

A mathematical model for co-digesting piggery, olive-mill and dairy wastewaters was developed by [57], the main characteristics of this model are described in section 5.47

Successively [74] developed and validated a two-stage mathematical model of acidogenesis and methanogenesis, including ammonia inhibition and pH prediction. In 1997 [75] proposed a simplified mathematical model that simulates the anaerobic co-digestion of different wastes, defining the waste by its general composition. The model takes into account only two conversion processes, i.e. hydrolysis/acidogenesis and methanogenesis. A more complete dynamic model was developed by [67]. The model, based on a model previously proposed [50], describes the anaerobic degradation of complex material

and the co-digestion of different types of wastes. The model includes 2 enzymatic hydrolytic steps, 8 bacterial steps and involves 19 chemical compounds (carbohydrates, lipids, and proteins, intermediates such as volatile fatty acids and long-chain fatty acids, and important inorganic components, i.e., ammonia, phosphate, cations, and anions). The model also includes pH prediction and free ammonia, acetate, volatile fatty acids (VFA) and long-chain fatty acids (LCFA) inhibition.

[76] used a model of the acidogenic stage based on the work of [77] in order to show that the hydrolysis in a two stage anaerobic digester could be achieved during a retention time of 3.1 days, as reported by [78].

3.3.2 Mathematical models based on the ADM1 approach

As reported in [79], when the ADM1 was applied under co-digestion conditions all authors considered the following two premises: (1) the ADM1 model components for composites cannot be used as an inflow fraction, and substrate characterisation should be done in terms of carbohydrates, proteins and lipids [80, 81, 47, 82], and (2) the disintegration/hydrolysis step is generally considered the rate-limiting step during the anaerobic digestion process [80, 1, 29, 83, 47, 82]. The first assumption was not used for the modified version of ADM1 proposed by [1] that considers two different input substrates (i.e. sewage sludge and OFMSW), with the possibility to apply different kinetics for each one, figure 3.1. Howewer several authors, after ADM1 publication, proposed co-digestion models that do not follow the ADM1 approach [84, 85, 86]. [80] proposed a modified version of the ADM1 where energy production by codigesting cattle manure and energy crops is evaluated. [81] published an extension of the ADM1 aimed at including phenol compounds degradation in the anaerobic digestion process. Applications of the ADM1 in the co-digestion of OFMSW and sewage sludge are proposed by [1, 87].

[87], using data obtained from a full scale anaerobic digester, showed the ADM1 potential as a tool for assisting in system operation and process control. [1] modified the ADM1 in order to include the possibility to model the disintegration of two different input substrates using different kinetics for each one. In particular, the model considers first order kinetics for sewage sludge disintegration and surface-based kinetics to model the OFMSW disintegration.

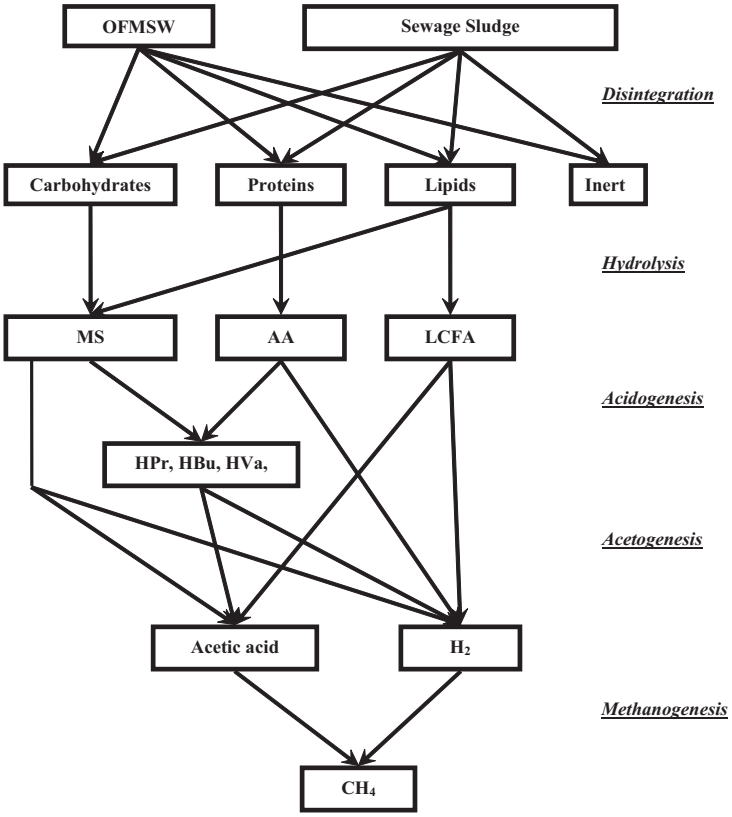

Figure 3.1: Flow chart of the modified version of the ADM1 proposed by [1]

Author	Steady state model	Dynamic model	Calibration	Validation	Substrates used in calibration validation
[80]	-	x	x	x	CM
[1]	-	x	-	-	-
[81]	-	x	x	x	OMW&OMSW
[87]	-	x	x	x	OFMSW&SW
[29]	-	x	-	x	-
[83]	-	x	x	x	sOFMSW&SW

Table 3.2: Mathematical models based on the ADM1 approach

When organic waste solids are present in the reactor influent, the disintegration process is the rate limiting step of the overall co-digestion process

and the main advantage of the proposed modelling approach is that the kinetic constant of such a process does not depend on the waste particles size distribution (PSD), but only on its nature and composition. This model has been upgraded in 2011 [29] in order to simulate the effect of LCFA production in pH prediction, also including the possibility to separate each product of the disintegration process (i.e. carbohydrates, proteins and lipids) into two fractions, i.e. a readily biodegradable fraction and a slowly biodegradable fraction. Biomethane potential test (BMP) experiments, conducted on synthetic organic waste, have been used to calibrate and validate this model [83].

3.3.3 Mathematical models not based on the ADM1 approach

[84] carried out anaerobic batch experiments combined with a mathematical model to study the anaerobic biodegradability of meat industry wastes. The authors proposed a simple mathematical model based on the assumption that the biodegradable fractions of the organic waste were divided into readily and slowly biodegradable fractions in agreement with [88] and [89]. The organic matter degradation is described using Monod kinetics without mutual interactions by a modification of the "Methane Production model" proposed by [90]. The model was calibrated with experimental data (cumulative methane production and VS degradation) from mesophilic anaerobic batch experiments in order to estimate the different biodegradable fractions (readly, slowly and inert) of the co-digested waste.

Author	Steady state model	Dynamic model	Calibration	Validation	Substrates used in calibration validation
[84]	-	x	x	x	WS; CW; RW; PCS
[91]	-	x	x	x	OFMSW; SW
[86]	x	-	x	x	SW and PS

Table 3.3: Mathematical models not based on the ADM1 approach

[91] carried out batch experiments with sewage sludge and OFMSW in large scale. The aim of such experiments was the determination of the process carbon balance and the proposal of a simple kinetic model of the anaerobic digestion. This is a two-stage acidogenesis and methanogenesis mathematical model which does not distinguish particular groups of microorganisms

and includes carbon dioxide formation both in hydrolytic and methanogenic steps. VFAs inhibition is also taken into account. [86] proposed a first-order model based on a previous work of [92]. To address the limitations of the models described by [92], the new model was developed to obtain the three different fractions in which organic matter can be classified in terms of biodegradability: readily biodegradable, slowly biodegradable and inert fraction. Several co-digestion experiments were carried out to calibrate the model. In such experiments vegetable oil, animal fats, cellulose and proteins were used to improve the anaerobic digestion of OFMSW.

Chapter 4

Mathematical model of suspended-growth anaerobic systems

4.1 Mathematical modelling of co-digestion of OFMSW and SS

During the last years much research aimed at modelling the anaerobic digestion of complex organic substrates has been carried out [79]. The mathematical modelling of the digestion process allows to reproduce several empirical behaviours on a computer in a short time. The possibility to obtain several data from model simulations can reduce the number of BMP tests needed to evaluate the biodegradability of a specific organic substrate. However the possibility to use a mathematical model to predict the results of BMP tests relies on a proper calibration of the model itself. Once the model is properly calibrated it can be used also to improve the performance of full-scale digesters.

Experiments, previously described, have been used to calibrate and validate the mathematical model proposed in this chapter.

The proposed mathematical model, described in details by equations in appendix A and B is based on the ADM1 approach, which was modified to take into account the peculiarities of a co-digestion system. The differential mass balance equations and the process kinetics and stoichiometry are modelled according to the ADM1, as well as the same biochemical conversion processes (i.e. disintegration, hydrolysis, acidogenesis, acetogenesis and methanogenesis) are taken into account. However the model is capable to consider two different influent substrates (i.e. sewage sludge and OFMSW),

which are modelled with different disintegration kinetics. In particular, a first-order kinetics is used to model the sewage sludge disintegration according to the ADM1, while a surface based kinetic expression [93, 1] is used to simulate the OFMSW disintegration process, which is a fundamental step when the substrate to be disintegrated is highly complex as the OFMSW. This expression (equation 1) takes into account the dependence of the OFMSW disintegration rate on the surface area (i.e. on the PSD) of the solid waste to be disintegrated. However the surface based kinetic expression proposed by [93] cannot be used in its original form (equation 4.1) as the model structure needs the substrates to be expressed in terms of concentrations, while equation 4.1 includes the organic particles in terms of mass:

$$\frac{dM}{dt} = -K_{sbk}A(t),\ 0 < t \leq T, \tag{4.1}$$

Therefore equation 4.1 has been reformulated in terms of concentrations (equation 4.4), by including the following two parameters, a and a^*, which characterize the disintegration process:

$$a = \frac{A}{V_{liq}} \tag{4.2}$$

$$a^* = \frac{A}{M} \tag{4.3}$$

$$\frac{dC}{dt} = -K_{sbk}a^*C(t),\ 0 < t \leq T, \tag{4.4}$$

where M is complex organic substrate mass $[M]$, K_{sbk} disintegration kinetic constant $[ML^{-2}T^{-1}]$ $A(t)$ disintegration surface area $[L^2]$, C concentration of the complex organic substrate in the digester $[ML^{-3}]$; V_{liq} liquid working volume of the anaerobic digester L^{-3}. Assuming that all organic solid particles have the same spherical shape and initial size and they are progressively and uniformly degraded in all directions from the outside towards the inside, the previous equation 4.3 can be rewritten as follows:

$$a^* = \frac{\sum_{i=1}^{n} A_i}{\sum_{i=1}^{n} M_i} = \frac{nA_i}{nM_i} = \frac{n4\pi R^2}{n\delta\frac{4}{3}\pi R^3} = \frac{3}{\delta R} \tag{4.5}$$

where A_i is the disintegration surface area of the organic solid particle i L^{-2}, M_i mass of the organic solid particle i $[M]$, n total number of organic solid particles $[dimensionless]$, δ complex organic substrate density $[ML^{-3}]$, $R(t)$ organic solid particles radius $[L]$, assumed time dependent in according with the following expression proposed by [93]:

$$R(t) = R_0 - K_{sbk}\frac{t}{\delta} \tag{4.6}$$

where R_0 initial organic solid particles radius $[L]$, specified as the initial condition for model application. 4.4 therefore results in the 4.7, which is used in the model:

$$\frac{dC}{dt} = -\left(\frac{3K_{sbk}}{\delta}\right)\frac{C}{R}, \tag{4.7}$$

Expressing C in 4.7 as the ratio between the mass of the organic solid particles and the digester volume, the following quadratic dependence of the disintegration process rate on the particles radius:

$$\frac{dC}{dt} = -K_{sbk}\frac{n4\pi R^2(t)}{V_{liq}}, \tag{4.8}$$

Because the radius of the organic solid particles varies in according with a linear law equation 4.7, equation 4.8 implies that the concentration of the complex organic substrate has to decrease in according with a cubic law, during the disintegration process. If this model is compared with the ADM1 first-order disintegration kinetics, the main advantage of this model is that K_{sbk} is the same for any OFMSW PSD and thus can be experimentally determined using OFMSW samples of any PSD. On the contrary, if a typical first-order kinetic expression is applied and organic waste samples are used to experimentally determine the kinetic constant, the latter can only be used to simulate the anaerobic digestion of OFMSWs with the same nature and PSD of the investigated organic waste samples. Numeric integration of the differential algebraic equations has been performed using a multi-step solving algorithm based on the numerical differentiation formulas in the software tool MATLAB®.

4.2 Numerical results

4.2.1 Parameter values used for the simulations

The mathematical model proposed in section 4.1 has been applied to simulate the co-digestion process and methane production in a digester of a typical MWWTP with a working volume of $12000 m^3$ and the hypothetical characteristics of the influent sewage sludge and OFMSW reported in Table 2. Values of the kinetic and stoichiometric parameters as well as Henry's constants according to the suggested parameter value for mesophilic solids [4], a kinetic disintegration constant K_{sbk} according to [93] and the hydrolysis kinetic constants reported in table 4.1 have been adopted for all simulations.

Parameter	Unit	Simulation Set1	Simulation Set2
Digester volume	m^3	12000	12000
Influent Sewage sludge flow rate	$m^3 d^{-1}$	430	430
Sewage sludge OLR	$kgCODd^{-1}m^{-3}$	1.43	1.43
Sewage sludge carbohydrates content	%	20	20
Sewage sludge proteins content	%	20	20
Sewage sludge lipids content	%	25	25
Sewage sludge inerts content	%	35	35
OFMSW OLR	$kgCODd^{-1}m^{-1}$	1.43	$0 \div 2,86$
OFMSW carbohydrates content	%	40	40
OFMSW proteins content	%	10	10
OFMSW lipids content	%	15	15
OFMSW inerts content	%	35	35
OFMSW particle initial radius	m	$2.5 \cdot 10^{-3} \div 5 \cdot 10^{-2}$	$5 \cdot 10^{-2}$
a^*	$m^2 kg^{-1}$	$9.09 \cdot 10^{-2} \div 1,82$	$9.09 \cdot 10^{-1}$
Gas pressure in the digester	Bar	1.25	1.25
Temperature	C	35	35

Table 4.1: Operational parameters used for model simulations

The LCFA dissociation constant K_{LCFA} in the acid base equilibria equations has been assumed equal to $1 \cdot 10^{3.5}$ according to [94]. Fractions of 50% readily biodegradable and 50% slowly biodegradable substrate have been assumed. Values of $2.16 d^{-1}$ and $3.84 d^{-1}$ [95] have been used for the $k_L a$ coefficients of the liquid-to-gas mass transfer of methane and hydrogen, respectively, whereas a value of $60 d^{-1}$ [96] has been applied for the carbon dioxide $k_L a$ coefficient. As the radius of the organic solid particles becomes smaller with time following a linear law [93], each simulation has been carried out assuming a^* constant and equal to the value resulting by equation (5), with the organic solid particles radius, R, equal to the arithmetic mean between its initial value, R_0, and the value calculated by means of equation (6) in correspondence of the digester SRT (Solid Retention Time). The initial values of the state variables reported in Table 4.1 have been used.

4.2.2 Effect of the OFMSW particle size on the digester performances

Figure 4.1 shows the results of model simulations (set 1, Table 4.1) performed to assess the effect of the OFMSW particle size on the digester performances in terms of COD removal efficiency and methane production. Different particle initial radius (R) of the OFMSW in the range $2.5 \cdot 10^{-3} \div 5 \cdot 10^{-2} m$ have been investigated, assuming a continuous addition of $17200 KgCOD d^{-1}$ of OFMSW into the digester for 160 days (i.e. from day 20 to day 180). An increase of the OFMSW particle size results in the increase of the COD fraction of the OFMSW added into the reactor that is not biodegraded (Figure 4.1 A) and remains in the effluent. The effluent COD due to sewage sludge is $3.35 KgCOD m^{-3}$. The latter is not included in the effluent COD reported in Figure 4.1 A, which is only related to the OFMSW.

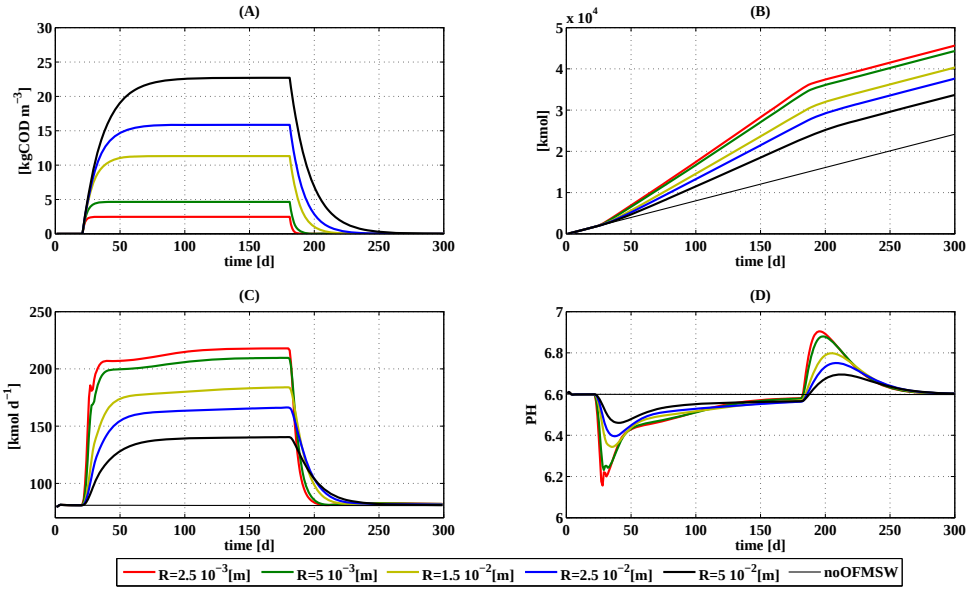

Figure 4.1: Effect of the OFMSW particle size on the effluent COD (A), methane cumulative formation (B), methane production rate (C) and pH (D)

The lower COD degradation due to a higher particle radius implies a lower methane production rate (Figure 4.1 C) and a lower cumulative methane formation (Figure 4.1 B). This points out the limiting effect of the disintegration step on the methane production, i.e. on the whole biological process. In fact, a larger particle size of the organic particles feeding the digester affects the

overall process efficiency, due to the decrease of the disintegration rate, which implies a limited (i.e. only partial) transformation in carbohydrates, proteins and lipids of these particles and, thus, a lower availability of substrates for the subsequent biological processes. As a consequence, a lower methane production is achieved. The OFMSW addition at day 20 also implies a sharp pH decrease (Figure 4.1 D) due to higher acids production by acidogenic bacteria. However these acids are degraded by acetogenic bacteria and when the biological system reaches new steady-state conditions the pH goes up to 6.6 again. A pH increase occurs when the OFMSW addition is stopped, i.e. at day 180, due to the decrease of acids production, but a pH of 6.6 is reached again around day 280.

4.2.3 Effect of the OFMSW OLR on the digester performances

Further simulations (set 2, Table 4.1) have been carried out to investigate the effect on the methane production of the OFMSW amount added into the sewage sludge digester. Continuous OFMSW additions from day 20 to day 180 have been simulated.

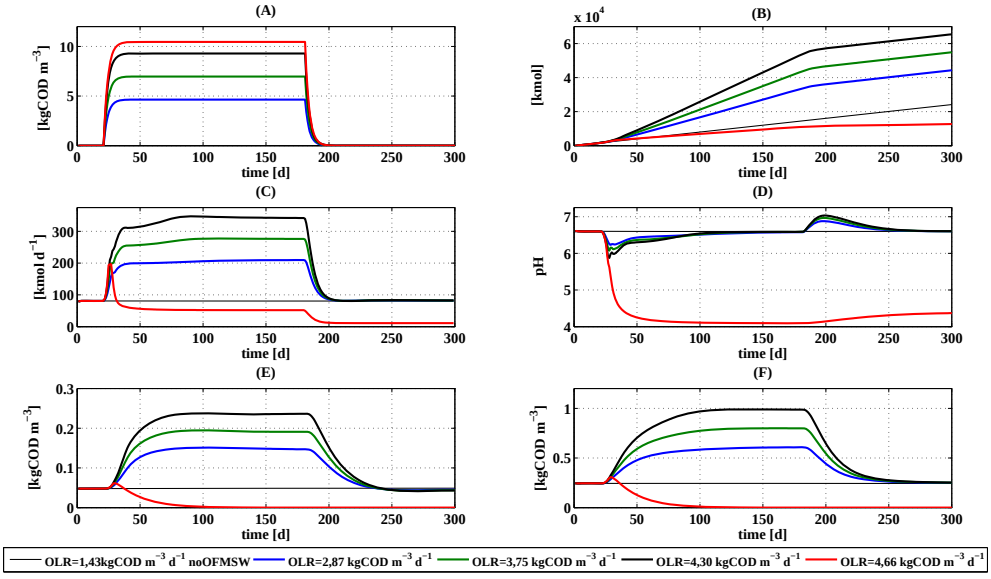

Figure 4.2: Effect of the OFMSW addition on the effluent COD (A), methane cumulative formation (B), methane production rate (C), pH (D), hydrogenotrophic methanogenic archea (E) and acetoclastic methanogenic archea (F)

The results show that increasing the OFMSW input from 0 to 34400 $KgCODd^{-1}$ (i.e. increasing the total organic loading rate, OLR, due to both sewage sludge and OFMSW from $1.43 KgCODm^{-3}d^{-1}$ to $3.29 KgCODm^{-3}d^{-1}$ results in an important increase of the OFMSW that is not biodegraded in the digester and thus remains in the effluent (Figure 4.2 A). Figures 4.2 B and C show the increase of the cumulative methane formation and methane production rate, respectively, which derive from the above cited increase of the OFMSW input from 0 to $34400 KgCODd^{-1}$. The pH decrease (Figure 4.2 D) due to the OFMSW addition at day 20 is higher when a higher OFMSW amount is added into the reactor. However for all OLRs investigated in the range $1.43 \div 3.29 KgCODm^{-3}d^{-1}$ the biological system slowly reaches new

steady-state conditions and the pH goes up to 6.6 again. Whereas when an overall OLR of $3.43 KgCODm^{-3}d^{-1}$ is considered, the pH drop is irreversible and results in the digester failure (Figure 4.2 D). The pH drop affects the microbial activity, resulting in a sharp decrease of the bacterial concentration in the digester. For instance, the acetoclastic and hydrogenotrophic methanogenic archea are completely washed out from the digester around day 100 (Figure 4.2 E) and day 105 (Figure 4.2 F), confirming the digester failure. Figure Figure 4.1 E also shows an increase of the concentration of acetoclastic methanogenic archea from 0.24 to $0.99 KgCODm^{-3}$, which results from the increase of the OLR from 1.43 to $3.29 KgCODm^{-3}d^{-1}$. The percentage increase of this concentration (412.5 %) of methanogenic archea is higher than the percentage increase of the OLR (300 %), confirming the potential of OFMSW addition into the digester to maximize the methane production.

4.2.4 Definition of optimal OFMSW particle size and OLR conditions

Figure 4.3 shows the results of a sensitivity analysis on the 2 operational parameters taken into account in this study, i.e. OFMSW particle size and OLR, aimed at assessing their combined effect on the digester performances and the occurrence of the digestion process failure. The model simulations have been carried out with the same digester volume and the same characteristics of the influent sewage sludge as reported in Table 2, but ranging the particle radius and the OLR between $5.0 \cdot 10^{-4}$ and $2.5 \cdot 10^{-2} m$ and 1.43 and $9.14 KgCOD m^{-3} d^{-1}$, respectively. Figure 4.3 shows that the higher is the particle size of the OFMSW, the higher is the OLR that induces the digester failure. This is due to the slower disintegration and thus slower acidification occurring for higher OFMSW particle sizes. However such larger particles imply the slow down of all the digestion processes, resulting in the decrease of the overall digestion efficiencies in terms of COD removal, as showed by the isoefficiency curves in Figure 4.3.

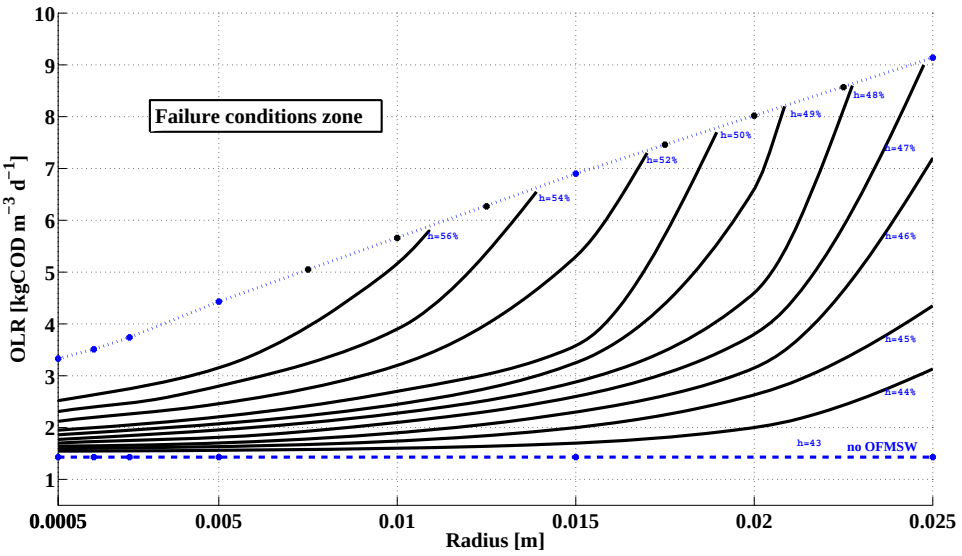

Figure 4.3: Combined effect of the OFMSW particle size and OLR on the digestion performances in terms of COD removal efficiency (η)

4.3 Proposed calibration and validation procedure

The mathematical model can be used to estimate several apparent kinetic rate constants. In this thesys model calibration was used to estimate K_{sbk}, $[ML^{-2}T^{-1}]$, i.e. the apparent kinetic rate constant of the surface-based disintegration process and $K_{dis}[T^{-1}]$, i.e. the first-order apparent kinetic rate constant of the disintegration process. Calibration was performed by comparing model results with experimental measurements of methane production and adjusting the unknown parameter until the model results adequately fit the experimental observations. Input, operational and output data from experiment A, B and C. (Table 2) were used, and a specific procedure was developed. In this text the calibration procedure is referred to K_{sbk}, even if it can be applied for any apparent kinetic rate constant. The calibration procedure is structured in four steps as follows.

1. Step 1 determines a variation range for K_{sbk}

2. Step 2 generates as many different values of K_{sbk} as the estimation accuracy requires. This calculation was performed taking n+1 constant step values of K_{sbk}, between the two bounds of the variation range, according to the following expression:

$$K_{sbk}^{j} = K_{sbk}^{j-1} + \Delta_{K_{sbk}},\ j = 1, ..., n, \tag{4.9}$$

   where $K_{sbk}^{0} = 0$ and $K_{sbk}^{n} = 1$ are the lower and upper bounds of the variation range, respectively, and $\Delta_{K_{sbk}}$ is the ratio between the width of the range and n. To set the accuracy of the results at two significant digits, n was fixed to be equal to 100

3. Step 3 Step 3 was performed by plotting a simulated curve for each value of K_{sbk} from the development of step 2 and by comparing simulated results with observed data. A comparison was performed by applying three methods that are commonly used for the model calibration process ([97]), the Modeling Efficiency (ME) method, the Index of Agreement (IoA) method and the Root Mean Square Error (RMSE) method, calculating the three following parameters:

$$ME = 1 - \frac{\sum_{i=1}^{k}(y_i - y_i^i)^2}{\sum_{i=1}^{k}(y_i - y_M^i)^2} \tag{4.10}$$

$$IoA = \frac{\sum_{i=1}^{k}(y_i - y_i^i)^2}{\sum_{i=1}^{k}(|y_i - y_M| - |y_i - y_M|)^2} \tag{4.11}$$

$$RMSE = \sqrt{\frac{\sum_{i=1}^{k}(y_i - y_i^i)^2}{K}} \tag{4.12}$$

4. Step 4 Step 4 determines the value of K_{sbk} that best fits the observed data using the three different criteria. Step 4 is performed by plotting three series of points using Cartesian coordinates with K_{sbk} as the first coordinate and the corresponding values of ME, IoA and RMSE, calculated in step 3, as the second coordinate. The last operation of the calibration process is the determination of K_{sbk} that either maximizes ME as well as IoA or minimizes RMSE for each series of plotted data.

4.4 Calibration and validation of OFMS-Sewage sludge co-digestion

The cumulative methane production data that were obtained from the experimental tests are reported in Figure 4.4. This figure shows that the gaps among the three curves resulting from tests A_1, B_1 and C_1, respectively, are noticeable for the initial 20 days and then progressively tend to vanish. Within this initial period, the three curves are plainly distinguishable as clearly indicated by the error bars of the experimental points (Figure 4.4). In particular, the differences are higher when the 2.5 mm curve is compared with the 0.5 or 1.5 mm curves. The differences among the three experimental curves are noticeable only during the initial 20 days, as the disintegration process of the solid particles occurs during this initial period. Once the solid particles have disintegrated, the anaerobic reactors continue to produce methane as long as all the organic matter is biodegraded, and the end points of the three curves coincide as each reactor was filled with the same amount of organic matter. The initial gap among the three curves is due to the effect of the solid particle size on the methane production, which cannot be properly modeled with the same first-order kinetic constant for the three experiments.

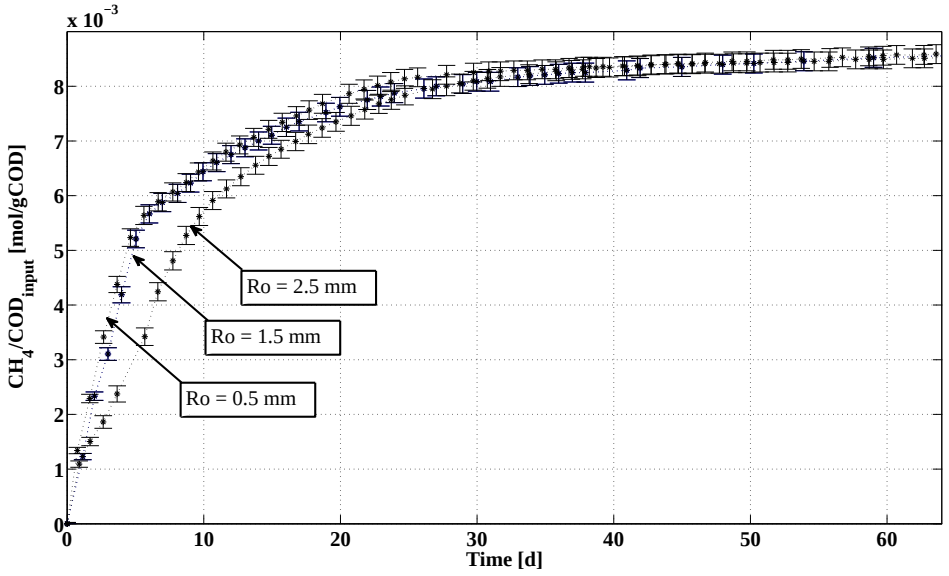

Figure 4.4: Cumulative methane production obtained in the experimental tests A_1, B_1 and C_1.

According to ADM1, a kinetic constant is required for each particle size.

The main difference of the proposed model as compared with the ADM1 is that the disintegration rate constant K_{sbk} is invariant with the substrate particle size.

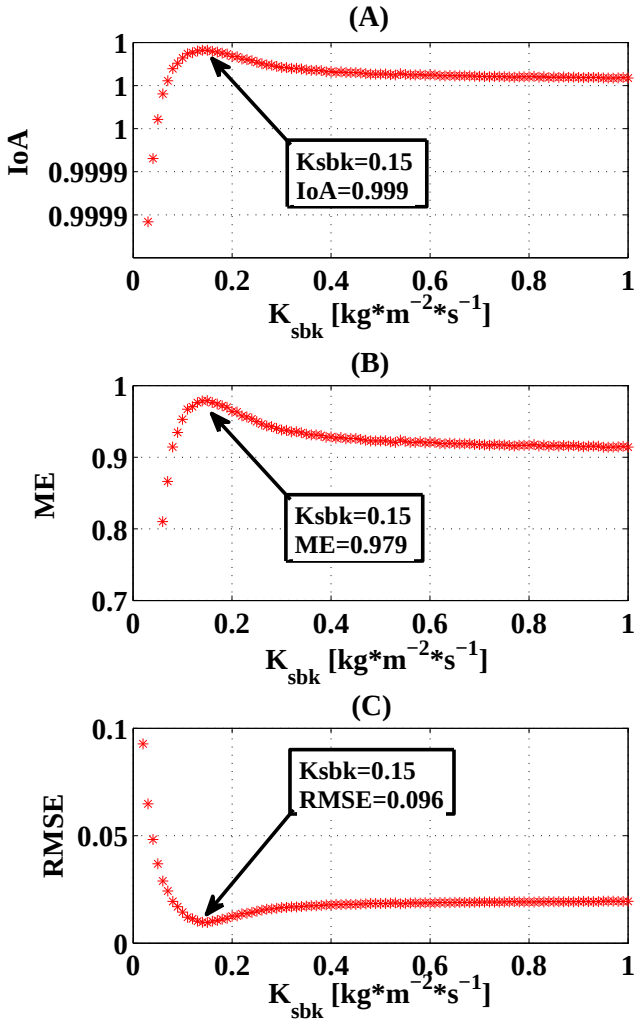

Figure 4.5: Dependence of ME on K_{sbk}.

The model calibration performed in this Thesis resulted in setting the kinetic constant K_{sbk} to $0.15 kgm^2s^{-1}$ when using values of the other kinetic and stoichiometric parameters as suggested by [4] for mesophilic solids.

This value of the kinetic constant K_{sbk} maximizes both ME and IoA and minimizes RMSE (Figures 4.5), making the gap between data simulated by model and experimental data used for the calibration process as small as possible. This K_{sbk} value fully meets the model calibration process requirements.

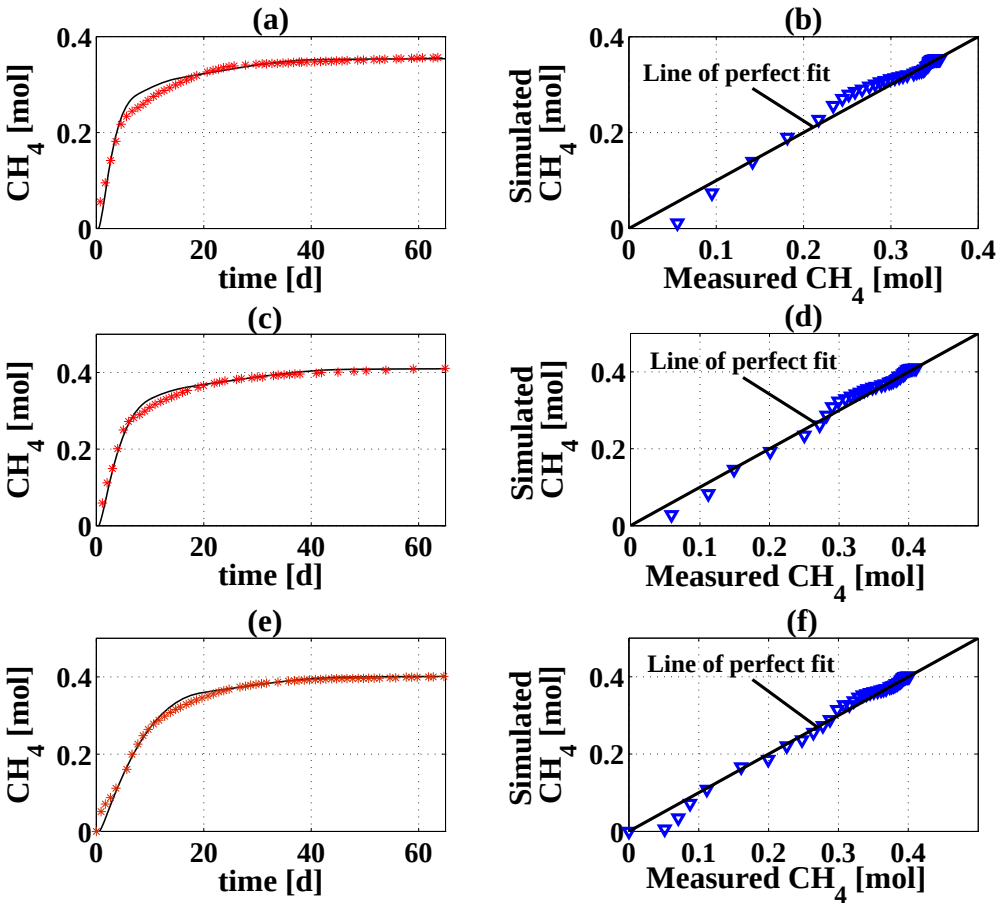

Figure 4.6: Comparison of measured and simulated by proposed model cumulative methane production for experiments A,B and C: overlapping between measured and simulated data (a,c and e); comparison with the line of perfect fit (b,d and e).

All curves represented in Figures 4.5 show a normal trend, characterized by a single monotone reversal located right in $K_{sbk} = 0.15 kgm^2 s^{-1}$. This reversal proves the existence of one and only one solution to the specific optimization problem that was used to calibrate the model. A further interesting aspect that emerges by analyzing the previous three graphs concerns the sensitivity of ME, IoA and RMSE to K_{sbk}: the closer K_{sbk} is to $1 kgm^{-2} s^{-1}$, the smaller the variations of ME, IoA and RMSE are in response to variations in K_{sbk}. This last observation validates the hypothesis that the procedure used to calibrate the model is based on, to assume $1 kgm^{-2} s^{-1}$ as the upper bound of the K_{sbk} variation range. The loss of sensitivity shown by the model toward

values of K_{sbk} of $1kgm^{-2}s^{-1}$ can be explained. K_{sbk} is a kinetic parameter used to describe the rate of a single process (i.e., disintegration) among the several processes involved in the anaerobic co-digestion of organic matter. The value of K_{sbk} can therefore affect the output of the model as long as it is small compared with the values of the other kinetic constants that are considered in the model (i.e., as long as disintegration is a limiting process). However, when the values of the different kinetic constants change, some processes that were not limiting become limiting and vice versa.

TEST	R_0	K_{sbk}	**ME**	**ME**	**RMSE**
	$[mm]$	$0.15kgm^{-2}s^{-1}$			
B	1.5	4.4	0.979	0.979	0.011
C	2.5	4.2	0.988	0.988	0.010

Table 4.2: Result of the model validation process.

Figure 4.6 shows the highest agreement between simulated and observed data for cumulative methane production achieved by the specific procedure that was used to calibrate the model. In Figure 4.6a, the good overlap between the two series of data is shown, with a very small shift between the points with simulated and observed data as coordinates and the line of perfect fit reported in Figure 4.6b. After calibrating the model using the cumulative methane production results from experiment A, the calibrated K_{sbk} value (i.e., $0.15kgm^{-2}s^{-1}$) was used to validate the model. Experiments B and C were used to validate the mathematical model, assessing

TEST	R_0 $[mm]$	K_{dis} s^{-1}	**ME**	**ME**	**RMSE**
B	1.5	0.406	0.985	0.999	0.010
C	2.5	0.406	0.909	0.996	0.031

Table 4.3: Result of the ADM1 validation process.

the agreement between simulated and observed data for cumulative methane production with the parameters ME, IoA and RMSE. The results of the validation process are graphically described in Figures 4.6b,c,d and e are numerically reported in Table 4.2. The graphs indicate a very good agreement between the simulated and observed data; the agreement is confirmed by the values of the fitting parameters reported in Table 4.2. Only a few experimental points close to the origin of the axes are not fitted by the simulation

results (Figure 4.6a), showing a slight shifting from the line of perfect fit in Figure 4.6b because of the readily biodegradable organic substrate present in the inoculum, which was not considered for the simulations.

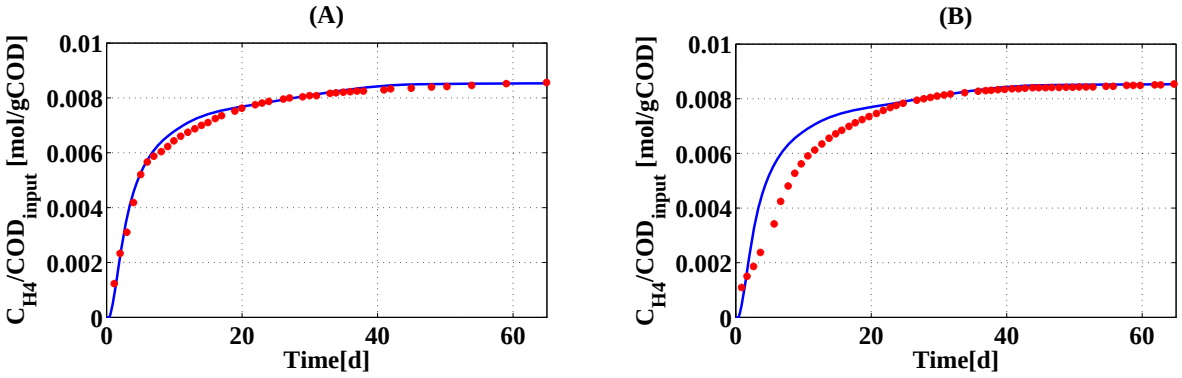

Figure 4.7: Comparison of measured and simulated by ADM1 cumulative methane production for experiment B.

The value assigned to K_{sbk}, as well as the modeling approach proposed in this work, is fully validated by experiments B and C. The same experimental data and the same calibration procedure applied to the proposed model were also used to calibrate and validate the ADM1 (Table 4.2 and Figures. 4.6c,d,e and f to assess the contribution of the proposed model as a potential upgrade for the ADM1. The calibration of the ADM1 resulted in a disintegration constant $K_{dis}0.406s^{-1}$, capable of maximizing both ME and IoA and minimizing RMSE (Figure 4.5A,B and C).The validation process still resulted in acceptable values of ME, IoA and RMSE, but the values were not as good as the values obtained using the proposed model. Figure 4.7 in particular shows an evident gap between the simulated and experimental data for the initial 25 days, i.e., when the particle size effect on the digestion process is more important. This gap confirms that the disintegration constant determined for a specific particle size cannot be properly used in ADM1 for a different particle size.

4.5 Calibration and validation of OFMS-Buffalo manure co-digestion

The results obtained from the BMP tests were used to calibrate and validate a mathematical model proposed in 4.1. For this aim, the procedure detailed in 4.3 has been applied, taking into account the Modelling Efficiency (ME)

method, the Index of Agreement (IoA) method and the Root Mean Square Error (RMSE) method [97].

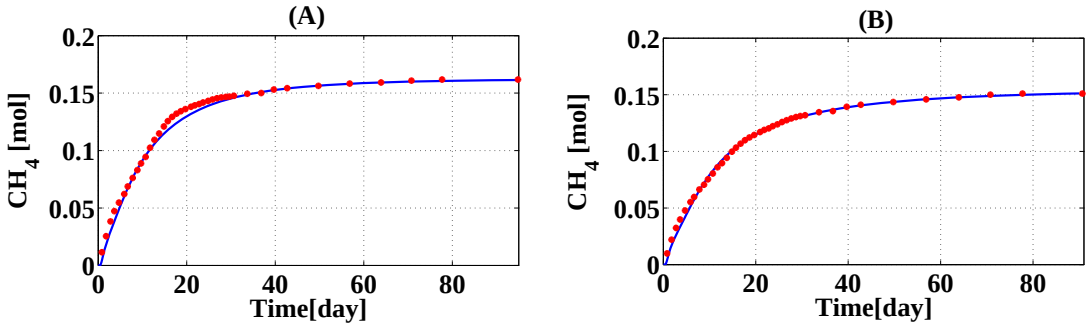

Figure 4.8: Comparison between the experimental (points) and simulated (line) bio-methane production from BMP tests T5 (a), T6 (b)

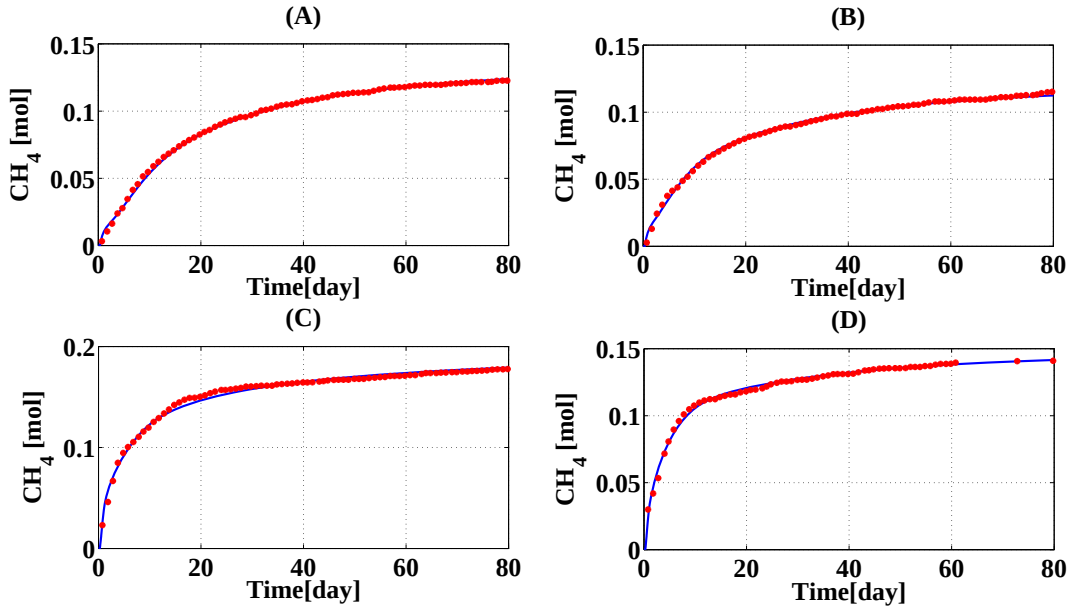

Figure 4.9: Comparison between experimental (points) and simulated (lines) bio-methane production from BMP tests T1 (a), T2 (b), T3 (c) and T4 (d)

The F_{ch}, F_{pr} and F_{li} parameters are shown in Table 1, whereas all other model parameters considered in the simulations are in agreement with [4, 98]. The calibration process was performed using the results of the BMP tests T1-T4, obtaining the kinetic constant of the disintegration process for each considered pure substrate (Table 3). Figure 4 shows a good fitting

between experimental and modeled data for all the curves related to each substrate. The constants related to BMP tests T1 and T3 were subsequently used to validate the model using the results obtained from BMP tests T5 and T6. (Table 4). The fitting between simulated and experimental curves of cumulative methane production is still remarkable (Figure 5). Therefore, once the disintegration kinetic constants of different substrates have been evaluated through the calibration process, the mathematical model can be used to predict the bio-methane produced from a co-digestion process fed with two substrates of any percentage, among all those considered during the calibration process.

4.6 Dynamic mathematical modelling of sulfate reducing gas-lift reactors

4.6.1 Introduction

Sulfate reduction in gas lift reactors, using hydrogen (H_2) and carbon dioxide (CO_2) as, respectively, electron donor and carbon source, represents a valuable solution for the treatment of specific wastewaters ([99, 100, 3]). Inorganic sulfate-rich wastewater such as acid rock drainage or flue gas scrubbing waters contain little or no organic compounds, thus biological sulfate reduction can only take place when electron donor and carbon source are added externally. A major problem of these hydrogen fed sulfate-reducing reactors is the formation of methane from hydrogen and carbon dioxide. Methane formation from hydrogen is undesired because it lowers the hydrogen utilization efficiency for sulfate reduction. Thermodynamic and Monod-kinetic data of heterotrophic sulfate reducing bacteria (HSRB), autotrophic sulfate reducing bacteria (ASRB), homoacetogenic bacteria (HB), methanogenic archaea (MA) and acetate degraders (AD) indicate that HSRB and ASRB can develop in these gas-lift reactors. ASRB out-compete MA and HB for hydrogen, HSRB are able to compete successfully with AD or/and MA for hydrogen and acetate. As far as HSRB are concerned, the above hypothesis has been confirmed experimentally for hydrogen ([101, 102, 103, 104]). With regard to the utilization of acetate in anaerobic reactors, literature data are ambiguous. Several researches show that during sulfate reduction HSRB can compete successfully with AD for acetate ([105, 106, 102, 107, 108, 109]) whereas others indicate that the latter is preferentially degraded to methane ([110, 111]). To explain the differences found, besides kinetic considerations, other factors influencing the competition process between HSRB and AD should be taken into account as well. These factors include the COD/SO_4^{2-}

ratio, Hydraulic Retention Time (HRT), and gas input flow ([3]). Other studies show that in a gas-lift reactor, ASRB are able to out-compete HB for hydrogen utilization ([100, 112, 113]). Such factors affect the outcome of the competition between ASRB and MA as well ([2]). In order to simulate the bacterial competition in these gas-lift reactors, a sulfate reduction dynamic mathematical model would be a valuable aid for design, operation and control. In this section the development of a mathematical model able to simulate under dynamic conditions the physical, chemical and biological processes prevailing in a biological sulfate reducing gas-lift reactor is presented. Calibration and validation of the proposed model are carried out using an experimental study ([3]) about the interaction between sulfate reduction and methanogenesis in a gas-lift anaerobic reactor. In the thesis, the model is applied for the following purposes: a) verification of a steady-state design model proposed by [2, 114]) assessment of the effect of the Hydraulic Retention Time (HRT) on the performances of a full-scale gas-lift reactor.

4.6.2 Mathematical model

Biochemical reactions

The proposed mathematical model, described in details by the equations in Table 1C and 2C (See Appendix), is based on mass balance equations for substrates, products, and bacterial groups and includes the bio-chemical reactions of the sulfate reduction process (Figure 4.10). The model considers the kinetics of microbial growth and decay.

In particular, the model takes five groups of bacteria, i.e. HSRB, ASRB, HB, MA, and AD; and six components (substrates and products), i.e. Hydrogen (H_2), Sulfate (SO_4^{2-}) (abbreviated as SO_4), Carbonic dioxide (CO_2), Acetate (Ac.), Sulphide (H_2S) and Inert, into account. Inert is substrate, which is not degraded within the typical HRTs of sulfate reducing gas-lift reactors. All substrates considered in the model are expressed as COD, except S_{so_4}. Thus, the coefficient 1.5 in the first column of Table 1C (See appendix) represents $1.5gS_{SO_4^{2-}}/gCOD$. The following assumptions were made to develop this model:

1. The biological reactor is a completely stirred tank reactor (CSTR).
2. HSRB, ASRB, HB, MA and AD can grow in the reactor.
3. The growth of each bacterial group proceeds according to Monod kinetics.
4. Bacterial decay is described by first order kinetics.

5. Chemical oxygen demand (COD) production from biomass decay is not degradable within the typical HRTs of sulfate reducing gas-lift reactors an thus is considered as inert in the model.

The sulphide toxicity was not taken into account due to a lack of quantitative data in the literature, which are often contradictory. The pH effect was neglected as gas-lift reactors are generally well buffered or controlled at a desired pH.

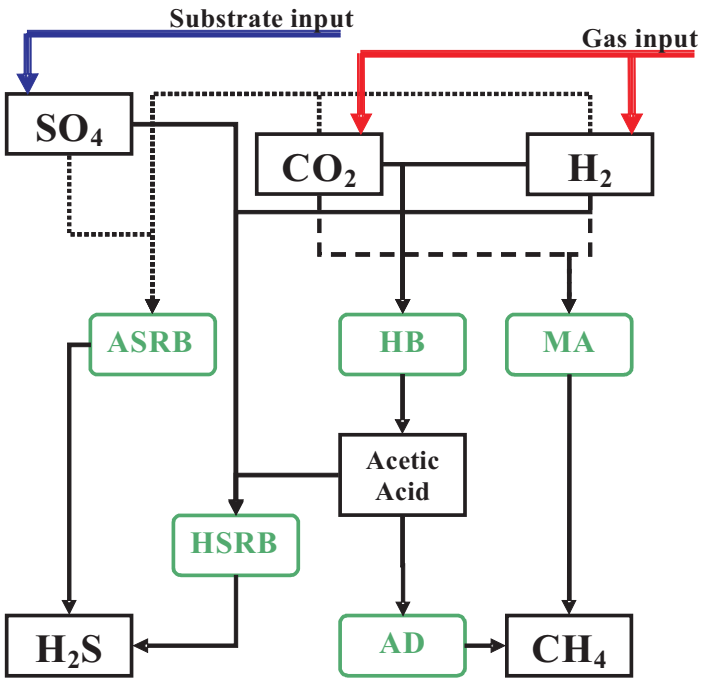

Figure 4.10: Schematic representation of the bioconversion pathways in the model

Gas transfer modelling

According to Henry's law, under steady state conditions the concentration of a gas in aqueous phase is in equilibrium with its partial pressure in the gaseous phase. Therefore an accurate evaluation of the gas-lift reactor system requires modelling of liquid-gas transfer processes involving all the gaseous products of the biological processes, i.e. H_2O, CO_2, CH_4, H_2 and H_2S. The mass balance equations have been considered for both liquid and gas phases, as follows:

$$\frac{d[S]_l}{dt} = \frac{q}{V_{liq}}([S]_{l,in} - [S]_l) - K_{la}([S]_l - [S^*]_l) + \sum_{i=1}^{N} \rho_i \nu_i, \tag{4.13}$$

$$\frac{d[S]_g}{dt} = \frac{V_{gas}}{V_{liq}} K_{la}([S]_l - [S^*]_l) - \frac{Q_{out,g}}{V_{gas}}[S]_g, \tag{4.14}$$

The total gas pressure P in the digester headspace is calculated as the sum of the partial pressures of saturated water (H_2O), carbon dioxide (CO_2), methane (CH_4), hydrogen (H_2) and sulphide (H_2S). The molar concentration of each gaseous component at thermodynamic equilibrium $[S^*]$ is given by Henry's law:

$$[S^*] = H_{gas} p_{gas} \tag{4.15}$$

where:

- H_{gas} = Henry's constant for the specific gas $[M^{-1}T^2L^{-2}]$
- p_{gas} = partial pressure of the specific gas, calculated according to the Dalton's law $[MT^{-2}L^{-1}]$.

Numeric integration

Numeric integration of the differential algebraic equations is performed using the solving algorithm ODE15S, a multi-step, variable-order solver based on the numerical differentiation formulas in the software tool MATLAB®.

4.6.3 Model calibration

Model calibration was aimed at estimating $Y_{HSRB,H_2}[ML^{-2}T^{-1}]$, i.e. the yield of HSRB on Hydrogen, which is a very sensitive model parameter. The calibration process was performed by comparing model results with experimental data and adjusting the unknown parameter as long as the model results adequately fitted the experimental observations. For this purpose input, operational and output data resulting from the experiments carried out by [2] were used (Figure 4.11), applying a specific procedure.

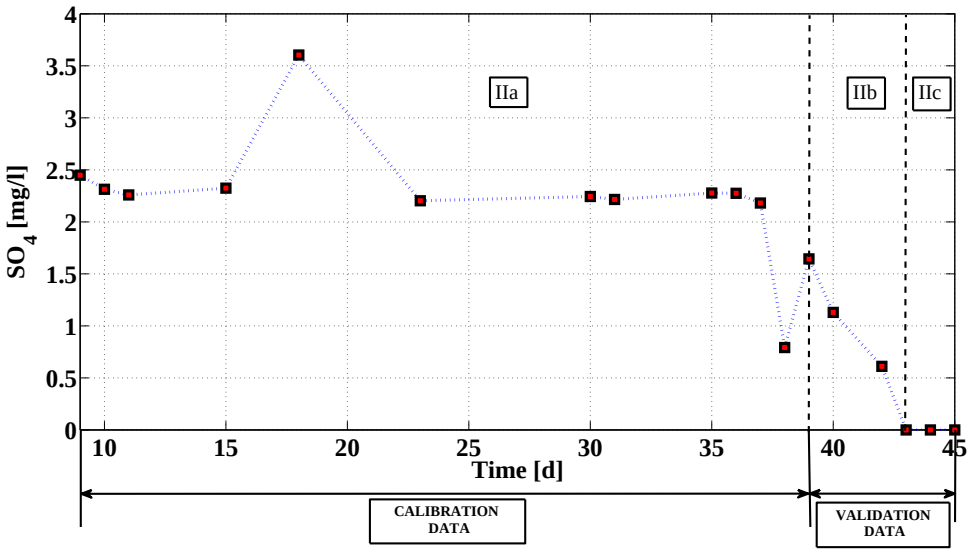

Figure 4.11: Experimental data used for model calibration and validation (from: [2])

The calibration procedure is structured in 5 steps as follows: i) experimental data definition; ii) determination of the variation range for Y_{HSRB,H_2}; iii) generation of as many different values of Y_{HSRB,H_2} as the estimation accuracy requires; iv) determination of simulated values of the sulfate concentration in the gas-lift reactor for all considered values of Y_{HSRB,H_2} and comparison between simulated and observed data and v) determination of the value of Y_{HSRB,H_2} that best fits the experimental data using three different criteria. The step ii) to iv) are the same presented in the section 4.3. Step 1 was performed to define the experimental data to be used in the subsequent steps. In this step, data differing more than the sample standard deviation from the mean value were removed(Figure4.12). The sample standard deviation is defined as follows:

$$\sigma = \sqrt{\frac{\sum_{i=1}^{N}(x_i - \overline{x})}{K-1}} \tag{4.16}$$

Where:

- x_i = is the observed value;
- $\overline{x}$ = is the observed value;
- K = number of observed values;

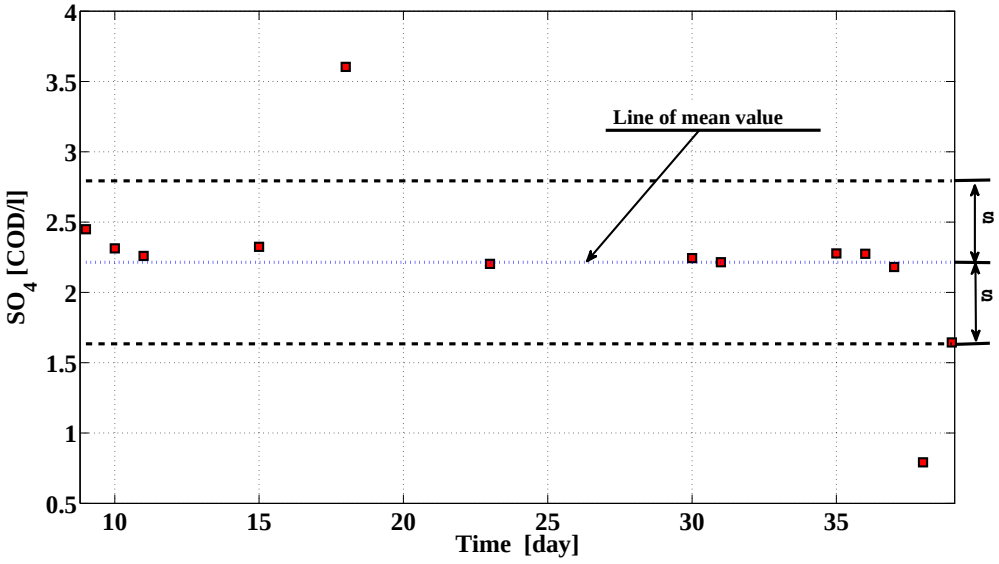

Figure 4.12: Mean value and sample standard deviation (σ) of the sulfate concentration in the experimental data

Model calibration resulted in setting the kinetic constant Y_{HSRB,H_2} to 0.96. This value maximises both ME and IoA and minimises RMSE, making the gap between model simulated and experimental data used for the calibration process as small as possible (4.13). Therefore, this Y_{HSRB,H_2} value fully meets the model calibration process requirements. All curves represented in Figure 4.13 show a regular trend, characterised by a single monotonicity reversal located at $Y_{HSRB,H_2} = 0.96$.

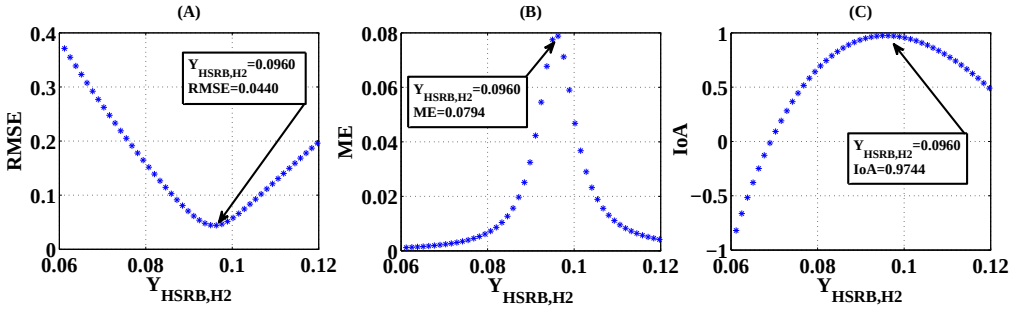

Figure 4.13: Dependence of ME (A), RMSE (B) and IoA (C) on Y_{HSRB,H_2}

4.6.4 Model Validation

After calibrating the model using the experimental data of period IIa (Figure 4.11), the calibrated Y_{HSRB,H_2} value (i.e. 0.960) was used for model validation. Experimental data of period IIb and period IIc (Figure 4.11) were used to validate the mathematical model evaluating the fitting between simulated and observed sulfate consumption data. The results of the validation process are graphically described in Figure 5 and numerically reported in Table 4.4. Figure 4.14 indicates a good fit between simulated and observed data, which is confirmed by the values of the fitting parameters reported in Table 4.4.

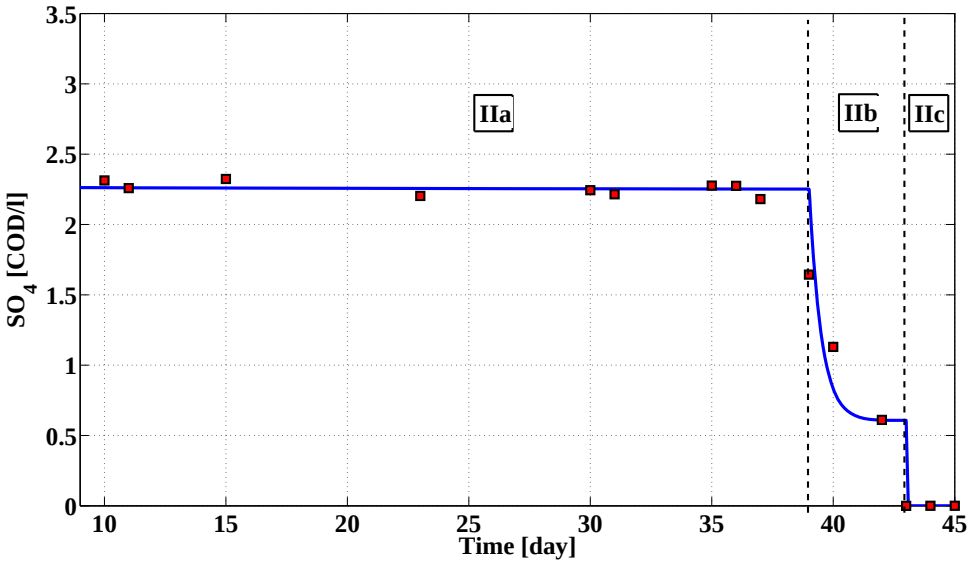

Figure 4.14: Comparison of measured and simulated concentrations of sulfate in the experimental gas lift reactor effluent. Data markers represent measured sulfate concentrations ([2])

PERIOD	K_{dis}	ME	ME	RMSE
IIa (Calibration)	0.960	0.0790	0.0440	0.9093
IIb (Calibration)	0.960	0.1401	0.3911	0.9603
IIc (Validation)	0.960	1	0	1

Table 4.4: Results of model calibration and validation.

Figures 4.15 and 4.16 show the comparison between measured and simulated concentrations of methane and sulfide, respectively, in the experimental

gas-lift reactor liquid and gas effluent.

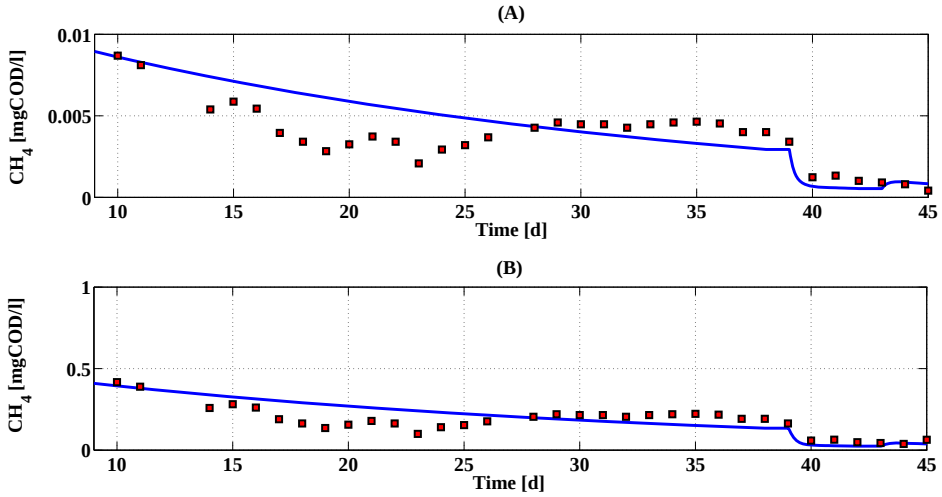

Figure 4.15: Comparison of measured and simulated concentrations of CH4 in the experimental gas lift reactor liquid (A) and gas (B) effluent. Data markers represent measured CH4 concentrations ([3])

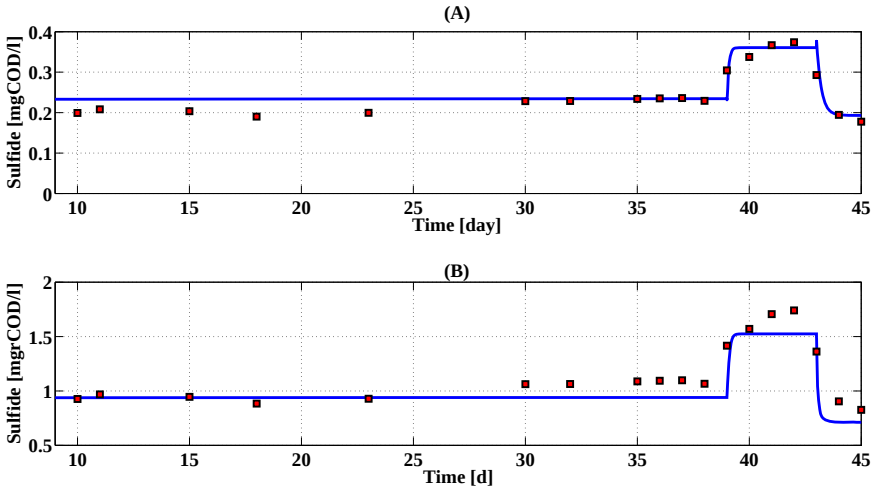

Figure 4.16: Comparison of measured and simulated concentrations of sulfide in the experimental gas lift reactor liquid (A) and gas (B) effluent. Data markers represent measured sulfide concentrations ([3])

Both Figures indicate that the simulated concentrations fit properly the

experimental data. In particular the good fitting between simulated and experimental concentrations in periods IIb and IIc shows the capability of the model to simulate the reactor performance when variations of the operational conditions occur.

4.6.5 Validation of the design model proposed by Esposito et al. (2009)

A proper design model of a biological reactor is a model capable to give the reactor volume when the desired treatment efficiency and the operational conditions are fixed ([3, 114]). A proper performance-prediction model gives the treatment efficiency when the bioreactor volume and the operational conditions are known ([3, 114]). A design model is typically a simplified model based on simplifying assumptions aimed at making the model easier to be applied ([115]). For instance steady-state instead of dynamic conditions are assumed, several microbial groups are neglected if they are not prevalent in the reactor, and bioconversion processes are neglected when they are not limiting for the overall biological process. All such assumptions need to be proven in order to demonstrate the model validity. This can be done experimentally using laboratory-scale bioreactors assessing the capability of the model to predict the treatment efficiency of a bioreactor with a known working volume. An alternative time and cost effective option to validate a design model is the use of a performance-prediction model, which is not affected by the simplifying assumptions of the design model. A performance-prediction model is typically a dynamic model which takes into account all bacterial groups growing in the reactor and all the bioconversion processes either if they are limiting or not ([116]). When the bioreactor volume is known and the operational conditions are set the results of the performance-prediction model simulations will predict which bacteria will prevail and which bacteria will be out-competed ([116]). Therefore, if a reactor volume is determined applying a design model which neglects some microbial groups, the validity of this assumption can be assessed applying a performance-prediction model which includes all bacteria capable to grow in the reactor. Applying the performance-prediction model with the reactor volume determined by the design model and the same operational conditions as set in the design model, if the performance-prediction model predicts the out-competition of the bacterial groups neglected in the design model, the assumptions of the design model can be considered correct. On the contrary, if the performance-prediction model predicts the growth of the bacterial groups neglected by the design model, it can be concluded that the design model is not reliable and thus its results are not reliable. This means that a design model, even if based on simplifying assumption, can give correct results if the assumptions are reliable. The above described approach is used in this section to validate the steady state mathematical model proposed by [3] for the design of sulfate reducing H_2/CO_2 fed gas-lift reactors. The model, named "model 1B" [3], described by the matrix in Appendix takes into account the bioconversion

pathways reported in Figure 4.17. The model takes three groups of bacteria, i.e. HSRB, HB, and MA, and five components (substrates and products), i.e. H_2, SO_4, CO_2, Ac and H_2S, into account. MA compete with HSRB and HB for H_2, but the model does not include competition between AD and HSRB for acetate. This assumption is based on the absence of AD in H_2/CO_2 fed gas-lift reactors ([100, 117, 3]). AD could be significant when acetate is externally added to the system, which is however not common in full scale applications of this reactor type.

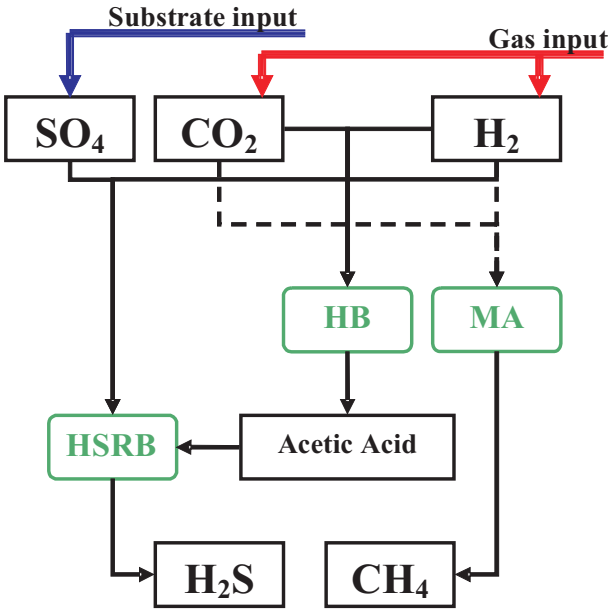

Figure 4.17: Schematic representation of bioconversion pathways in model 1B ([3]).

In order to validate the hypothesis of model 1B ([3]), i.e. to show that AD are outcompeted in H_2/CO_2 fed gas-lift reactors, the dynamic performance-prediction model proposed in this section has been applied to predict the bacterial concentrations in the reactor when it is operated with the same operational conditions, influent characteristics and input gas flow as considered for the simulations carried out with model 1B (Table 4.5). In particular, two sets of simulations were performed, with different working and headspace reactor volumes and different H_2 input concentrations (Table 4.5).

Parameter	Unit	Simulation set 1	Simulation set 2
Digester volume	m^3	53.89	241.09
Headspace reactor volume	m^3	19.90	80.40
Influent sulfate concentration	gl^{-1}	0.681	0.681
HRT	d	0.27	1.205
Liquid flow rate	m^3d^{-1}	200	200
Gas flow rate	m^3d^{-1}	400	400
Input H_2 concentration	$gCODl^{-1}$	10	2
R	–	0.46276	0.41612
σ	–	3.1	3.1
Temperature	C	35	35

Table 4.5: Operational parameters used for model simulations

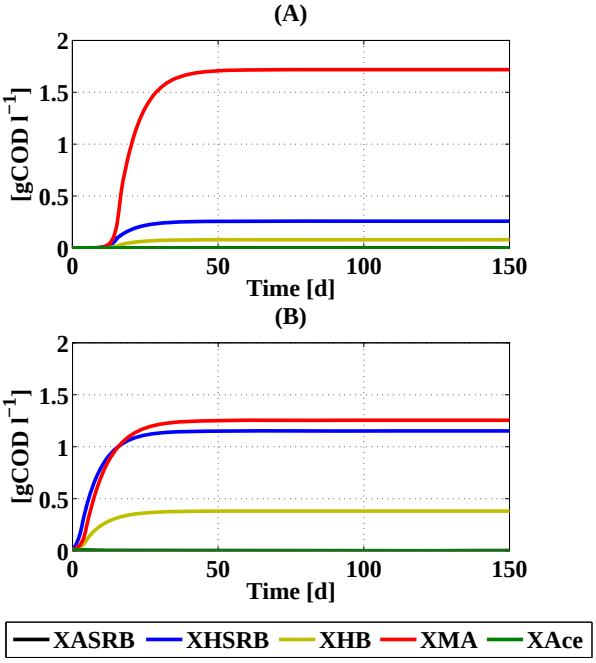

Figure 4.18: Competition between ASRB, HSRB, HB, MA and AD in the reactor when applying the proposed model with set 1 (A) and set 2 (B) operational parameters

Figure 4.18 shows the concentrations of the bacterial species prevailing in the reactor, which agree with the results of the design model of [3] for operational conditions of both Set 1 and Set 2 (Table 4.6). In particular,

Figure 4.18 shows that AD are completely out-competed by HSRB, MA and HB, confirming the above-cited assumption of model 1B.

Bacterial species	**Unit**	Model 1B		Model proposed	
		set A	**set B**	**set A**	**set B**
X_{HSRB}	$gCODl^{-1}$	0.256	1.150	0.256	1.150
X_{MA}	$gCODl^{-1}$	2.300	1.260	1.720	1.250
X_{HB}	$gCODl^{-1}$	0.041	0.180	0.079	0.381
X_{ASRB}	$gCODl^{-1}$	nc	nc	0	0
X_{AD}	$gCODl^{-1}$	nc	nc	0	0

Table 4.6: Operational parameters used for model simulations (nc = not considered)

4.6.6 Effect of the HRT on the gas-lift reactor performances

Parameter values used for the simulations

The mathematical model proposed before has been applied to simulate the sulfate reduction process in a gas lift reactor with a working volume of $200m^3$ and a headspace reactor volume of $65m^3$. The reactor engineering parameters, the hypothetical characteristics of the influent sulfate-rich wastewater and the input gas flow are reported in Table 4.7. Values of the kinetic and stoichiometric parameters according to [3] were used except for $Y_{HSRB,H_2} = 0.960$, which resulted from the calibration and validation procedure. A Henry's constant according to [118] was adopted. Figures 4.19,4.20,4.21 show the results of model simulations performed to asses the HRT effect on the reactor performances in terms of: i) species and concentrations of bacteria growing in the gas lift reactor for a 500 days time simulation; ii) concentration of components in aqueous phase for a 500 days time simulation and iii) concentration of components in gaseous phase for a 500 days time simulation. Differences in HRT, varying in the range of $0.02 - 0.5$ days were investigated.

Parameter	Unit	set A	set B	set C	set D
Digester volume	m^3	200	200	200	200
Headspace reactor volume	m^3	65	65	65	65
Influent sulfate concentration	gl^{-1}	2	2	2	2
HRT	d	0.5	0.1	0.05	0.02
Liquid flow rate	m^3d^{-1}	400	2000	4000	10000
Gas flow rate	m^3d^{-1}	400	4000	8000	20000
Input H_2 concentration	$gCODl^{-1}$	20	20	20	20
R	–	0.468	0.468	0.468	0.468
σ	–	3.1	3.1	3.1	3.1
Temperature	C	35	35	35	35

Table 4.7: Operational parameters used for model simulations

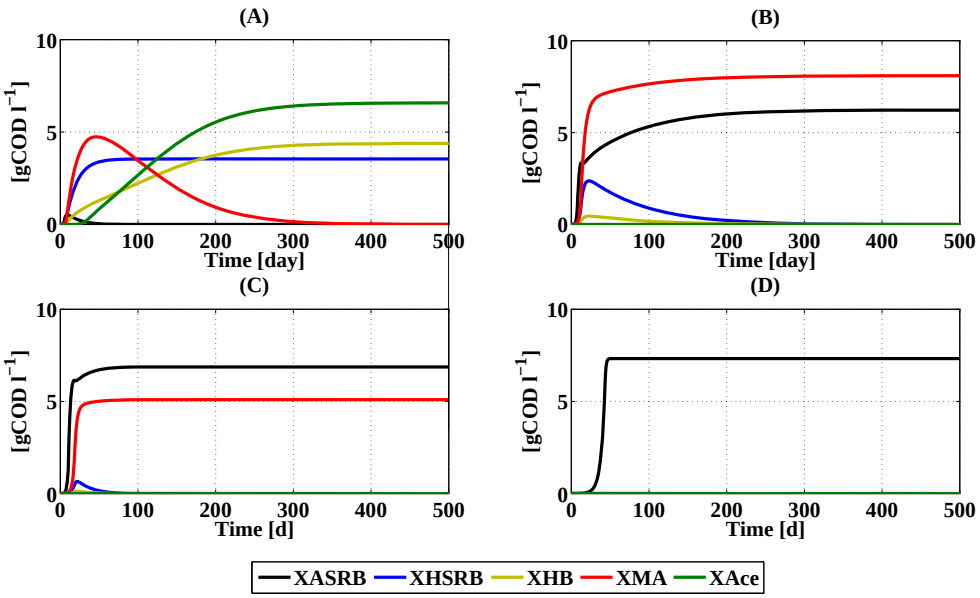

Figure 4.19: Effect of the HRT on the bacterial species and concentrations in the reactor. (A) HRT = 0.5 d; (B) HRT = 0.1 d; (C) HRT = 0.05 d; (D) HRT = 0.02 d

Species and concentrations of bacteria growing in the gas lift reactor

A decrease of the HRT results in the variation of species and concentrations of bacteria prevailing in the reactor (Figure 4.19). When the HRT is 0.5 days there is formation of HSRB with HB as well as MA and AD (Figure 4.19 A). At a HRT of 0.1 days there is an initial coexistence of HSRB and ASRB but after 100 days ASRB out-compete HSRB. After 250 days, there is only ASRB and MA in the system. Figure 4.19 shows the undesired high concentration of MA. A stable coexistence between ASRB and MA with a minor concentration of MA is obtained after 40 days in a reactor with HRT = 0.05 days (Figure 4.19 C), whereas there are only ASRB in the reactor when HRT is 0.02 days (Figure 4.19 D). However, the results reported in Figures 4.19 C and 4.19 D are not applicable for full scale applications as the HRTs are very short.

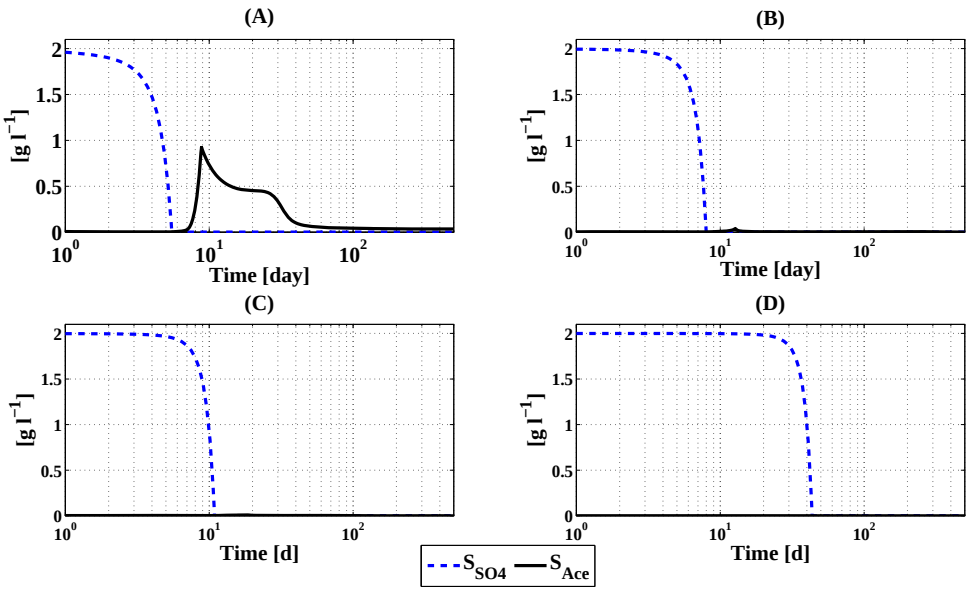

Figure 4.20: Effect of HRT on the concentration of components in aqueous phase. (A) HRT = 0.5 d; (B) HRT = 0.1 d; (C) HRT = 0.05 d; (D) HRT = 0.02 d.

Concentration of components in aqueous phase

The different kinds of bacterial species growing in the reactor at different HRTs imply a different kind and concentration of components in the reactor system. It is possible to see the presence of acetic acid only for an HRT higher than 0.1 days (Figure 4.20 A and B). Figure 4.20 shows that a HRT decrease causes an increase of the time delay of sulfate reduction. The time delay increases because different kinds of bacteria develop in the reactor at lower HRTs.

Concentration of components in gaseous phase

Figure 4.21 shows that an HRT increase results in a decrease of the hydrogen content in the effluent gas flow, whereas with lower HRT values there is the presence of methane due to the action of AD and MA (Figure 4.21 A) or only MA (Figure 4.21 B and C). When the HRT is 0.02 days, there is a high concentration of hydrogen in the effluent gas flow as only ASRB are present in the reactor.

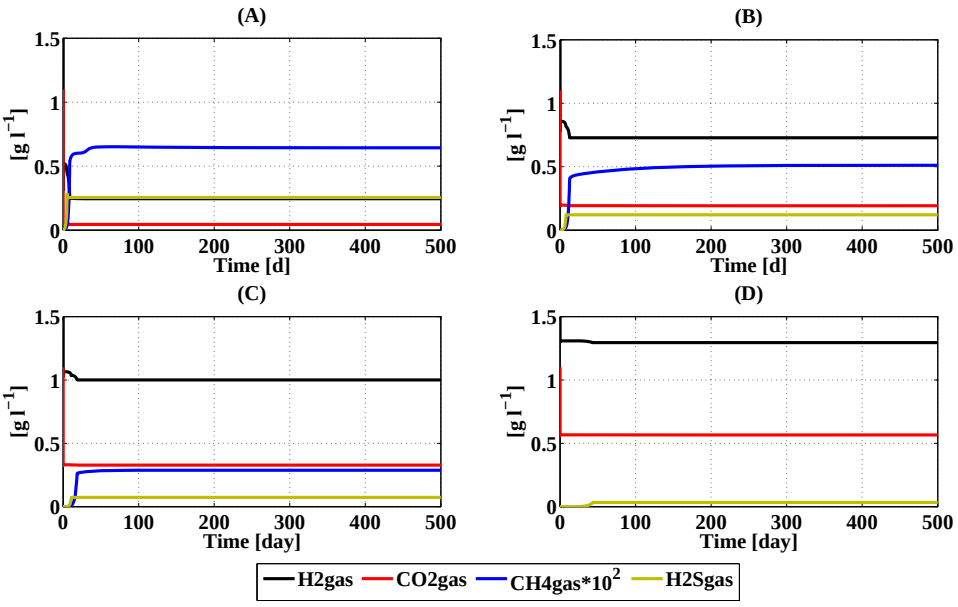

Figure 4.21: Effect of HRT on the concentration of components in gaseous phase. . (A) HRT = 0.5 d; (B) HRT = 0.1 d; (C) HRT = 0.05 d; (D) HRT = 0.02 d.

Chapter 5

Mathematical modeling of attached-growth anaerobic systems

5.1 Introduction

For long time, in the history of microbiology, the bacteria were considered only as planktonic bacteria that can rapidly multiply and disperse. In 1600s Anton Van Leeuwenhoek, with his primitive microscope, scraped the plaque from his teeth and observed the *animaluculae* that formed a microbial community. The following studies leaded to discover the sessile microbial communities, i.e. biofilm, different from planktonic bacteria.

The complete definition of biofilm is: *a layer of prokaryotic and eukaryotic cells anchored to a substratum surface and embedded in an organic matrix of biological origin* [119].

The planktonic bacteria can adhere to support surface and begin the formation of biofilm even if there is continuous water flux. The formation of biofilm is a complex and dynamic process formed by several step: adhesion to support, formation of attached monolayer and cell proliferation (microcolonies), development of mature biofilm, and detachment as schematically depicted in fig. 5.1.

The advantage of disposing bacteria in biofilms is very important in environmental industrial application. The bacteria in biofilm can not be washed away with the water flow, as suspended bacteria. The bacterial biofilms allow to achieve higher biomass concentration value in bioreactors, and allow the growth of bacteria in bioreactor locations where their food remains abundant. Also two main characteristics of biofilms offer great advantages

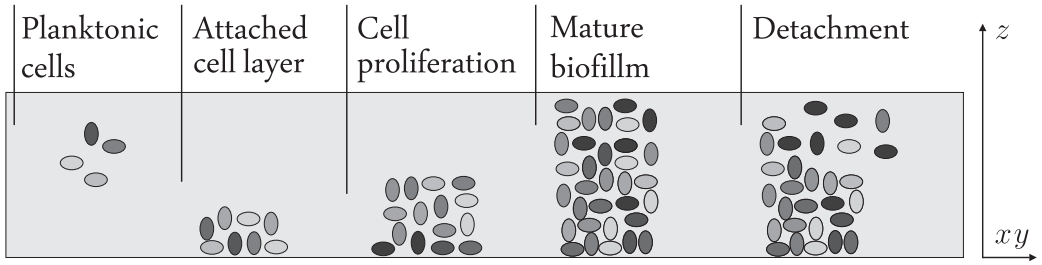

Figure 5.1: Biofilm growth

in environmental application: resistance to antimicrobial agents and formation in biofilm of several bacterial species. The resistance of antimicrobial agents allows a better resistance of bacteria when inhibiting agents reach the wastewater treatment plant (i.e. shock loading). The formation in biofilm of several bacterial species allows to treat simultaneously both organic and inorganic substrates. In recent years, the environmental engineering processes that use bacterial biomass attached to media have generally been referred to as fixed-growth reactor.

Mathematical modelling of biofilms growth was extensively performed during the last decades. The first models are based on a continuum description of the biofilms material and conservation principles, [120, 121, 122, 123, 124]. These studies are mostly centered on the biofilm growth dynamics including the biofilms thickness and spatial distribution of microbial species and substrate concentration. The authors modelled the evolution of biofilms thickness, with biomass detachment, dynamics and spatial distribution of microbial species and substrates in the biofilm. Later, discrete continuum models were developed capable to simulate the biochemical processes of the biofilms growth, [125, 126, 127, 128, 129]. These models can capture various biofilm growth patterns observed in experiments and strongly suggest that the biofilm structure is largely determined by the surrounding substrate concentration. These continuum models can be related to the underlying description offered by models at the microscopic scale as documented in [130].

Biofilm growth is governed by complex systems of nonlinear partial differential equations that are mostly integrated numerically in the above mentioned papers. Qualitative analysis has been performed only for special problems, e.g. [131, 132, 133]. A wide bibliography is reported in [134].

This work presents an analysis of solutions to a free boundary value problem related to the multispecies biofilm model introduced by [123]. The model contains two groups of nonlinear partial differential equations. The first system of n nonlinear hyperbolic partial differential equations describes the grow

of microbial species in biofilms. The evolution of the free boundary is essentially dominated by this system. The second group of m nonlinear parabolic partial differential equations governs the diffusion of substrates. The two biological processes are reciprocally influenced and so are the two systems. The integer numbers n and m are arbitrary and may assume different values. They represent the number of microbial species and the number of substrates, respectively. The mathematical system is quite general and can include a large variety of special situations.

The equations which govern the biofilm evolution are considered in section 5.2, where the equation for the free boundary is also derived. In section 3 is presented a qualitative analysis of a mathematical model for the attached cell layer in multispecies biofilm formation. In section 5.4 the model introduced in section 5.1 has been applied to a biological sulfate reducing biofilm.

5.2 1D Model

Consider the 1D grow of multispecies biofilms. The following notations will be used:

$f_i(z,t)$ volume fraction of the microbial species i, $\sum_{i=1}^{n} f_i = 1$,
ρ_i constant density,
$X_i = \rho_i f_i(z,t)$ concentration of the microorganism,
$S_j(z,t)$ concentration of substrate j, $j = 1, ..., m$,
$r_{mi}(z,t,X_i,S_j)$ specific growth rate,
$u(z,t)$ velocity of the microbial mass,
$g_i(z,t) = u(z,t)\rho_i f_i(z,t) = u(z,t)X_i(z,t)$ biomass flux,
$L(t)$ biofilm thickness,
A constant cross sectional area,
$(z_2 - z_1)A$ 1D control volume.

The mass balance for the microbial species i gives

$$A\frac{\partial}{\partial t}\int_{z_1}^{z_2} \rho_i f_i \, dz = A[g_i(z_1,t) - g_i(z_2,t)] + A\int_{z_1}^{z_2} \rho_i r_{mi} \, dz,$$

$$\int_{z_1}^{z_2} \rho_i \frac{\partial f_i}{\partial t} \, dz = -\int_{z_1}^{z_2} \frac{\partial g_i}{\partial z} \, dz + \int_{z_1}^{z_2} \rho_i r_{mi} \, dz, \tag{5.1}$$

Differentiate equation (5.1) with respect to z_2, then let $z_2 = z$:

$$\frac{\partial f_i}{\partial t} + \frac{\partial}{\partial z}(u f_i) = r_{mi}, \tag{5.2}$$

Summing (5.2) on i yields

$$\frac{\partial u}{\partial z} = \sum_{i=1}^{n} r_{mi}, \tag{5.3}$$

Equation (5.2) is equivalent to $\sum_{i=1}^{n} f_i = 1$. The remaining part of this statement will be proved in Sec. 5.2.2.

Equations (5.2) and (5.3) were initially presented in [123], [124]. In the first sections we will assume

$$r_{mi} = r_{mi}(z, t, \rho_i f_1, ..., , \rho_i f_n) = r_{mi}(z, t, X_1, ..., X_n). \tag{5.4}$$

The situation where r_{mi} depends also on substrates will be considered in Sec. 5.2.4.

Free boundary

Consider the mass balance on $[0, L(t)]$ and denote by $\rho_i \sigma_i(L(t), t)$ the biomass flux between biofilm and bulk liquid

$$\frac{\partial}{\partial t} \int_0^{L(t)} \rho_i f_i \, dz = -\rho_i \sigma_i + \int_0^{L(t)} \rho_i r_{mi} \, dz, \ i = 1, ..., n, \ t > 0. \tag{5.5}$$

Summing on i and using (5.3) and $(5.10)_2$ yields

$$\dot{L}(t) = u(L(t), t) - \sigma, \ t > 0, \tag{5.6}$$

where

$$\sigma = \sum_{i=1}^{n} \sigma_i. \tag{5.7}$$

The initial condition for differential equation (5.6) will be

$$L(0) = L_0, \tag{5.8}$$

where L_0 denotes the initial thickness of biofilm.

5.2.1 Integral system

Consider system (5.2)-(5.3) rewritten in terms of X_i

$$\begin{cases} \frac{\partial X_i}{\partial t} + u \frac{\partial X_i}{\partial z} = \rho_i r_{mi} - \frac{\partial u}{\partial z} X_i, \\ \frac{\partial u}{\partial z} = \sum_i r_{mi}, \end{cases} \quad i = 1, ..., n \ 0 \le z \le L(t), \ t > 0, \tag{5.9}$$

with the following initial-boundary conditions

$$X_i(z,0) = \varphi_i(z),\ u(0,t) = 0. \tag{5.10}$$

The functions $\varphi_i(z)$ represent the generic initial concentrations. Condition $(5.10)_2$ is apparent. Using $(5.9)_2$ in $(5.9)_1$ gives the following system of nonlinear hyperbolic equations

$$\frac{\partial X_i}{\partial t} + u\frac{\partial X_i}{\partial z} = \rho_i r_{mi} - X_i \sum_{h=1}^{n} r_{mh},\ i = 1, ..., n. \tag{5.11}$$

The characteristics are the lines $z = s(z_0, t)$ defined by

$$\frac{\partial s}{\partial t}(z_0,t) = u(s(z_0,t),t),\ s(z_0,0) = z_0,\ z_0 \in [0, L_0]. \tag{5.12}$$

By setting

$$F_i = \rho_i r_{mi} - X_i \sum_j r_{mj} = F_i(z,t,X_1,...,X_n) = F_i(z,t,\mathbf{X}), \tag{5.13}$$

and considering (5.12), system (5.11) reduces to the following system of ordinary differential equations

$$\frac{d}{dt}X_i(s(z_0,t),t) = F_i(s,t,\mathbf{X}),\ i = 1, ..., n,\ 0 \le z_0 \le L_0,\ t > 0, \tag{5.14}$$

with initial conditions

$$X_i(s(z_0,0),0) = X_i(z_0,0) = \varphi_i(z_0),\ 0 \le z_0 \le L_0,\ i = 1, ..., n. \tag{5.15}$$

Solving system (5.14)-(5.15) gives X_i along the characteristics. However, this does not solve the problem, since the characteristics are unknown. In addition, note that differential system (5.14)-(5.15) is equivalent to the integral system

$$\begin{cases} X_i(s(z_0,t),t) = \varphi_i(z_0) + \int_0^t F_i(s(z_0,\tau),\tau,\mathbf{X}(s(z_0,\tau),\tau))\ d\tau, \\ i = 1, ..., n,\ 0 \le z_0 \le L_0,\ t > 0, \end{cases} \tag{5.16}$$

which incorporates the initial conditions (5.15).

Now, the integral equation for characteristics is derived. From (5.12)

$$s(z_0,t) = z_0 + \int_0^t u(s(z_0,\tau),\tau)\ d\tau. \tag{5.17}$$

On the other hand

$$\frac{\partial}{\partial z_0}u(s(z_0,t),t) = \sum_{h=1}^{n} r_{mh}(s(z_0,t),t,\mathbf{X}(s(z_0,t),t))\frac{\partial s}{\partial z_0}(z_0,t),$$

where equation $(5.9)_2$ has been employed. Hence,

$$u(s(z_0,t),t) = \int_0^{z_0}\sum_{h=1}^{n} r_{mh}(s(\zeta,t),t,\mathbf{X}(s(\zeta,t),t))\frac{\partial s}{\partial z_0}(\zeta,t)\ d\zeta. \tag{5.18}$$

Inserting the equation above into (5.17) gives the desired integral equation for $s(z_0,t)$

$$s(z_0,t) = z_0 + \int_0^t d\tau \int_0^{z_0}\sum_{h=1}^{n} r_{mh}(s(\zeta,\tau),\tau,\mathbf{X}(s(\zeta,\tau),\tau))\frac{\partial s}{\partial z_0}(\zeta,\tau)\ d\zeta, \tag{5.19}$$

which incorporates the initial condition $s(z_0,0) = z_0$. Moreover, since $\partial s/\partial z_0$ is involved, we also need

$$\frac{\partial s}{\partial z_0}(z_0,t) = 1 + \int_0^t \sum_{h=1}^{n} r_{mh}(s(z_0,\tau),\tau,\mathbf{X}(s(z_0,\tau),\tau))\frac{\partial s}{\partial z_0}(z_0,\tau)\ d\tau, \tag{5.20}$$

which follows easily from (5.19).

Finally, the integral equation for the free boundary is obtained by (5.6)

$$L(t) = L_0 + \int_0^t u(L(\tau),\tau)\ d\tau - \int_0^t \sigma(L(\tau),\tau)\ d\tau. \tag{5.21}$$

5.2.2 Existence and uniqueness of solutions

The integral system derived in Sec. 5.2.1 will be discussed first in the situation

$$\sigma = 0. \tag{5.22}$$

Under this hypothesis, the mentioned system is expressed as

$$X_i(s(z_0,t),t) = \varphi_i(z_0) + \int_0^t F_i(s(z_0,\tau),\tau,\mathbf{X}(s(z_0,\tau),\tau))\ d\tau,\ \ i = 1,...,n, \tag{5.23}$$

$$s(z_0,t) = z_0 + \int_0^t d\tau \int_0^{z_0}\sum_{h=1}^{n} r_{mh}(s(\zeta,\tau),\tau,\mathbf{X}(s(\zeta,\tau),\tau))\frac{\partial s}{\partial z_0}(\zeta,\tau)\ d\zeta, \tag{5.24}$$

$$\frac{\partial s}{\partial z_0}(z_0,t) = 1 + \int_0^t \sum_{h=1}^{n} r_{mh}(s(z_0,\tau),\tau,\mathbf{X}(s(z_0,\tau),\tau))\frac{\partial s}{\partial z_0}(z_0,\tau)\ d\tau, \quad (5.25)$$

$$0 \le z_0 \le L_0,\ 0 < t \le T. \quad (5.26)$$

Note that equation (5.21) is included in (5.24) for $z_0 = L_0$.

By setting

$$x_i(z_0,t) = X_i(s(z_0,t),t),\ i = 1,...,n, \quad (5.27)$$

$$x_{n+1}(z_0,t) = s(z_0,t),\ x_{n+2}(z_0,t) = \frac{\partial s}{\partial z_0}(z_0,t),\ \mathbf{x} = (x_1,...,x_{n+2}), \quad (5.28)$$

$$F_{n+1}(t,\mathbf{x}(z_0,t)) = \sum_{h=1}^{n} r_{mh}(s(z_0,t),t,\mathbf{X}(s(z_0,t),t))\frac{\partial s}{\partial z_0}(z_0,t),\ F_{n+2} = F_{n+1}, \quad (5.29)$$

system is rewritten as

$$x_i(z_0,t) = \varphi_i(z_0) + \int_0^t F_i(\tau,\mathbf{x}(z_0,\tau))\ d\tau,\ i = 1,...,n, \quad (5.30)$$

$$x_{n+1}(z_0,t) = z_0 + \int_0^t d\tau \int_0^{z_0} F_{n+1}(\tau,\mathbf{x}(\zeta,\tau))\ d\zeta, \quad (5.31)$$

$$x_{n+2}(z_0,t) = 1 + \int_0^t F_{n+2}(\tau,\mathbf{x}(\mathbf{z_0},\tau))\ d\tau, \quad (5.32)$$

$$0 \le z_0 \le L_0,\ 0 < t \le T. \quad (5.33)$$

Theorem 1. *Assume F_h, $h = 1,...,n+2$, Lipschitz continuous and φ_i, $i = 1,...,n$, continuous:*

$$|F_k(\mathbf{x},t) - F_k(\tilde{\mathbf{x}},t)| \le \lambda_k \sum_{h=1}^{n+2} |x_h - \tilde{x}_h|,\ k = 1,...,n+2,\ \varphi_i \in C([0,L_0]). \quad (5.34)$$

Then, if (5.22) holds, there exists a unique continuous solution to system (5.30)-(5.33):

$$x_h = x_h(z_0,t),\ h = 1,...,n+2,\ z_0 \in [0,L_0],\ 0 < t \le T,\ T > 0.$$

Proof. Consider the vector space V of the function $x_h(z_0,t)$ continuous on $C(I)$, $I = [0,L_0] \times [0,T]$ with norm

$$||\mathbf{x}|| = \sum_{h=1}^{n+2} \sup_I \exp(-\gamma_1 z_0 - \gamma_2 t)|x_h(z_0,t)|. \quad (5.35)$$

Here, γ_1, γ_2 are positive constants that will be fixed later on. Consider the map $y = A\mathbf{x}$ of V into itself defined by

$$A\mathbf{x} = \text{ right-hand side of system (5.30) – (5.32).} \tag{5.36}$$

Let us show that A is a contractive map. Denote by $\tilde{y} = A\tilde{\mathbf{x}}$ and obtain

$$|y_i - \tilde{y}_i| \leq \lambda_i \int_0^t \sum_{h=1}^{n+2} |x_h(z_0,\tau),\tau) - \tilde{x}_h(z_0,\tau),\tau)|\ d\tau,\ i = 1, ..., n,$$

$$|y_i - \tilde{y}_i| \exp(-\gamma_1 z_0 - \gamma_2 t) \leq$$

$$\lambda_i \int_0^t \exp(-\gamma_2(t-\tau)) \sum_{h=1}^{n+2} \exp(-\gamma_1 z_0 - \gamma_2\tau)|x_h(z_0,\tau),\tau) - \tilde{x}_h(z_0,\tau),\tau)|\ d\tau \leq$$

$$\lambda_i ||\mathbf{x} - \tilde{\mathbf{x}}|| \int_0^t \exp(-\gamma_2(t-\tau))\ d\tau \leq \frac{\lambda_i}{\gamma_2} ||\mathbf{x} - \tilde{\mathbf{x}}||,\ i = 1, ..., n, \tag{5.37}$$

$$|y_{n+1} - \tilde{y}_{n+1}| \leq \lambda_{n+1} \int_0^t\ d\tau \int_0^{z_0} \sum_{h=1}^{n+2} |x_h(\zeta,\tau),\tau) - \tilde{x}_h(\zeta,\tau),\tau)|\ d\zeta,$$

$$|y_{n+1} - \tilde{y}_{n+1}| \exp(-\gamma_1 z_0 - \gamma_2 t) \leq$$

$$\lambda_{n+1} \int_0^t\ d\tau \int_0^{z_0} e^{-\gamma_1(z_0-\zeta)-\gamma_2(t-\tau)} \sum_{h=1}^{n+2} e^{-\gamma_1\zeta-\gamma_2\tau}|x_h(\zeta,\tau),\tau) - \tilde{x}_h(\zeta,\tau),\tau)|\ d\zeta \leq$$

$$\lambda_{n+1} ||\mathbf{x} - \tilde{\mathbf{x}}|| \int_0^t\ d\tau \int_0^{z_0} e^{-\gamma_1(z_0-\zeta)-\gamma_2(t-\tau)}\ d\zeta \leq \frac{\lambda_{n+1}}{\gamma_1\gamma_2} ||\mathbf{x} - \tilde{\mathbf{x}}||, \tag{5.38}$$

$$|y_{n+2} - \tilde{y}_{n+2}| \leq \lambda_{n+2} \int_0^t \sum_{h=1}^{n+2} |x_h(z_0,\tau),\tau) - \tilde{x}_h(z_0,\tau),\tau)|\ d\tau,$$

$$|y_{n+2} - \tilde{y}_{n+2}| \exp(-\gamma_1 z_0 - \gamma_2 t) \leq$$

$$\lambda_{n+2}\int_0^t e^{-\gamma_2(t-\tau)}\sum_{h=1}^{n+2} e^{-\gamma_1 z_0-\gamma_2\tau}|x_h(z_0,\tau),\tau)-\tilde{x}_h(z_0,\tau),\tau)|\ d\tau \leq$$

$$\lambda_{n+2}||\mathbf{x}-\tilde{\mathbf{x}}||\int_0^t e^{-\gamma_2(t-\tau)}\ d\tau \leq \frac{\lambda_{n+2}}{\gamma_2}||\mathbf{x}-\tilde{\mathbf{x}}||. \tag{5.39}$$

Summing (5.37)-(5.39) gives

$$||\mathbf{y}-\tilde{\mathbf{y}}|| \leq \left(\sum_{i=1}^{n}\frac{\lambda_i}{\gamma_2}+\frac{\lambda_{n+1}}{\gamma_1\gamma_2}+\frac{\lambda_{n+2}}{\gamma_2}\right)||\mathbf{x}-\tilde{\mathbf{x}}||, \tag{5.40}$$

Therefore, map $y = A\mathbf{x}$ is a contraction if γ_1 and γ_2 are selected such that

$$\frac{\sum_{i=1}^{n}\lambda_i+\lambda_{n+2}}{\gamma_2}<\frac{1}{2},\ \frac{\lambda_{n+1}}{\gamma_1\gamma_2}<\frac{1}{2}.$$

So, the theorem is proved.

Now, properties of solution are derived from Th. 1.

Corollary 1 *Under the same hypotheses as* Th. 1, *if* $\sum_{j=1}^{n} r_{mj} \geq 0$ *then*

$$\frac{\partial s}{\partial z_0}(z_0,t) \geq 1. \tag{5.41}$$

Proof. Consider the integral equation

$$\frac{\partial s}{\partial z_0}(z_0,t) = 1+\int_0^t\sum_{j=1}^{n} r_{mj}(\mathbf{X}(s(z_0,\tau),\tau),s(z_0,\tau),\tau)\frac{\partial s}{\partial z_0}(z_0,\tau)\ d\tau.$$

Consider Picard's process of successive approximations. We start by setting

$$\left(\frac{\partial s}{\partial z_0}\right)_0(z_0,t)=1$$

and determine $\left(\frac{\partial s}{\partial z_0}\right)_1(z_0,t)$

$$\left(\frac{\partial s}{\partial z_0}\right)_1(z_0,t)=1+\int_0^t\left(\sum_{j=1}^{n} r_{mj}\frac{\partial s}{\partial z_0}\right)_0(z_0,\tau)\ d\tau.$$

By continuing in this manner we obtain an infinite sequence of approximating functions which are not less than 1 and so is the solution.

Corollary 2 *Under the same hypotheses as* Th. 1, *if* $\sum_{j=1}^{n} r_{mj} \geq 0$ *then the characteristics do not intersect.*

Proof. Consider the characteristics $z = s(z_1, t)$ and $z = s(z_2, t)$, where $z_2 > z_1$. Then,

$$s(z_2, t) - s(z_1, t) = \int_{z_1}^{z_2} \frac{\partial s}{\partial z_0}(z_0, t)\, dz_0 \geq z_2 - z_1 > 0.$$

Corollary 3 *Under the same hypotheses as* Th. 1, *if* $\sum_{j=1}^{n} r_{mj} \geq 0$ *then* X_i *can be determined as function of* z, t.

Proof. The function $z = s(z_0, t)$ can be inverted and gives $z_0 = s^{-1}(z, t)$. Therefore,

$$x_i(z_0, t) = x_i(s^{-1}(z, t), t) = X_i(z, t).$$

Corollary 4 *Under the same hypotheses as* Th. 1, *if* $F_i \geq 0$, $\varphi_i \geq 0$ *then*

$$X_i \geq 0. \tag{5.42}$$

Proof. Consider equation (5.23) and use Picard's process of successive approximations with $(X_i)_0 = \varphi_i$.

Corollary 5 *Under the same hypotheses as* Th. 1

$$\sum_{i=1}^{n} f_i = 1 \;\Leftrightarrow\; \frac{\partial u}{\partial z} = \sum_{i=1}^{n} r_{mi}. \tag{5.43}$$

Proof. Consider equation $(5.9)_1$, rewritten in terms of fraction volume f_i

$$f_i = \varphi_i/\rho_i + \int_0^t (r_{mi} - f_i \frac{\partial u}{\partial z})\, d\tau,\ i = 1, ..., n, \tag{5.44}$$

where

$$\sum_{i=1}^{n} \varphi_i/\rho_i = 1,$$

since φ_i/ρ_i, $i = 1, ..., n$, represent the initial volume fractions. Summing (5.44) gives

$$\sum_{i=1}^{n} f_i = \sum_{i=1}^{n} \varphi_i/\rho_i + \int_0^t (\sum_{i=1}^{n} r_{mi} - \sum_{i=1}^{n} f_i \frac{\partial u}{\partial z})\, d\tau, \tag{5.45}$$

Hence, if $\sum_{i=1}^{n} f_i = 1$,

$$0 = \int_0^t (\sum_{i=1}^{n} r_{mi} - \frac{\partial u}{\partial z})\, d\tau,\ \forall t,$$

and after differentiating with respect with respect to t

$$\sum_{i=1}^{n} r_{mi} = \frac{\partial u}{\partial z}. \tag{5.46}$$

Conversely, under hypothesis (5.46), the function $\sum_{i=1}^{n} f_i = 1$ is the unique solution to integral equation (5.45).

Corollary 6 *Under the same hypotheses as* Th. 1, *if* $F_i \geq 0$, $\varphi_i \geq 0$ *then*

$$0 \leq f_i \leq 1. \tag{5.47}$$

Proof. Indeed, f_i, $i = 1, ..., n$, are positive because of (5.42) and less than 1 since $\sum_i f_i = 1$.

5.2.3 Biomass detachment

The free boundary evolution is governed by equation (5.6), rewritten for convenience,

$$\dot{L}(t) = u(L(t), t) - \sigma(L(t), t),\ L(0) = L_0, t > 0. \tag{5.48}$$

As outlined earlier, if $\sigma = 0$, equation (5.48) reduces to the characteristic of initial point $z_0 = L_0$

$$s(L_0, t), \tag{5.49}$$

and the problem has been solved in Sec 5.2.2. Now, we consider $\sigma \geq 0$. A typical expression is σ =constant$\times L^2$. In this hypothesis the mathematical problem describes biomass detachment, loss of biomass due to shear or sloughing.

Assume that the hypotheses of Corollary 1 hold and σ Lipshitz continuous

$$|\sigma(L, t) - \sigma(\tilde{L}, t)| \leq \lambda |L - \tilde{L}|. \tag{5.50}$$

For any time t denote by $z_0(t)$ the initial point of the characteristic through $L(t)$

$$L(t) = s(z_0(t), t). \tag{5.51}$$

Hence,

$$\dot{L}(t) = \frac{\partial s}{\partial z_0}(z_0(t), t)\dot{z}_0(t) + \frac{\partial s}{\partial t}(z_0(t), t) = \frac{\partial s}{\partial z_0}(z_0(t), t)\dot{z}_0(t) + u(L(t), t). \tag{5.52}$$

From (5.48) and (5.52) it follows that

$$\frac{\partial s}{\partial z_0}(z_0(t), t)\dot{z}_0(t) = -\sigma(L(t), t), \tag{5.53}$$

and, since $\partial s/\partial z_0 \geq 1$,

$$\dot{z}_0(t) \leq 0. \tag{5.54}$$

Therefore, the tangent to the free boundary in any point is not grater than the tangent of the characteristic trough the same point. Since this fact is also true initially we may conclude that $L(t)$ is not greater than the characteristic of equation (5.49). The solution X_i for $z \leq s(L_0, t)$ is known. So we can use it to obtain the free boundary, as shown below.

From (5.48)

$$L(t) = L_0 + \int_0^t u(L(\tau), \tau)\ d\tau - \int_0^t \sigma(L(\tau), \tau)\ d\tau, \tag{5.55}$$

and considering $(5.9)_2$

$$L(t) = L_0 + \int_0^t d\tau \int_0^{L(\tau)} \sum_{j=1}^{n} r_{mj}(\zeta, \tau)\ d\zeta - \int_0^t \sigma(L(\tau), \tau)\ d\tau. \tag{5.56}$$

The function space for solution is: $C([0, T])$, with norm

$$||L(t)|| = \sup_{[0,T]} \exp(-\gamma t)|L(t)|,\ \gamma \text{ positive constant.} \tag{5.57}$$

Consider the map $L_1 = BL$, $C([0, T]) \rightarrow\ C([0, T])$ defined by

$$BL = \text{ right-hand side of(5.56)} \tag{5.58}$$

and prove that B is a contractive map. Indeed,

$$L_1 - \tilde{L}_1 = \int_0^t d\tau \int_{\tilde{L}(\tau)}^{L(\tau)} \sum_{j=1}^{n} r_{mj}(\zeta, \tau)\ d\zeta - \int_0^t [\sigma(L(\tau), \tau) - \tilde{\sigma}(L(\tau), \tau)]\ d\tau. \tag{5.59}$$

Setting

$$M = \max |\sum_{j=1}^{n} r_{mj}(z,t)|,\ 0 \le z \le s(L_0,t),\ 0 \le t \le T, \tag{5.60}$$

we get

$$|L_1 - \tilde{L}_1| \le (M+\lambda) \int_0^t |L(\tau) - \tilde{L}(\tau)|\ d\tau, \tag{5.61}$$

$$|L_1 - \tilde{L}_1| \exp(-\gamma t) \le \frac{M+\lambda}{\gamma} ||L - \tilde{L}||, \tag{5.62}$$

$$||L_1 - \tilde{L}_1|| < ||L - \tilde{L}||, \tag{5.63}$$

if γ is selected greater than $M + \lambda$.

5.2.4 Substrates

Biofilm growth depends on nutrients: the substrates. In this section the influence of substrates on biofilm growth is considered and it is assumed

$$r_{mi} = r_{mi}(z,t,\mathbf{X},\mathbf{S}), \tag{5.64}$$

where $\mathbf{S}(z,t) = (S_1(z,t),...,S_m(z,t))$ and $S_j(z,t)$ denotes the concentration of substrate j, $j = 1,...,m$.

The diffusion of substrates is governed by the equation

$$\frac{\partial S_j}{\partial t} - D_j \frac{\partial^2 S_j}{\partial z^2} = r_{Sj}(z,t,\mathbf{X},\mathbf{S}),\ 0 < z < L(t),\ 0 < t \le T,\ j = 1,...,m, \tag{5.65}$$

where D_j denotes the diffusivity coefficient and $r_{Sj}(z,t,\mathbf{X},\mathbf{S})$ the conversion rate of substrate j. The following initial-boundary conditions will be associated to equation (5.65)

$$S_j(z,0) = S_{j0}(z),\ 0 \le z \le L_0,\ j = 1,...,m, \tag{5.66}$$

$$\frac{\partial S_j}{\partial z}(0,t) = 0,\ S_j(L(t),t) = S_{jL}(t),\ 0 < t \le T,\ j = 1,...,m, \tag{5.67}$$

$$S_{j0}(L_0) = S_{jL}(0),\ S_{j0}(0) = 0. \tag{5.68}$$

Assume r_{Sj} Lipschitz continuous with respect to $\mathbf{S}$, $\mathbf{X}$ and

$$S_{j0} \in C_1([0,L_0]),\ S_{jL} \in C_1([0,T]). \tag{5.69}$$

Under the hypotheses above the solution to system (5.65)-(5.68) can be expressed in terms of integral equations by using known results on the heat equation in general regions [135]

$$S_j(z,t) = \int_0^{L_0} S_{j0}(\zeta)N(z,\zeta,t)\ d\zeta + \int_0^t D_j w_j(\tau)N(z,L(\tau),t-\tau)\ d\tau$$

$$+ \int_0^t S_{jL}(\tau)[N(z,L(\tau),t-\tau)\dot{L}(\tau) - D_j N\zeta(z,L(\tau),t-\tau)]\ d\tau$$

$$+ \int_0^t d\tau \int_0^{L(\tau)} r_{Sj}(\zeta,\tau,\mathbf{X}(\zeta,\tau),\mathbf{S}(\zeta,\tau))N(z,\zeta,t-\tau)\ d\zeta,\ j=1,...,m, \quad (5.70)$$

$$w_j(t) = \int_0^{L_0} S'_{j0}(\zeta)G(z,\zeta,t)\ d\zeta + 2\int_0^t \dot{S}_{Lj}(\tau)G(L(t),L(\tau),\tau)\ d\tau$$

$$+2\int_0^t d\tau \int_0^{L(\tau)} r_{Sj}(\zeta,\tau,\mathbf{X}(\zeta,\tau),\mathbf{S}(\zeta,\tau))N_z(L(t),\zeta,t-\tau)\ d\zeta$$

$$+2\int_0^t D_j w_j(\tau)N_z(L(t),L(\tau),t-\tau)\ d\tau,\ j=1,...,m, \quad (5.71)$$

where the following notations have been introduced

$$K(z,t) = \frac{\exp(-z^2)/4D_j t}{\sqrt{4\pi D_j t}},\ N(z,\zeta,t-\tau) = K(z-\zeta,t-\tau) + K(z+\zeta,t-\tau), \quad (5.72)$$

$$w_j(t) = \frac{\partial S_j}{\partial z}(L(t),t),\ G(z,\zeta,t-\tau) = K(z-\zeta,t-\tau) - K(z+\zeta,t-\tau). \quad (5.73)$$

Systems (5.70)-(5.71) and (5.30)-(5.33) must be considered simultaneously, since they are mutually connected by the forcing terms r_{Sj} and r_{mi}. In Picard's process of successive approximations, they are solved in series. The starting approximations are the functions:

$$\varphi_i(z),\ S_{0j}(z),\ L_0,\ 0 \le z \le L_0. \quad (5.74)$$

Using (5.74) in system (5.30)-(5.33) yields approximating solutions for X_i and $L(t)$, which are employed in system (5.70)-(5.71) to find S_j. Then, the process is repeated.

Of course, system (5.65) can be solved numerically, as in the example in following section.

5.3 Initial Cell Layer in Multispecies Biofilm Formation

Mathematical modelling of biofilms growth was extensively performed during the last decades. Essentially, two different classes of models have been developed: continuum models, e.g. among others [123, 124, 134, 136], and differential-discrete models, e.g. [137, 138]. In principles, methods of statistical mechanics can be used to derive macroscopic equations form the underlying description at the cellular scale [130].

Usually, an initial nonzero thickness in biofilm growth is assumed and the formation of attached cell layer is neglected, fig. 5.4 (A), (B). Nevertheless, this biological process can last several days or months, since it depends on many factors such as physical and chemical characteristics of substratum, nutrient concentration, hydrodynamic conditions and concentration of planktonic bacteria in the bulk. Therefore, the formation of attached cell layer is very important in environmental industrial application for wastewater treatment, in particular in the start-up of fixed-growth treatment reactors.

In this section is presented a qualitative analysis of a mathematical model for the attached cell layer in mutispecies biofilm formation. This biological process is described by a free boundary problem for nonlinear hyperbolic equations where the initial biofilm thickness is zero. This problem is different from similar free boundary problems for biofilm growth, since the free boundary is a space-like line. Furthermore, no fictitious initial conditions for biomass concentrations and biofilm thickness are required. We only need to know the concentrations of biomass in the bulk liquid and the biomass flux from bulk liquid.

The objective of this section is the qualitative analysis of solutions and of properties of the free boundary. The mathematical model is introduced and the complete free boundary problem is described. The differential equations are converted, into an equivalent system of Volterra integral equations. Subsequently, an existence and uniqueness theorem is proved by the classical fixed point theorem and suitable weighted norms. The properties of solutions are analized. It will be shown that the solutions are positive and the sum of fraction volumes is equal to 1. In addition, it is proved that the free boundary is an increasing function of time.

5.3.1 Mathematical modelling of initial cell layer

Consider the initial phase in one-dimensional multispecies biofilm growth. Let $f_i(z,t)$ be the volume fraction of the microbial species i, $\sum_{i=1}^{n} f_i = 1$, ρ_i

the constant density, $X_i = \rho_i f_i(z,t)$ the concentration of the microorganism i, $\mathbf{X} = (X_1, ..., X_n)$, $r_{M,i}(z,t,X_i)$ the specific growth rate, $u(z,t)$ the velocity of the microbial mass, $L(t)$ biofilm thickness. In addition, denote by $\sigma(t)$ the biomass flux from bulk liquid to biofilm. This is the most used convention. On the other hand, if an opposite definition is adopted, as in [136], $\sigma(t)$ must be replaced by $-\sigma(t)$ and represents the biomass flux from biofilm to bulk liquid.

The initial growth process for multispecies biofilms in one space dimension may be described by the following free boundary problem

$$\frac{\partial}{\partial t}X_i(z,t) + u(z,t)\frac{\partial}{\partial z}X_i(z,t) = \rho_i r_{M,i}(z,t,\mathbf{X}) - X_i(z,t)\frac{\partial}{\partial z}u(z,t), \quad (5.1)$$

$$\frac{\partial}{\partial z}u(z,t) = \sum_{i=1}^{n} r_{M,i}(z,t,\mathbf{X}),\ 0 < z \leq L(t),\ t > 0, \quad (5.2)$$

$$\dot{L}(t) = u(L(t),t) + \sigma(t),\ t > 0, \quad (5.3)$$

where $i = 1, ...n$. Equations (5.1)-(5.3) are derived from the mass balance for the microbial species as in [123, 124, 136]. The following boundary conditions will be associated to system (5.1)-(5.3)

$$X_i(L(t),t) = \psi_i(t),\ u(0,t) = 0,\ \sigma(t) \geq \sigma_L > 0,\ L(0) = 0. \quad (5.4)$$

Condition $(5.4)_1$ states that the biomass concentrations at the biofilm boundary are the same as the bulk liquid. Therefore, they are the boundary conditions in this specific problem, although they are often named initial conditions in a general mathematical context. Equation $(5.4)_2$ is a no flux condition between substratum and biofilm.

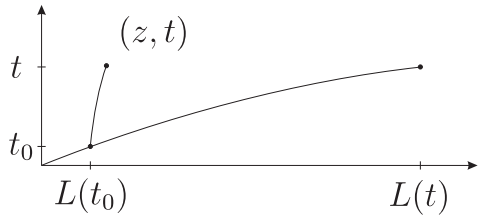

Figure 5.1: Free boundary problem.

The characteristics $z = z(t)$ of system (5.1) are defined by $\partial z/\partial t = u$. Since they also depend on the initiation point $(L(t_0), t_0)$, fig. 5.1, we will

use the notation $z = c(t_0, t)$. Thus, the characteristics are defined by the following initial value problem

$$\frac{\partial}{\partial t} c(t_0, t) = u(c(t_0, t), t), \quad c(t_0, t_0) = L(t_0). \tag{5.5}$$

Condition $(5.4)_3$ essentially means that the initial curve is not a characteristic. By using the notations

$$G(z, t, \mathbf{X}) = \sum_{i=1}^{n} r_{M,i}, \;\; F_i(z, t, \mathbf{X}) = \rho_i r_{M,i} - X_i G, \tag{5.6}$$

system (5.1) is rewritten as follows:

$$\frac{d}{dt} X_i(c(t_0, t), t) = F_i(c(t_0, t), t, \mathbf{X}(c(t_0, t), t)), \;\; 0 \le t_0 \le t \le T, \tag{5.7}$$

and after integrating over (t_0, t)

$$X_i(c(t_0, t), t) = \psi_i(t_0) + \int_{t_0}^{t} F_i(c(t_0, \tau), \tau, \mathbf{X}(c(t_0, \tau), \tau)) \; d\tau. \tag{5.8}$$

Let us now consider equation (5.2)

$$\frac{\partial}{\partial z} u(c(t_0, t), t) = G(c(t_0, t), t, \mathbf{X}(c(t_0, t), t)). \tag{5.9}$$

Hence,

$$\frac{\partial u}{\partial t_0}(c(t_0, t), t) = \frac{\partial u}{\partial z} \frac{\partial c}{\partial t_0} = G(c(t_0, t), t, \mathbf{X}(c(t_0, t), t)) \frac{\partial c}{\partial t_0}(t_0, t),$$

and

$$\frac{\partial u}{\partial \tau}(c(\tau, t), t) = G(c(\tau, t), t, \mathbf{X}(c(\tau, t), t)) \frac{\partial c}{\partial \tau}(\tau, t), 0 < \tau \le t_0.$$

Integrating over $(0, t_0)$ yields

$$u(c(t_0, t), t) = \int_{0}^{t_0} G(c(\tau, t), t, \mathbf{X}(c(\tau, t), t)) \frac{\partial c}{\partial \tau}(\tau, t) \; d\tau, \tag{5.10}$$

since $u(c(0, t), t) = u(0, t) = 0$.

Consider equation (5.3)

$$\dot{L}(t_0) = u(L(t_0), t_0) + \sigma(t_0) = u(c(t_0, t_0), t_0) + \sigma(t_0), \tag{5.11}$$

and use (5.10)

$$\dot{L}(t_0) = \sigma(t_0) + \int_0^{t_0} G(c(\tau, t_0), t_0, \mathbf{X}(c(\tau, t_0), t_0)) \frac{\partial c}{\partial \tau}(\tau, t_0) d\tau. \tag{5.12}$$

Hence,

$$\dot{L}(\theta) = \sigma(\theta) + \int_0^{\theta} G(c(\tau, \theta), \theta, \mathbf{X}(c(\tau, \theta), \theta)) \frac{\partial c}{\partial \tau}(\tau, \theta) d\tau, 0 < \theta \leq t_0,$$

and, after integration over $(0, t_0)$,

$$L(t_0) = \int_0^{t_0} \sigma(\theta)\ d\theta + \int_0^{t_0}\ d\theta \int_0^{\theta} G(c(\tau, \theta), \theta, \mathbf{X}(c(\tau, \theta), \theta)) \frac{\partial c}{\partial \tau}(\tau, \theta) d\tau. \tag{5.13}$$

Consider equation (5.5)

$$\frac{\partial}{\partial \theta} c(t_0, \theta) = u(c(t_0, \theta), \theta),\ c(t_0, t_0) = L(t_0),\ t_0 < \theta \leq t.$$

Integrate over (t_0, t)

$$c(t_0, t) = L(t_0) + \int_{t_0}^{t} u(c(t_0, \theta), \theta)\ d\theta,$$

and use (5.10)

$$c(t_0, t) = L(t_0) + \int_{t_0}^{t} d\theta \int_0^{t_0} G(c(\tau, \theta), \theta, \mathbf{X}(c(\tau, \theta), \theta)) \frac{\partial c}{\partial \tau}(\tau, \theta) d\tau. \tag{5.14}$$

Differentiation of (5.14) with respect to t_0 and some simple manipulations yield

$$\frac{\partial}{\partial t_0} c(t_0, t) = \sigma(t_0) + \int_{t_0}^{t} G(c(t_0, \theta), \theta, \mathbf{X}(c(t_0, \theta), \theta)) \frac{\partial c}{\partial t_0}(t_0, \theta) d\theta. \tag{5.15}$$

The differential system (5.5), (5.7), (5.11) is equivalent to the integral system (5.8), (5.13), (5.14), (5.15). Indeed, if a solution exists for the integral system, this can be differentiated and the differential system is recovered.

In the most general biological process the function $r_{M,i}$ can also depend on substrates. This dependence has been omitted here, since inessential in the mathematical problem discussed in this work.

5.3.2 Volterra system

Consider the following positions

$$x_i(t_0,t) = X_i(c(t_0,t),t),\ \mathbf{x}(x_1,...,x_n), \tag{5.16}$$

$$\Phi_i(\mathbf{x}(t_0,t),c(t_0,t),t) = F_i(c(t_0,t),t,\mathbf{x}(t_0,t)),\ i=1,...,n. \tag{5.17}$$

$$\Phi_{n+1}(\mathbf{x}(t_0,t),c(t_0,t),c_{t_0}(t_0,t),t) = G(c(t_0,t),t,\mathbf{x}(t_0,t))c_{t_0}(t_0,t), \tag{5.18}$$

$$\Phi_{n+2} = \Phi_{n+1}. \tag{5.19}$$

By using definitions (5.16)-(5.19), equations (5.8), (5.13), (5.14), (5.15) are rewritten as

$$x_i(t_0,t)) = \psi_i(t_0) + \int_{t_0}^{t} \Phi_i(\mathbf{x}(t_0,\tau),c(t_0,\tau),\tau)d\tau, \tag{5.20}$$

$$\begin{aligned} c(t_0,t) = &\int_0^{t_0} \sigma(\theta)\ d\theta + \int_0^{t_0} d\theta \int_0^{\theta} \Phi_{n+1}(\mathbf{x}(\tau,\theta),c(\tau,\theta),c_\tau(\tau,\theta),\theta)\ d\tau \\ &+ \int_{t_0}^{t} d\theta \int_0^{t_0} \Phi_{n+1}(\mathbf{x}(\tau,\theta),c(\tau,\theta),c_\tau(\tau,\theta),\theta)d\tau, \end{aligned} \tag{5.21}$$

$$c_{t_0}(t_0,t) = \sigma(t_0) + \int_{t_0}^{t} \Phi_{n+2}(\mathbf{x}(t_0,\theta),c(t_0,\theta),c_{t_0}(t_0,\theta),\theta)d\theta, \tag{5.22}$$

$$L(t_0) = \int_0^{t_0} d\theta \int_0^{\theta} G(c(\tau,\theta),\theta,\mathbf{x}(\tau,\theta))c_\tau(\tau,\theta)\ d\tau + \int_0^{t_0} \sigma(\theta)\ d\theta, \tag{5.23}$$

where $i = 1,...n$ and $0 \le t_0 \le t \le T$.

Note that equation (5.23) is separated from system (5.20)-(5.22). Thus, this system is solved firstly. Then, the solution is used in equation (5.23) to find L. The following theorem holds for system (5.20)-(5.22).

Theorem 1. Assume σ, ψ_i, $i = 1,...,n$, continuous and Φ_j Lipschitz continuous

$$\sigma, \psi_i \in C([0,T]),\ i = 1,...,n, \tag{5.24}$$

$$|\Phi_i(\mathbf{x},c,t) - \Phi_i(\tilde{\mathbf{x}},\tilde{c},t)| \le L_i \left[\sum_{h=1}^{n} |x_h - \tilde{x}_h| + |c-\tilde{c}|\right], i = 1,...,n, \tag{5.25}$$

$$|\Phi_i(\mathbf{x},c,c_{t_0},t) - \Phi_i(\tilde{\mathbf{x}},\tilde{c},\tilde{c}_{t_0},t)| \le L_i \left[\sum_{h=1}^{n} |x_h - \tilde{x}_h| + |c-\tilde{c}| + |c_{t_0} - \tilde{c}_{t_0}|\right],\ i = n+1, n+2. \tag{5.26}$$

Then, there exists a unique continuous solution $x_i, c, c_{t_0} \in C(I)$ to Volterra system (5.20)-(5.22), where $I = \{(t_0,t) : 0 \le t_0 \le t \le T\}$, $T > 0$.

Proof. Consider the vector space S of the continuous functions $x_i, c, c_{t_0} \in C(I)$ with norm

$$||(\mathbf{x}, c, c_{t_0})|| = \sum_{i=1}^{n} \max_I e^{-\gamma_1 t_0 - \gamma_2 t} |x_i(t_0,t)| + \max_I e^{-\gamma_1 t_0 - \gamma_2 t} |c(t_0,t)| + \max_I e^{-\gamma_1 t_0 - \gamma_2 t} |c_{t_0}(t_0,t)|,$$

where γ_1 and γ_1 are positive constants. Let $(\mathbf{y}, C, C_{t_0}) = A(\mathbf{x}, c, c_{t_0})$ be the map defined by the equations below

$$y_i(t_0,t)) = \psi_i(t_0) + \int_{t_0}^{t} \Phi_i(\mathbf{x}(t_0,\tau), c(t_0,\tau), \tau) d\tau, \tag{5.27}$$

$$C(t_0,t) = \int_0^{t_0} \sigma(\theta)\, d\theta + \int_0^{t_0} d\theta \int_0^{\theta} \Phi_{n+1}(\mathbf{x}(\tau,\theta), c(\tau,\theta), c_\tau(\tau,\theta), \theta)\, d\tau$$
$$+ \int_{t_0}^{t} d\theta \int_0^{t_0} \Phi_{n+1}(\mathbf{x}(\tau,\theta), c(\tau,\theta), c_\tau(\tau,\theta), \theta) d\tau, \tag{5.28}$$

$$C_{t_0}(t_0,t) = \sigma(t_0) + \int_{t_0}^{t} \Phi_{n+2}(\mathbf{x}(t_0,\theta), c(t_0,\theta), c_{t_0}(t_0,\theta), \theta) d\theta, \tag{5.29}$$

where $i = 1, ...n$ and $0 \le t_0 \le t \le T$. Denote by $(\tilde{\mathbf{y}}, \tilde{C}, \tilde{C}_{t_0}) = A(\tilde{\mathbf{x}}, \tilde{c}, \tilde{c}_{t_0})$ and consider equation (5.27)

$$|y_i(t_0,t)) - \tilde{y}_i(t_0,t))| e^{-\gamma_1 t_0 - \gamma_2 t}$$

$$\le L_i \int_{t_0}^{t} \left[\sum_{h=1}^{n} |x_h(t_0,\tau) - \tilde{x}_h(t_0,\tau)| + |c(t_0,\tau) - \tilde{c}(t_0,\tau)| \right] e^{-\gamma_1 t_0 - \gamma_2 \tau} e^{-\gamma_2 (t-\tau)} d\tau.$$

Hence,

$$|y_i(t_0,t)) - \tilde{y}_i(t_0,t))| e^{-\gamma_1 t_0 - \gamma_2 t} \le L_i ||(\mathbf{x}, c, c_{t_0}) - (\tilde{\mathbf{x}}, \tilde{c}, \tilde{c}_{t_0})|| / \gamma_2, \tag{5.30}$$

$i = 1, ..., n$. Consider equation (5.28)

$$|C(t_0,t)) - \tilde{C}(t_0,t))| e^{-\gamma_1 t_0 - \gamma_2 t} \le L_{n+1} \int_0^{t_0} d\theta \int_0^{\theta} \left[\sum_{h=1}^{n} |x_h(\tau,\theta) - \tilde{x}_h(\tau,\theta)| \right.$$
$$\left. + |c(\tau,\theta) - \tilde{c}(\tau,\theta)| + |c_\tau(\tau,\theta) - \tilde{c}_\tau(\tau,\theta)| \right] e^{-\gamma_1 t_0 - \gamma_2 \tau} e^{-\gamma_1 (t_0 - \tau)} e^{-\gamma_2 (t-\theta)} d\tau$$
$$+ L_{n+1} \int_{t_0}^{t} d\theta \int_0^{t_0} \left[\sum_{h=1}^{n} |x_h(\tau,\theta) - \tilde{x}_h(\tau,\theta)| + |c(\tau,\theta) - \tilde{c}(\tau,\theta)| \right.$$
$$\left. + |c_\tau(\tau,\theta) - \tilde{c}_\tau(\tau,\theta)| \right] e^{-\gamma_1 t_0 - \gamma_2 \tau} e^{-\gamma_1 (t_0 - \tau)} e^{-\gamma_2 (t-\theta)} d\tau.$$

Hence,

$$|C(t_0,t)) - \tilde{C}(t_0,t))|e^{-\gamma_1 t_0 - \gamma_2 t} \leq 2L_{n+1}||(\mathbf{x}, c, c_{t_0}) - (\tilde{\mathbf{x}}, \tilde{c}, \tilde{c}_{t_0})||/(\gamma_1\gamma_2). \quad (5.31)$$

Consider equation (5.29)

$$|C_{t_0}(t_0,t)) - \tilde{C}_{t_0}(t_0,t))|e^{-\gamma_1 t_0 - \gamma_2 t} \leq L_{n+2}\int_0^{t_0}\left[\sum_{h=1}^{n}|x_h(t_0,\theta) - \tilde{x}_h(t_0,\theta)|\right.$$

$$\left.+|c(t_0,\theta) - \tilde{c}(t_0,\theta)| + |c_{t_0}(t_0,\theta) - \tilde{c}_{t_0}(t_0,\theta)|\right] e^{-\gamma_1 t_0 - \gamma_2 \tau}e^{-\gamma_2(t-\theta)}d\theta.$$

Hence,

$$|C_{t_0}(t_0,t)) - \tilde{C}_{t_0}(t_0,t))|e^{-\gamma_1 t_0 - \gamma_2 t} \leq L_{n+2}||(\mathbf{x}, c, c_{t_0}) - (\tilde{\mathbf{x}}, \tilde{c}, \tilde{c}_{t_0})||/\gamma_2. \quad (5.32)$$

From (5.30)-(5.32) it follows that

$$||(\mathbf{y}, C, C_{t_0}) - (\tilde{\mathbf{y}}, \tilde{C}, \tilde{C}_{t_0})|| \leq p||(\mathbf{x}, c, c_{t_0}) - (\tilde{\mathbf{x}}, \tilde{c}, \tilde{c}_{t_0})||,$$

where

$$p = \frac{1}{\gamma_2}\sum_{i=1}^{n} L_i + \frac{2}{\gamma_1\gamma_2}L_{n+1} + \frac{1}{\gamma_2}L_{n+2}.$$

If the positive constants γ_1, γ_2 are chosen large enough, then $p < 1$ and A is a contractive map. So, the theorem is proved.

Corollary 1. Under the same hypotheses as Th. 1 the function $L \in C([0,T])$.

Proof. See equation (5.23).

5.3.3 Solution to free boundary problem

The integral system in Sec. 5.3.2 provides the solution for the biomass concentrations in the form

$$X_i = X_i(c(t_0,t),t),\ i = 1,...,n, \quad (5.33)$$

whereas the original problem requires the solution in the form

$$X_i = X_i(z,t),\ i = 1,...,n. \quad (5.34)$$

Since

$$z = c(t_0,t), \quad (5.35)$$

we immediately realize that a problem of inversion of the function c with respect to t_0 arises. This issue is analyzed in the following;

Theorem 2. Under the same hypotheses as Th. 1, if

$$\sigma(t_0) \geq \sigma_L > 0,\ G(c(t_0,t),t,\mathbf{x}(c(t_0,t),t)) \geq 0,\ 0 \leq t_0 \leq t \leq T, \tag{5.36}$$

then

$$c(t_0,t) > 0,\ c_{t_0}(t_0,t) > 0,\ 0 \leq t_0 \leq t \leq T. \tag{5.37}$$

In addition,

$$L(t_0) > 0,\ 0 < t_0 \leq t \leq T,\ \dot{L}(t_0) > 0,\ 0 \leq t_0 \leq t \leq T. \tag{5.38}$$

Proof. Inequalities (5.37) follow from the application of Picard's process of successive approximations to integral equations (5.21)-(5.22). Estimates (5.38) are easily derived from (5.12) and (5.23).

Now, the function c can be inverted and the function (5.34) is obtained.

Theorem 3. Under the same hypotheses as Th. 1, if

$$\psi_i(t_0) \geq 0,\ F_i(c(t_0,t),t,\mathbf{x}(c(t_0,t),t)) \geq 0,\ 0 \leq t_0 \leq t \leq T, \tag{5.39}$$

$i = 1, ..., n$, then

$$x_i(t_0,t) \geq 0,\ 0 \leq t_0 \leq t \leq T,\ i = 1, ..., n. \tag{5.40}$$

Proof. Inequality (5.39) follows from the application of Picard's process of successive approximations to integral equations (5.20).

Consider integral equation (5.8) rewritten in terms of fraction volumes $f_i = X_i/\rho_i$

$$f_i(c(t_0,t),t) = \psi_i(t_0)/\rho_i + \int_{t_0}^{t} (r_{M,i} - f_i G)\ d\tau,\ i = 1, ..., n. \tag{5.41}$$

Since $\psi_i(t_0)/\rho_i$, $i = 1, ..., n$, represent the initial fraction volumes, we must assume

$$\sum_{i=1}^{n} \psi_i(t_0)/\rho_i = 1. \tag{5.42}$$

Now, we expect that the same condition is satisfied by the sum of functions f_i at any time

$$f(c(t_0,t),t) = \sum_{i=1}^{n} f_i = 1 \ \forall t. \tag{5.43}$$

This result will be proved in Th. 4.

Theorem 4. Under the same hypotheses as Th. 1, if hypothesis (5.42) holds, then condition (5.43) is satisfied.

Proof. Summing (5.40) on i and using (5.42) yields

$$f(c(t_0,t),t) = 1 + \int_{t_0}^{t} G(1-f)\ d\tau,\ 0 \le t_0 \le t \le T, \tag{5.44}$$

with initial condition

$$f(c(t_0,t_0),t_0) = 1. \tag{5.45}$$

The initial value problem (5.44)-(5.45) has the unique solution $f = 1$.

5.4 Biological sulfate reducing biofilm

5.4.1 Introduction

Increasing anthropogenic activity has contributed to local imbalances in the natural sulfur cycle, leading to serious environmental problems. Industrial wastewater containing sulfate has contributed to this sulfur imbalance [139].

Sulfate can be removed from wastewaters by chemical precipitation or desalination processes but at high costs. Biological methods for the removal of sulfate from wastewater represent an attractive alternative.

A variety of reactors have been applied for biological treatment of sulfate rich wastewater such as batch reactors [129], baffled reactors [140] and gas-lift reactors [141, 142] that involve suspended-growth bacteria. In the last years biological sulfate reducing processes have been developed that involve a bacterial biomass attached to a media (biofilm), i.e. fixed bed reactors or fluidized bed reactors [143]. The environmental engineering processes that use a bacterial biomass attached to a media have generally been referred to as fixed-growth processes.

Under anaerobic conditions dissimilatory sulfate reducing bacteria (SRB) use sulfate as a terminal electron acceptor for the degradation of organic compounds [144]. In this anaerobic process sulfate is reduced to sulfide by the action of SRB which have the ability of coupling the oxidation of organic matter (electron donor) to the reduction of sulfate (electron acceptor) and depend on hydrolytic and fermentative bacteria that degrade complex organic matter [145].

The advantage of bacteria disposing in biofilm is very important in environmental industrial application. The bacteria in biofilm differently from suspended bacteria cannot be washed out with the water flow. This allows to retain the biomass within the reactor and therefore to operate at shorter hydraulic retention time (HRT). The bacterial biofilm allows to achieve higher biomass concentration in bioreactors, and allows the growth of bacteria in bioreactor locations where their food remains abundant. Also two main characteristics of biofilms offer great advantages in environmental applications: resistance to antimicrobial agents and formation in biofilm of several bacterial species. The resistance of antimicrobial agents allows a better resistance of bacteria when undesired inhibiting agents reach the wastewater treatment plant (shock loading). The formation in biofilm of several bacterial species allows to treat different organic and inorganic substrates at the same time. Biological sulfate reduction in anaerobic fixed growth reactors has been investigated extensively at lab-scale. In particular, it was pointed out that the composition of the microbial community influences the performance and

stability of the overall biological sulfate reducing process [146].

The model proposed in this section includes sulfate reduction by complete and incomplete sulfate reducing bacteria; COD removal by sulfate reduction and by acetogenic bacteria; acetate consumption via methanogenesis [146, 147, 4]. The biochemical mechanisms which regulate the competition between these trophic groups growing in anaerobic fixed growth reactors are nevertheless still mostly unknown. Thus, further research is needed to asses the effect of different process conditions on this competition and to define control criteria to favor the dominance of one species over the other. Mathematical models aimed at simulating the biochemical process prevailing in an anaerobic fixed growth reactor should be coupled to experimental studies in order to: i) address the laboratory experimental procedure; ii) enhance the design and operation of the treatment systems [116]; and iii) optimize the reactor process control criteria [142]. In this study a mathematical model was developed to describe the bacterial competition in sulfate reducing biofilms.

The objectives of this study include:

- to propose a new mathematical modelling approach to study population dynamics competition between sulfate reducing and acetate degrading bacteria in biofilms;
- to propose a new numerical approach to solve a multispecies biofilm model;
- to describe substrate dynamics, i.e. mass transport of substrates and their microbial conversion, which take place within the biofilm.

5.4.2 Mathematical model

The dynamics of a biological sulfate reducing biofilm are discussed. Physical, chemical and biological transient processes are analyzed. The kinetics of microbial growth and decay are modelled. The model considers the kinetics of three microbial species: complete oxidizers heterotrophic SRB (X_1), which completely oxidise lactate to CO_2, incomplete oxidizers heterotrophic SRB (X_2), which oxidise lactate to acetate, acetate degraders (X_3), and three reacting components (substrates and products): sulfate (S_1), lactate (S_2), acetate (S_3), fig. 5.2. The sulfate is used for the lactate oxidation by complete and incomplete SRB. inert residues (X_4) are also taken into account.

The undesired formation of acetate allows the development of acetate degraders which compete for space in the biofilm with complete and incomplete heterotrophic SRB.

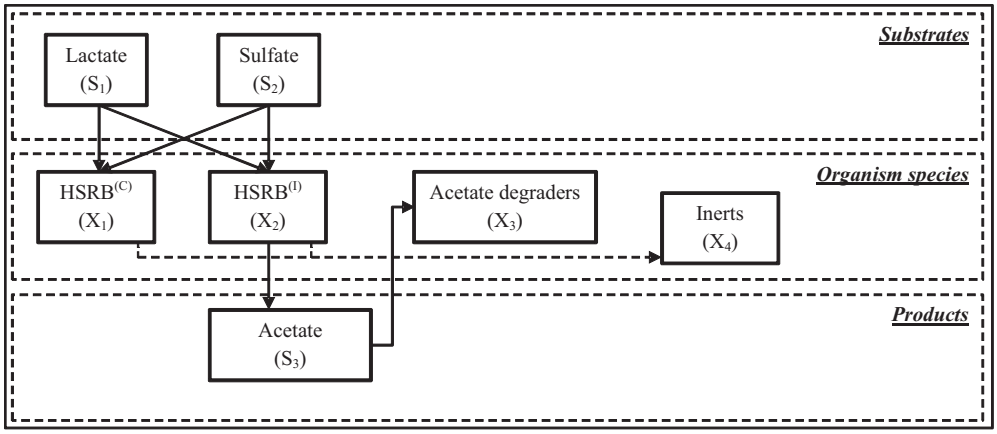

Figure 5.2: Main pathways of biological process

The biofilm growth is governed by the following equations [123, 136],

$$\frac{\partial X_i}{\partial t}+\frac{\partial}{\partial z}(uX_i) = \rho_i r_{M,i}(z,t,\mathbf{X},\mathbf{S}),\ 0 \le z \le L(t),\ t>0,\ i=1,2,3,4 \quad (5.46)$$

$$\frac{\partial u}{\partial z} = \sum_{i=1}^{3} r_{M,i}(z,t,\mathbf{X},\mathbf{S}),\ 0 < z \le L(t),\ t>0, \quad (5.47)$$

where $X_i = \rho_i f_i(z,t)$ denotes the concentration of the microbial species and inert residues $i = 1,2,3,4$, f_i volume fraction of microbial species i, $\sum_{i=1}^{4} f_i = 1$, ρ_i the constant density, $u(z,t)$ the velocity of the microbial mass displacement with respect to the biofilm support interface, $S_j(z,t)$ the concentration of substrate $j = 1,2,3$, $r_{M,i}(z,t,X_i,S_j)$ the biomass growth rate, $L(t)$ the biofilm thickness, $\mathbf{X} = (X_1,X_2,X_3,X_4)$ and $\mathbf{S} = (S_1,S_2,S_3)$.

In addition, the biomass growth rates are given by:

$$r_{M,1} = \mu_{\max,1} X_1 \frac{S_1}{K_{1,1}+S_1}\frac{S_2}{K_{2,1}+S_2} - b_{m,1}X_1, \quad (5.48)$$

$$r_{M,2} = \mu_{\max,2} X_2 \frac{S_1}{K_{1,2}+S_1}\frac{S_2}{K_{2,2}+S_2} - b_{m,2}X_2, \quad (5.49)$$

$$r_{M,3} = \mu_{\max,3} X_3 \frac{S_3}{K_{1,3}+S_3} - b_{m,3}X_3, \quad (5.50)$$

while for inert residues

$$r_{M,4} = b_{m,1}X_1 + b_{m,2}X_2 + b_{m,3}X_3, \quad (5.51)$$

where $\mu_{\max,i}$ denotes the maximum net growth rate for biomass i, $K_{i,j}$ the half-saturation constant of substrate j for biomass i, $b_{m,i}$ the decay-inactivation-rate concentration for biomass i.

The diffusion of substrates is governed by the equations

$$\frac{\partial S_j}{\partial t} - D_j \frac{\partial^2 S_j}{\partial z^2} = r_{S,j}(z,t,\mathbf{X},\mathbf{S}),\ 0<z<L(t),\ 0<t\le T,\ j=1,2,3, \quad (5.52)$$

where D_j denotes the diffusivity coefficient and $r_{S,j}(z,t,\mathbf{X},\mathbf{S})$ the conversion rate of substrate j. These are expressed by

$$r_{S,1} = -\frac{\mu_{\max,1}}{Y_1} X_1 \frac{S_1}{K_{1,1}+S_1}\frac{S_2}{K_{2,1}+S_2} - \frac{\mu_{\max,2}}{Y_2} X_2 \frac{S_1}{K_{1,2}+S_1}\frac{S_2}{K_{2,2}+S_2}, \quad (5.53)$$

$$r_{S,2} = -1.5\frac{(1-Y_1)\mu_{\max,1}}{Y_1} X_1 \frac{S_1}{K_{1,1}+S_1}\frac{S_2}{K_{2,1}+S_2} - 1.5\frac{(1-Y_2)\mu_{\max,2}}{Y_2} X_2 \frac{S_1}{K_{1,2}+S_1}\frac{S_2}{K_{2,2}+S_2}, \quad (5.54)$$

$$r_{S,3} = \frac{(1-Y_2)\mu_{\max,2}}{Y_2} X_2 \frac{S_1}{K_{1,2}+S_1}\frac{S_2}{K_{2,2}+S_2} - \frac{\mu_{\max,3}}{Y_3} X_3 \frac{S_3}{K_3+S_3}, \quad (5.55)$$

where Y_i denotes the yield for biomass i.

The following initial-boundary conditions will be considered for equations (5.1), (5.47) and (5.52)

$$X_i(z,0) = \varphi_i(z),\ u(0,t)=0,\ 0\le z\le L_0,\ 0<t\le T,\ i=1,2,3,4, \quad (5.56)$$

$$S_j(z,0) = S_{j0}(z),\ 0\le z\le L_0,\ j=1,2,3, \quad (5.57)$$

$$\frac{\partial S_j}{\partial z}(0,t)=0,\ S_j(L(t),t)=S_{jL}(t),\ 0<t\le T,\ j=1,2, \quad (5.58)$$

$$\frac{\partial S_3}{\partial z}(0,t) = \frac{\partial S_3}{\partial z}(L(t),t) = 0,\ 0<t\le T. \quad (5.59)$$

The functions $\varphi_i(z), i=1,...,n$, represent the initial concentrations. Condition $(5.56)_2$ follows from the relationship $g_i(0,t) = u(0,t)X_i(0,t)$ of the biomass flux at $z=0$. The functions $S_{j0}(z)$ represent the initial values of substrates. The functions $S_{jL}(t)$ in $(5.58)_2$ are the values of concentrations in the bulk liquid.

The free boundary evolution is governed by the following ordinary differential equation

$$\frac{dL}{dt}(t) = u(L(t),t), \quad (5.60)$$

with initial condition:

$$L(0) = L_0, \tag{5.61}$$

where L_0 denotes the initial biofilm thickness. Equation (5.59) is derived from the general equation of free boundary by setting the biomass flux $\sigma = 0$.

An existence and uniqueness theorem for the free boundary problem (5.1)-(5.60) was proved in [136] under quite general hypotheses. In addition, a number of properties for solutions was shown. Numerical methods will be discussed in the following section.

5.4.3 Numerical methods

The qualitative analysis of system (5.1)-(5.60) developed in [136] was based on the method of characteristics. The success suggests that this method can be also used in the numerical analysis. In this section we show that the method can be applied very easily. In addition, it is less expensive than other methods and allows us to perform computational analysis of transient biofilm processes very efficiently.

The characteristics of system (5.1) are the lines $z = s(s^0, t)$ defined by

$$\dot{s}(s^0, t) = u(s(s^0, t), t),\ s(s^0, 0) = s^0,\ 0 \le s^0 \le L_0,\ t > 0. \tag{5.62}$$

By introducing the characteristics and using the notations

$$G = \sum_i^4 r_{M,i} = G(z, t, \mathbf{X}, \mathbf{S}), \tag{5.63}$$

$$F_i = \rho_i r_{M,i} - X_i G = F_i(z, t, \mathbf{X}, \mathbf{S}), \tag{5.64}$$

system (5.1)-(5.47) is rewritten as

$$\frac{\partial u}{\partial s}(s, t) = G(s, t, \mathbf{X}, \mathbf{S}),\ 0 < s \le L(t),\ t > 0, \tag{5.65}$$

$$\dot{X}_i(s(s^0, t), t) = F_i(s(s^0, t), t, \mathbf{X}, \mathbf{S}),\ i = 1, 2, 3, 4,\ t > 0, \tag{5.66}$$

Consider equation (5.62). Integrating equation (5.62) over (t_n, t_{n+1}) yields

$$s_m^{n+1} - s_m^n = \int_{t_n}^{t_{n+1}} u(s(s_m^n, \tau), \tau)\ d\tau, \tag{5.67}$$

where $s_m^n = s(s^m, t_n)$. Consider equation (5.65). Integrating over (s_m^n, s_{m+1}^n) yields

$$u(s_{m+1}^n, t_n) - u(s_m^n, t_n) = \int_{s_m^n}^{s_{m+1}^n} G(s, t_n, \mathbf{X}, \mathbf{S})\ ds. \tag{5.68}$$

Consider the free boundary equation (5.58). Integrating over (t_n, t_{n+1}) yields

$$L(t_{n+1}) - L(t_n) = \int_{t_n}^{t_{n+1}} u(L(\tau), \tau)\ d\tau. \tag{5.69}$$

Furthermore, integrating equation (5.66) over (t_n, t_{n+1}) gives

$$X_i(s(s_m^n, t_{n+1}), t_{n+1}) - X_i(s(s_m^n, t_n), t_n) = \int_{t_n}^{t_{n+1}} F_i(s(s_m^n, \tau), \tau, \mathbf{X}, \mathbf{S})\ d\tau. \tag{5.70}$$

In Sec. 5.2.2, equations (5.67)-(5.70) will be integrated by using a fourth-order Runge-Kutta method. The flow-chart is illustrated in fig. 5.3.

Consider diffusion equation (5.52). Finite difference methods for parabolic equations can be used, e.g. [148]. Recent finite difference methods introduced in [149, 150] could also be experienced in future 2D and 3D applications. In Sec. 5.2.2, in the forward Euler method will be used and we obtain

$$S_{j,m}^{n+1} = S_{j,m}^n + \frac{\Delta t}{(\Delta z)^2}(S_{j,m-1}^n - 2S_{j,m}^n + S_{j,m+1}^n) + \Delta t r_{S,j,m}^n, \tag{5.71}$$

where

$$r_{S,j,m}^n = r_{S,j}(m\Delta z, n\Delta t, \mathbf{X}_m^n, \mathbf{S}_m^n). \tag{5.72}$$

5.4.4 Results and discussion

5.4.5 Simulation set 1: Effect of the COD/SO_4^{2-} ratio on the biofilm sulfate removal performances

Parameter values used for the simulations

The mathematical model proposed in this section has been applied to simulate the sulfate reduction process in a biological biofilm with an initial thickness of 2 mm. The initial conditions and biological parameters adopted in the simulations are reported in table 5.1. Values of the kinetic parameters, stoichiometric parameters and mass transfer coefficients according to [142] and [151] were used except for lactate mass transfer coefficient which resulted from the procedure proposed by [152].

By application of empirical formula of [153], the molecular diffusion coefficient, earlier in water D_w and after in biofilm D_f, was determined. The formula can be described as follows:

$$D_w = 7.4 \times 10^{-8} \frac{(\varphi_b M_b)^{0.5} T}{\mu_b V_a^{0.6}}$$

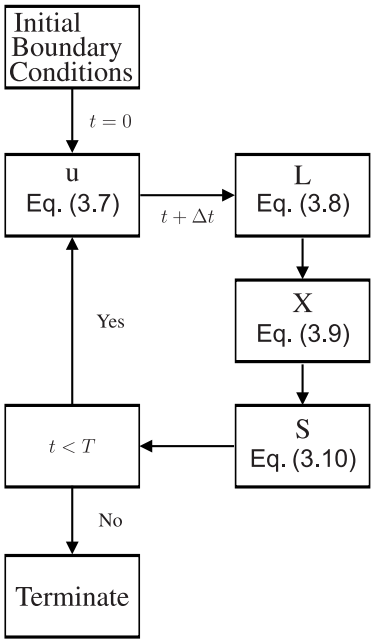

Figure 5.3: Flow-chart

where φ_b is solvent association parameter (2.6 for water), M_b molecular weight of solvent (18 g for water), T absolute temperature (expressed in K), μ_b solvent absolute viscosity (0.7208 cp for water at 35^oC), V_a molecular volumes of solute as liquid at its normal boiling point ($cm^3 mol^{-1}$). To obtain the diffusion coefficients in biofilm, the diffusion coefficients in water were multiplied by a factor of 0.8 to correct the additional diffusion resistance in the biofilm [154].

The computed values of molecular diffusion coefficients in dm^2 per *day* for sulfate, lactate and acetate are 0.00732 (dm^2/d), 0.00980 (dm^2/d) and 0.00835 (dm^2/d) respectively.

Figs. 5.4 and 5.5 show the results of model simulations performed to assess the COD/SO_4^{2-} ratio effect on the reactor performances in terms of volume fractions of bacteria and concentration trends of substrates in biofilm for a 0.5 days time simulation. COD/SO_4^{2-} ratios, in the range 0.125-1 were investigated.

Species and volumetric fractions of bacteria growing in the biofilm

Firstly the influence of the COD/SO_4^{2-} ratio on the bacteria prevailing in the biofilm was studied. The simulated film structures at four different COD/SO_4^{2-} ratios are shown in fig. 5.4. This figure indicates a high presence

Parameter	Unit	Set A	Set B	Set C	Set D
COD Concentration	$gCODl^{-1}$	0.2	0.1	0.05	0.025
Sulfate Concentration	gl^{-1}	0.2	0.2	0.2	0.2
Time Simulation	h	12	12	12	12
Initial Biofilm thickness	mm	2	2	2	2
Initial Volume Fraction of SRB	–	0.3	0.3	0.3	0.3
Initial Volume Fraction of SRB	–	0.3	0.3	0.3	0.3
Initial Volume Fraction of AD	–	0.3	0.3	0.3	0.3
Initial Volume Fraction of Inert	–	0.1	0.1	0.1	0.1

Table 5.1: Operational parameters used for model simulations. Set 1

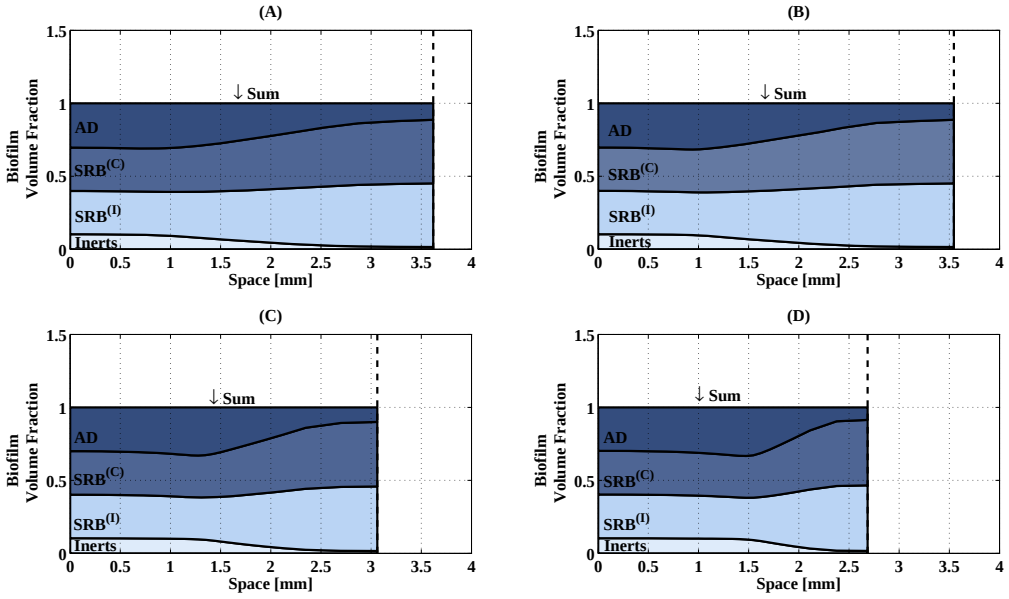

Figure 5.4: Effect of the COD/SO_4^{2-} ratio on the volumetric fraction of the bacterial species in biofilm. A: COD/SO_4^{2-}=1, B: COD/SO_4^{2-}=0.5, C: COD/SO_4^{2-}=0.25, D: COD/SO_4^{2-}=0.125

of acetate degraders at the inner layer of biofilm whereas SRB are dominant over acetate degraders at the outmost layer of biofilm. It is interesting to note that the area of acetate degraders in the biofilm becomes broader at decreasing COD/SO_4^{2-} ratios, figure 5.4 C and D. This occurs since the decreasing of COD surface load implies a lower sulfate reduction by the action of complete and incomplete SRB. In the deeper of biofilm sulfate

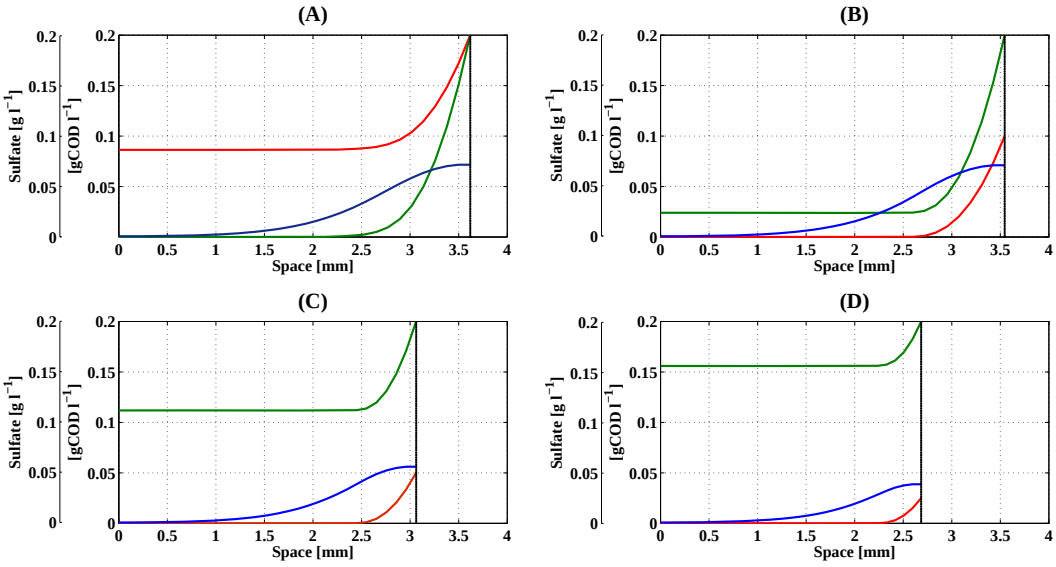

Figure 5.5: Effect of the COD/SO_4^{2-} ratio on the substrate trends in biofilm. Green line: sulfate concentration; red line: COD concentration; blue line: acetate concentration A: COD/SO_4^{2-}=1, B: COD/SO_4^{2-}=0.5, C: COD/SO_4^{2-}=0.25, D: COD/SO_4^{2-}=0.125

concentrations are lower than in the superficial layer of biofilm, therefore the acetate degraders prevail over the SRB. When the COD/SO_4^{2-} ratio is low the volumetric fraction of bacterial species is less homogeneous than at high COD/SO_4^{2-} ratios, fig. 5.4 C and D. .

Trends of substrate concentrations in biofilm

The different kinds of bacterial species growing in the biofilm at different COD/SO_4^{2-} ratios imply a different concentration trend of substrates in the biofilm. Figure 5.5 shows that a COD/SO_4^{2-} ratio increase causes an increase of sulfate reduction. When the COD/SO_4^{2-} ratio is 1, (fig. 5.5 A) there is a sharp decrease of sulfate concentration troughout the biofilm depth, with a concentration near to zero in the inner layer of biofilm. This occurs because the concentration of COD is not limiting for SRB metabolism.

When the COD/SO_4^{2-} ratio is less than 0,5 (figure 5.5, B, C and D) COD is limiting implying a decrease of the sulfate reduction rate. Many authors have reported the accumulation of acetic acid in several types of reactors working under sulfate-reducing conditions, and most of them agree that acetate is the bottleneck of sulfate reducing processes [146]. It is interesting to

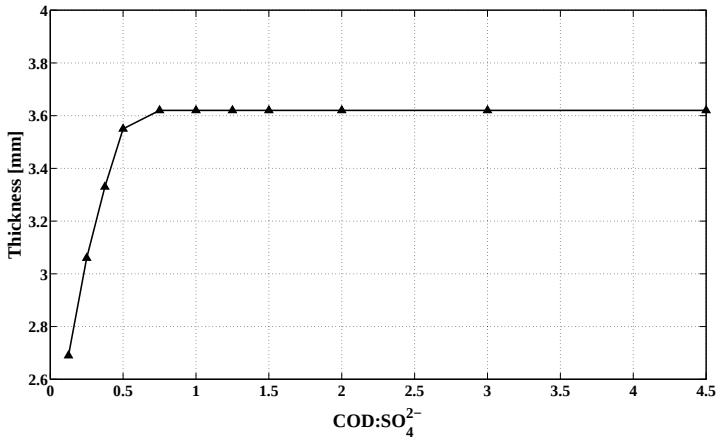

Figure 5.6: Effect of the COD/SO_4^{2-} ratio on biofilm thickness

note that the acetate production becomes broader at higher COD/SO_4^{2-} ratios. This was expected, since, at high COD/SO_4^{2-} ratio both complete and,

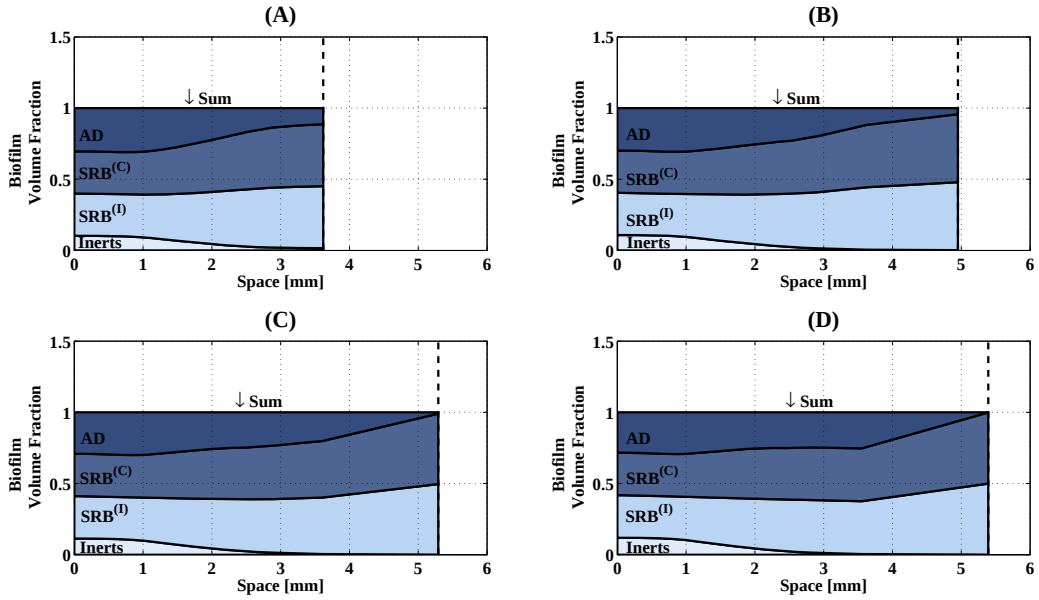

Figure 5.7: Effect of simulation time on the volumetric fraction of the bacterial species in biofilm. A: Simulation time=12h, B: Simulation time=24h, C: Simulation time=36h, D: Simulation time=48h

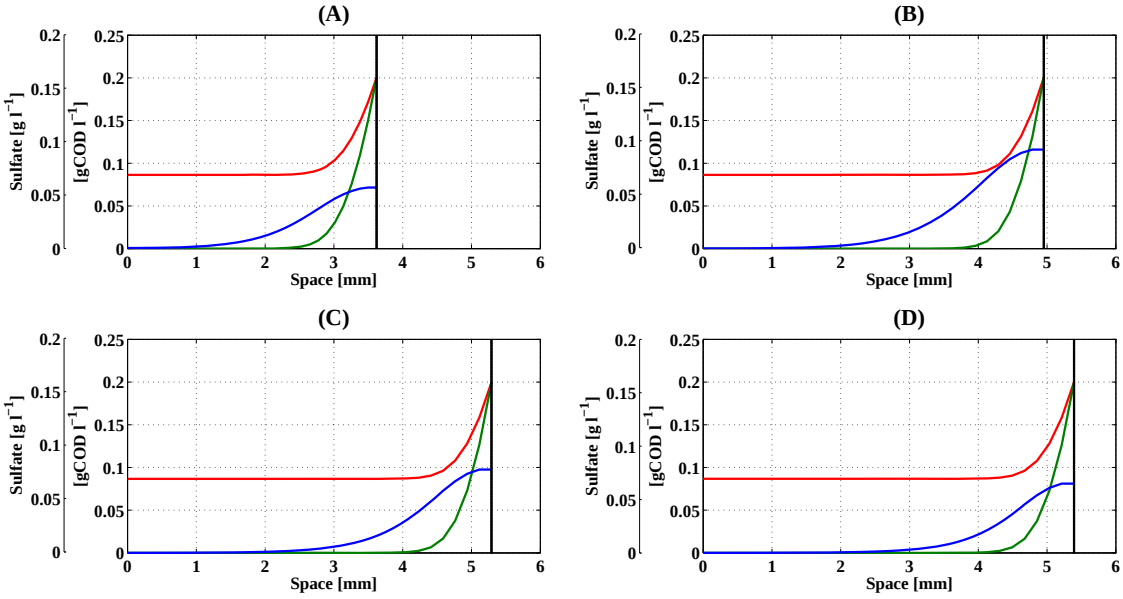

Figure 5.8: Effect of simulation time on the substrate trends in biofilm. Green line: sulfate concentration; red line: COD concentration; blue line: acetate concentration. A: Simulation time=12h, B: Simulation time=24h, C: Simulation time=36h, D: Simulation time=48h

in particular, incomplete SRB increase their metabolic activity, according to equations 5.48 and 5.49.

The relationship between COD/SO_4^{2-} ratio and biofilm thickness is shown in figure 5.6. At high COD/SO_4^{2-} ratios there is no increase of biofilm thickness. This is because SO_4^{2-} becomes a limiting substrate for biofilm bacteria metabolism and hence for biofilm growth.

5.4.6 Simulation set 2: Effect of simulation time on the biofilm sulfate removal performances

Species and volumetric fractions of bacteria growing in the biofilm

The effect of different simulation times was studied. When the simulation time increases the biofilm thickness increases, as expected. The effect of four different time simulations, and therefore, four different biofilm thicknesses are shown in figure 5.7 . The initial conditions and biological parameters adopted in the simulations are reported in table 5.2. Difference in biofilm

Parameter	Unit	Set A	Set B	Set C	Set D
COD Concentration	$gCODl^{-1}$	0.2	0.2	0.2	0.2
Sulfate Concentration	gl^{-1}	0.2	0.2	0.2	0.2
Time Simulation	h	12	24	36	48
Initial Biofilm thickness	mm	2	2	2	2
Initial Volume Fraction of SRB	–	0.3	0.3	0.3	0.3
Initial Volume Fraction of SRB	–	0.3	0.3	0.3	0.3
Initial Volume Fraction of AD	–	0.3	0.3	0.3	0.3
Initial Volume Fraction of Inert	–	0.1	0.1	0.1	0.1

Table 5.2: Operational parameters used for model simulations. Set 2

structure occurs when the time of simulation is greater than 1 day (figures 5.7 C and D). In this cases AD are predominantly active at the inner layer of the biofilm, while both complete and incomplete oxidizers SRB are found to be predominant at the outmost layer of biofilm.

Trends of substrate concentrations in biofilm

The four different diffuse substrate concentration trends in biofilm, for four different time simulations, are shown in figure 5.8. The trends of sulfate, COD and acetate concentrations is quite similar for all four simulations, in agreement with Dirichlet boundary condition.

Conclusions

- The experimental tests demonstrate the advantages for the anaerobic digestion process resulting from mixing different organic wastes. The first benefit is related to the possibility to make the digestion process faster, producing a significant amount of methane even in digesters sized with a low hydraulic retention time (HRT).
- Mixing OFMSW with a lower degradable but ammonia richer substrate, such as livestock manure, implies that the system is better shelter by sharp drop in pH, that is the main cause of the digestion process failure.
- Once the characteristics of the pure substrates are known, the mathematical model permits to evaluate a priori which substrates should be mixed and their percentages to optimize the performance of the process. Therefore the mathematical model can be reasonably applied for the co-digestion systems design.
- The mathematical model proposed is capable to assess the effect of the OFMSW particle size on the methane production rate and cumulative formation of a system performing an OFMSW and sewage sludge co-digestion process.
- The mathematical model can be used to assess the maximum OLR increase due to OFMSW addition that an anaerobic digester can tolerate. In particular, it can be applied to optimize the OFMSW addition into the anaerobic digesters of the MWWTPs. Model simulations show as an OLR excess results in a pH drop and thus a digester failure.
- The experiments demonstrated that K_{sbk} depends only on the nature and composition of the organic waste, while K_{sbk} is independent of the PSD of the OFMSW. The model calibration can therefore be performed on organic waste of any PSD and a PSD variation (e.g., if the OFMSW is pre-triturated) does not affect the calibrated K_{sbk} value.

- In the mathematical model of biological sulfate reduction gas-lift reactor, special attention is given to the competition between sulfate reduction and methanogenesis in the biological system. The proposed model adequately simulates the bioconversion processes in the gas-lift reactor, both under steady state and dynamic conditions. The model, also, gives a good prediction of the gas production and transfer from the liquid to the gas phase. The effects of the variations of the operational conditions on the bacterial competition in the gas-lift reactor can be properly predicted with this model, which thus can be used for process optimisation and control. Application of the present model shows that the hypotheses of the design model proposed by [3] are correct, confirming that the design model of [3] is a proper tool for sizing such bioreactors.

- In this work an analysis of solutions to a free boundary value problem for a multispecies biofilm growth model in one space dimension has been presented. The mathematical model is quite general and can include a large variety of special situations. An existence and uniqueness theorem is discussed and properties of solutions are given. The proposed model is able to simulate the competition among the bacteria growing in the biofilm. The method of characteristics is introduced for the numerical process. As in the qualitative analysis of solutions, where it was first presented, this method seems to be a powerful tool in this situation also. The model has been applied to simulate the sulfate reduction process in a biofilm for several purposes. In particular the effect of the COD/SO_4^{2-} ratio and the effect of different simulation times on the reactor performances in terms of volume fraction of bacterial species and substrate diffusion trends in biofilm have been assessed.

- The initial attached cell layer in multispecies biofilm growth is considered. The corresponding mathematical model leads to discuss a free boundary problem for a system of nonlinear hyperbolic partial differential equations, where the initial biofilm thickness is equal to zero. No assumptions on initial conditions for biomass concentrations and biofilm thickness are required. The data that the problem needs are the concentration of biomass in the bulk liquid and biomass flux from the bulk liquid. The method of characteristics is used to convert the differential system to Volterra integral equations for which an existence and uniqueness theorem is proved.

Appendix A

APPENDIX

A.1 Table 1A

	Component	1	2	3	4	5	6	7	8	9	10	11	12	rate ρ[kgCOD m^{-3} d^{-1}]
	Process	S_{su}	S_{aa}	S_{fa}	S_{va}	S_{bu}	S_{pro}	S_{ac}	S_{h2}	$S_{ch/4}$	S_{IC}	S_{IN}	S_I	
													$f_{SI,Xc}$	K_{shd} C a^*
1	Disintegration of OFMSW													$K_{dis,XSh}$ X_{Sh}
2	Disintegration of Sludge													$K_{dis\_ch\_R}$ X_{ch_R}
3	Hydrolysis of Carbohydrates (readily)													$K_{hyd\_ch\_R}$ X_{ch_R}
4	Hydrolysis of Carbohydrates (slowly)													$K_{hyd\_ch\_S}$ X_{ch_S}
5	Hydrolysis of Proteins (readily)		1											$K_{hyd\_pr\_R}$ X_{pr_R}
6	Hydrolysis of Proteins (slowly)		1											$K_{hyd\_pr\_S}$ X_{pr_S}
7	Hydrolysis of Lipids (readily)	1	$f_{fa,li}$											$K_{hyd\_li\_R}$ X_{li_R}
8	Hydrolysis of Lipids (slowly)	1	$f_{fa,li}$											$K_{hyd\_li\_S}$ X_{li_S}
9	Uptake of Sugars	1				$(1-Y_{su})f_{bu,su}$	$(1-Y_{su})f_{pro,su}$	$(1-Y_{su})f_{ac,su}$	$(1-Y_{su})Y_{h2,su}$		$C_{i,9}-f_{i,13}C_{i,28}$	$(Y_{su})N_{bac}$		$K_{m,su}\dfrac{S_{su}}{K_s+S_{su}}X_{su}\ I_1$
10	Uptake of Amino Acids		1		$(1-Y_{aa})f_{va,aa}$	$(1-Y_{aa})f_{bu,aa}$	$(1-Y_{aa})f_{pro,aa}$	$(1-Y_{aa})f_{ac,aa}$	$(1-Y_{aa})f_{h2,aa}$		$C_{i,10}-f_{i,13}C_{i,28}$	$(Y_{aa})N_{bac}$		$K_{m,aa}\dfrac{S_{aa}}{K_s+S_{aa}}X_{aa}\ I_1$
11	Uptake of LCFA			1				$(1-Y_{fa})0.7$	$(1-Y_{fa})0.3$			$(Y_{fa})N_{bac}$		$K_{m,fa}\dfrac{S_{fa}}{K_s+S_{fa}}X_{fa}\ I_2$
12	Uptake of Valerate				1			$(1-Y_{C4})0.31$	$(1-Y_{C4})0.15$			$(Y_{C4})N_{bac}$		$K_{m,C4}\dfrac{S_{va}}{K_s+S_{va}}X_{C4}\ \dfrac{1}{1+\frac{S_{bu}}{S_{va}}}\ I_2$
13	Uptake of Butyrate					1		$(1-Y_{C4})0.8$	$(1-Y_{C4})0.2$			$(Y_{C4})N_{bac}$		$K_{m,C4}\dfrac{S_{bu}}{K_s+S_{bu}}X_{C4}\ \dfrac{1}{1+\frac{S_{va}}{S_{bu}}}\ I_2$
14	Uptake of Propionate						$(1-Y_{pro})0.57$	$(1-Y_{pro})0.43$			$C_{i,14}-f_{i,13}C_{i,28}$	$(Y_{pro})N_{bac}$		$K_{m,pro}\dfrac{S_{pro}}{K_s+S_{pro}}X_{pro}\ I_2$
15	Uptake of Acetate						1			$(1-Y_{ac})$	$C_{i,15}-f_{i,13}C_{i,28}$	$(Y_{ac})N_{bac}$		$K_{m,ac}\dfrac{S_{ac}}{K_s+S_{ac}}X_{ac}\ I_3$
16	Uptake of Hydrogen							1		$(1-Y_{h2})$	$C_{i,16}-f_{i,13}C_{i,28}$	$(Y_{h2})N_{bac}$		$K_{m,h2}\dfrac{S_{h2}}{K_s+S_{h2}}X_{h2}\ I_1$
17	Decay of X_{su}										$C_{i,17}-f_{i,13}C_{i,26}$	$N_{i,17}-f_{i,13}N_{i,26}$		$K_{dec,Xsu}\ X_{su}$
18	Decay of X_{aa}										$C_{i,18}-f_{i,13}C_{i,26}$	$N_{i,18}-f_{i,13}N_{i,26}$		$K_{dec,Xaa}\ X_{aa}$
19	Decay of X_{fa}										$C_{i,19}-f_{i,13}C_{i,26}$	$N_{i,19}-f_{i,13}N_{i,26}$		$K_{dec,Xfa}\ X_{fa}$
20	Decay of X_{C4}										$C_{i,20}-f_{i,13}C_{i,26}$	$N_{i,20}-f_{i,13}N_{i,26}$		$K_{dec,XC4}\ X_{C4}$
21	Decay of X_{pro}										$C_{i,21}-f_{i,13}C_{i,26}$	$N_{i,21}-f_{i,13}N_{i,26}$		$K_{dec,Xpro}\ X_{pro}$
22	Decay of X_{ac}										$C_{i,22}-f_{i,13}C_{i,26}$	$N_{i,22}-f_{i,13}N_{i,26}$		$K_{dec,Xac}\ X_{ac}$
23	Decay of X_{h2}										$C_{i,23}-f_{i,13}C_{i,26}$	$N_{i,23}-f_{i,13}N_{i,26}$		$K_{dec,Xh2}\ X_{h2}$

Figure A.1: Petersen matrix of model equations for anaerobic co-digestion, part1.

A.2 Table 1B

	Component	13	14	15	16	17	18	19	20	21	22	23	24	25	26	27	28	
	Process	C	X_{ch_R}	X_{ch_S}	X_{Pr_R}	X_{Pr_S}	X_{li_R}	X_{li_S}	X_{su}	X_{aa}	X_{fa}	X_{C4}	X_{pro}	X_{ac}	X_{h2}	X_I	X_{xbi}	$rate$ $_j$ [$kgCOD$ m^{-3} d^{-1}]
1	Disintegration o f OFMSW	1	f_{Ch_Xc}	f_{Pr_Xc}	f_{Li_Xc}	f_{Xc}										f_{XI_Xc}	1	K_{dis_xbi} C a^* X_{xbi}
2	Disintegration o f Sludge	1	f_{Ch_Xbiu}	f_{Pr_Xbiu}	f_{Li_Xbiu}	f_s												$K_{hyd\_ch\_R}$ X_{ch_R}
3	Hydrolysis o f Carbohydrates (readily)		f_r	1														$K_{hyd\_ch\_S}$ X_{ch_S}
4	Hydrolysis o f Carbohydrates (slowly)		f_{Ch_Xc}		1													$K_{hyd\_pr\_R}$ X_{pr_R}
5	Hydrolysis o f Proteins (readily)		f_{Pr_Xc}			1												$K_{hyd\_pr\_S}$ X_{pr_S}
6	Hydrolysis o f Proteins (slowly)		f_r				1											$K_{hyd\_li\_R}$ X_{li_R}
7	Hydrolysis o f Lipids (readily)		f_{Li_Xc}					1										$K_{hyd\_li\_S}$ X_{li_S}
8	Hydrolysis o f Lipids (slowly)		f_s															
9	Uptake of Sugars								Y_{su}									$K_{m,su}$ $\frac{S_{su}}{K_s + S_{su}}$ X_{su} I_1
10	Uptake of Amino Acids									Y_{aa}								$K_{m,aa}$ $\frac{S_{aa}}{K_s + S_{aa}}$ X_{aa} I_1
11	Uptake of LCFA										Y_{fa}							$K_{m,fa}$ $\frac{S_{fa}}{K_s + S_{fa}}$ X_{fa} I_2
12	Uptake of Valerate											Y_{C4}						$K_{m,C4}$ $\frac{S_{va}}{K_s + S_{va}}$ X_{C4} $1 - \frac{1}{S_{va}/S_{bu}}$ I_2
13	Uptake of Butyrate											Y_{C4}						$K_{m,C4}$ $\frac{S_{bu}}{K_s + S_{bu}}$ X_{C4} $1 - \frac{1}{S_{va}/S_{bu}}$ I_2
14	Uptake of Propionate												Y_{pro}					$K_{m,pro}$ $\frac{S_{pro}}{K_s + S_{pro}}$ X_{pro} I_2
15	Uptake of Acetate													Y_{ac}				$K_{m,ac}$ $\frac{S_{ac}}{K_s + S_{ac}}$ X_{ac} I
16	Uptake of Hydrogen														Y_{h2}			$K_{m,h2}$ $\frac{S_{h2}}{K_s + S_{h2}}$ X_{h2} I_1
17	Decay of X_{su}	1							1									$K_{dec,Xsu}$ X_{su}
18	Decay of X_{aa}	1								1								$K_{dec,Xaa}$ X_{aa}
19	Decay of X_{fa}	1									1							$K_{dec,Xfa}$ X_{fa}
20	Decay of X_{C4}	1										1						$K_{dec,Xc4}$ X_{c4}
21	Decay of X_{pro}	1											1					$K_{dec,Xpro}$ X_{pro}
22	Decay of X_{ac}	1												1				$K_{dec,Xac}$ X_{ac}
23	Decay of X_{h2}	1													1			$K_{dec,Xh2}$ X_{h2}

Figure A.2: Petersen matrix of model equations for anaerobic co-digestion, part2.

A.3 Table 1C

Components →	1	2	3	4	5	6	7	8	9	10	11	12	13	14	15	16	
Process ↓	S_{SO_4}	$S_{H_2}^{liq}$	$S_{H_2}^{gas}$	$S_{CO_2}^{liq}$	$S_{CO_2}^{gas}$	$S_{CH_4}^{liq}$	$S_{CH_4}^{gas}$	$S_{H_2S}^{liq}$	$S_{H_2S}^{gas}$	S_{Ace}	X_{ASRB}	X_{HSRB}	X_{HB}	X_{MA}	X_{AD}	X_I	**Rate** ρ_j [kgCOD m^{-3} d^{-1}]
Sulfate Reduction by X_{ASRB}	-1.5(1-$Y_{ASRB,H2}$)	-1		-1				(1-$Y_{ASRB,H2}$)			$Y_{ASRB,H2}$						$\nu_{ASRB} \cdot X_{ASRB}$
Sulfate Reduction by X_{HSRB}	-1.5(1-$Y_{HSRB,H2}$)	-1						(1-$Y_{HSRB,H2}$)		-1		$Y_{HSRB,H2}$					$\nu_{HSRB} \cdot X_{HSRB}$
Uptake of Hydrogen by X_{HB}		-1		-1						1- $Y_{HB,H2}$			$Y_{HB,H2}$				$\nu_{HB} \cdot X_{HB}$
Uptake of Hydrogen by X_{MA}		-1		-1		(1-$Y_{MA,Ac}$)								$Y_{MA,H2}$			$\nu_{MA} \cdot X_{MA}$
Uptake of Acetate						(1-$Y_{AD,Ac}$)				-1					$Y_{AD,H2}$		$\nu_{AD} \cdot X_{AD}$
Decay of X_{ASRB}											-1					+1	$K_{dec,X_{ASRB}} \cdot X_{ASRB}$
Decay of X_{HSRB}												-1				+1	$K_{dec,X_{HSRB}} \cdot X_{HSRB}$
Decay of X_{HB}													-1			+1	$K_{dec,X_{HB}} \cdot X_{HB}$
Decay of X_{MA}														-1		+1	$K_{dec,X_{MA}} \cdot X_{MA}$
Decay of X_{AD}															-1	+1	$K_{dec,X_{AD}} \cdot X_{AD}$
H_2 transfer		-1	+1														$K_{La,H_2} \cdot \left(S_{H_2}^{liq} - S_{H_2}^{gas} H_{H_2}\right)$
CO_2 transfer				-1	+1												$K_{La,CO_2} \cdot \left(S_{CO_2}^{liq} - S_{CO_2}^{gas} H_{CO_2}\right)$
CH_4 transfer						-1	+1										$K_{La,CH_4} \cdot \left(S_{CH_4}^{liq} - 64 \cdot \left(K_{H,CH_4} \cdot P_{gas,CH_4}\right)\right)$
H_2S transfer		-1	+1														$K_{La,H_2S} \cdot \left(S_{H_2S}^{liq} - 48 \cdot \left(K_{H,H_2S} \cdot P_{gas,CH_4}\right)\right)$

Figure A.3: Petersen Matrix for suspended-growth sulfate reducing model

A.4 Table 2C

	Rate ρ_j [kgCOD m^{-3} d^{-1}]
ASRB	$\hat{}_{ASRB} \frac{S_{H_2}^{liq}}{K_{SRB,H_2} + S_{H_2}^{liq}} \frac{S_{H_2tSRB}}{S_{H_2tSRB}} \frac{S_{SO_4}}{K_{SRB,SO_4} + S_{SO_4}} \frac{S_{SO_4tSRB}}{S_{SO_4tSRB}} \frac{S_{CO_2}^{liq}}{K_{SRB,CO_2} + S_{CO_2}^{liq}}$
HSRB	$\hat{}_{HSRB} \frac{S_{H_2}^{liq}}{K_{SRB,H_2} + S_{H_2}^{liq}} \frac{S_{H_2tSRB}}{S_{H_2tSRB}} \frac{S_{SO_4}}{K_{SRB,SO_4} + S_{SO_4}} \frac{S_{SO_4tSRB}}{S_{SO_4tSRB}} \frac{S_{Ace}}{K_{SRB,Ac} + S_{Ace}}$
HB	$\hat{}_{HB} \frac{S_{H_2}^{liq}}{K_{HB,H_2} + S_{H_2}^{liq}} \frac{S_{H_2tHB}}{S_{H_2tHB}} \frac{S_{CO_2}^{liq}}{K_{HB,CO_2} + S_{CO_2}^{liq}}$
MA	$\hat{}_{MA} \frac{S_{H_2}^{liq}}{K_{MA,H_2} + S_{H_2}^{liq}} \frac{S_{H_2tMA}}{S_{H_2tMA}} \frac{S_{CO_2}^{liq}}{K_{MA,CO_2} + S_{CO_2}^{liq}}$
AD	$\hat{}_{AD} \frac{S_{Ace}}{K_{AD,Ace} + S_{Ace}}$

Figure A.4: Net specific utilization rates for suspended-growth sulfate reducing model

A.5 Table 3C

	Components ?	2	3	6	8	11	12	13	14	15	16	
	Process ?	S_{SO_4}	$S_{H_2}^{liq}$	$S_{CO_2}^{liq}$	$S_{H_2S}^{liq}$	S_{Ace}	$S_{CH_4}^{liq}$	X_{HSRB}	X_{HB}	X_{MA}	X_I	**Rate** ρ_j [kgCOD m^{-3} d^{-1}]
1	Sulphate Reduction by X_{HSRB}	-1,5(1-$Y_{HSRB,H2}$)	-1		(1-$Y_{HSRB,H2}$)	-1		$Y_{HSRB,H2}$				$\hat{}_{HSRB} \frac{S_{H_2e}}{K_{SRB,H_2}} \frac{S_{H_2}}{S_{H_2e}} \frac{S_{H_2SRB}}{S_{H_2SRB}} \frac{S_{SO_4e}}{K_{SRB,SO_4}} \frac{S_{SO_4SRB}}{S_{SO_4e}} \frac{S_{SO_4SRB}}{S_{SO_4SRB}} \frac{S_{Ace}}{K_{SRB,Ac}} \frac{S_{Ace}}{S_{Ace}} X_{HSRB}$
2	Uptake of Hydrogen by X_{HB}		-1	-1		+1			$Y_{HB,H2}$			$\hat{}_{HB} \frac{S_{H_2e}}{K_{HB,H_2}} \frac{S_{H_2HB}}{S_{H_2e}} \frac{S_{H_2HB}}{S_{H_2HB}} \frac{S_{CO_2e}}{K_{HB,CO_2}} \frac{S_{CO_2e}}{S_{CO_2e}} X_{HB}$
3	Uptake of Hydrogen by X_{MA}		-1	-1			+1			$Y_{MA,H2}$		$\hat{}_{HB} \frac{S_{H_2e}}{K_{MA,H_2}} \frac{S_{H_2MA}}{S_{H_2e}} \frac{S_{H_2MA}}{S_{H_2MA}} \frac{S_{CO_2e}}{K_{MA,CO_2}} \frac{S_{CO_2e}}{S_{CO_2e}} X_{MA}$
4	Decay of X_{HSRB}							-1			+1	$K_{dec,X_{HSRB}} X_{HSRB}$
5	Decay of X_{HB}								-1		+1	$K_{dec,X_{HB}} X_{HB}$
6	Decay of X_{MA}									-1	+1	$K_{dec,X_{MA}} X_{MA}$
		Sulphate	Liquid phase concentration for hydrogen	Liquid phase concentration for dioxide carbon	Liquid phase concentration for hydrogen sulphide	Acetate		Heterotrophic sulphate reducing bacteria	Homoacetogenic bacteria		Inert	

Figure A.5: Petersen Matrix for model 1B proposed by Esposito et al. (2009)

Bibliography

[1] G Esposito, L Frunzo, A Panico, and G d' Antonio. Mathematical modelling of disintegration–limited co–digestion of ofmsw and sewage sludge. *Water Sci Technol*, 58(7):1513–1519, 2008.

[2] G Esposito, J Wejma, F Pirozzi, and P N L Lens. Effect of the sludge retention time on H_2 utilization in a sulfate reducing gas-lift reactor. *Process Biochem*, 39:491–498, 2003.

[3] G Esposito, P N L Lens, and F Pirozzi. User-friendly mathematical model for the design of sulfate reducing H_2/CO_2 fed bioreactors. *J Environ Eng ASCE*, 135:167–175, 2009.

[4] D J Batstone, J Keller, I Angelidaki, S V Kalyuzhnyi, Pavlostathis S V, A Rozzi, W T M Sanders, H Siegrist, and VA Vavilin. *Anaerobic digestion model no.1.* Rep. No. 13 IWA Publishing, London, 2002.

[5] F Blumensaat and J Keller. Modelling of two–stage anaerobic digestion using the iwa anaerobic digestion model no. 1 (adm1). *Water Res*, 39(1):171–183, 2005.

[6] P Plaza, P Robredo, O Pacheco, and A Saravia Toledo. Anaerobic treatment of municipal solid waste. *Water Sci Technol*, 33:169–175, 1996.

[7] M Ward S Poschl and P Owende. Evaluation of energy efficiency of various biogas production and utilization pathways. *Appl Ener*, 87:3305–33321, 2010.

[8] A Karagiannidis and G. Perkoulidis. A multi–criteria ranking of different technologies for the anaerobic digestion for energy recovery of the organic fraction of municipal solid wastes. *Bioresource Technol*, 100:2355–2360, 2009.

[9] F Tambone, P Genevini, D' Imporzano G, and F. Adani. Assessing amendment properties of digestate by studying the organic matter composition and the degree of biological stability during the anaerobic digestion of the organic fraction of msw. *Bioresource Technol*, 100:3140–3142, 2009.

[10] J Mata-Alvarez, Macé S, and P. Llabrés. Anaerobic digestion of organic solid wastes. an overview of research achievements and perspectives. *Bioresource Technol*, 74:3–16, 2000.

[11] A Donoso Bravo, J Mailier, J Martin, C Rodriguez, C A Aceves Lara, and A V Wouwer. Model selection, identification and validation in anaerobic digestion: A review. *Water Res*, 45(17):5347–5364, 2011.

[12] J Mata Alvarez. Fundamentals of the anaerobic digestion process. In J Mata Alvarez, editor, *Biomethanization of the Organic Fraction of Municipal Solid Wastes*, pages 1–20. IWA publishing, Alliance House, 12 Caxton street, London UK, 2002.

[13] P Mähnert and B Linke. Kinetic study of biogas production from energy crops and animal waste slurry. effect of organic loading rate and reactor size. *Environ Technol*, 30(1):93–99, 2009.

[14] L Björnsson, M Murto, and B Mattiasson. Evaluation of parameters for monitoring an anaerobic co-digestion process. *Appl Microbiol Biot*, 54:844–849, 2000.

[15] M Henze, P Harremöes, J la Cour Jansen, and E Arvin. *Wastewater treatment: biological and chemical processes (3rd Ed.)*. Springer, Berlin, 2001.

[16] M Hansson, A Nordberg, I Sundh, and B Mathisen. Early warning of disturbances in a laboratory-scale msw biogas process. *Water Sci Technol*, 45(10):255–260, 2002.

[17] I Angelidaki, M Alves, D Bolzonella, L Borzacconi, J L Campos, A J Guwi, S Kalyuzhnyi, Jenicek P, and J B Van Lier. Defining the biomethane potential (bmp) of solid organic wastes and energy crops: a proposed protocol for batch assays. *Water Sci Technol*, 59:927–934, 2009.

[18] Pagga U and D B Beimborn. Anaerobic biodegradation test for organic compounds. *Chemosphere*, 27:1499–1509, 1993.

[19] F Raposo, V Fernandez-Cegri, M A De la Rubia, R Borja, F Beline, C Cavinato, G Demirer, B Fernandez, M Fdz-Polanco, J C Frigon, R Ganesh, P Kaparaju, J Koubova, R Mendez, G Menin, A Peene, P Scherer, M Torrijos, H Uellendahl, Wierinckm I, and V DeWilde. Biochemical methane potential (bmp) of solid organicsubstrates: evaluation of anaerobic biodegradability using data from an international-interlaboratory study. *J Chem Technol Biot*, 86:1088–1098, 2001.

[20] K J Chae, Jang A, S K Yim, and S Kim. The effects of digestion temperature and temperature shock on the biogas yields from the mesophilic anaerobic digestion of swine manure. *Bioresource Technol*, 99:1–6, 2008.

[21] A Del Borghi, A Converti, E Palazzi, and M Del Borghi. Hydrolysis and thermophilic anaerobic digestion of sewage sludge and organic fraction of municipal solid waste. *Bioprocess Engin*, 20:553–560, 1999.

[22] Gungor-Demirci G and G N Demirer. Effect of initial cod concentration, nutrient addition, temperature and microbial acclimation on anaerobic treatability of broiler and cattle manure. *Bioresource Technol*, 93:109–117, 2004.

[23] W F Owen, D C Stuckey, JB Healy Jr., Young L Y, and P L McCarty. Bioassay for monitoring biochemical methane potential and anaerobic toxicity. *Water Res*, 13:485–492, 1979.

[24] T Forster-Carneiro, Perez M, and L I Romero. Influence of total solid and inoculum contents on performance of anaerobic reactors treating food waste. *Bioresource Technol*, 99:6994–7002, 2008.

[25] N Hamzawi, Kennedy K J, and D D Mclean. Anaerobic digestion of co-mingled municipal solid-waste and sewage-sludge. *Water Sci Technol*, 38(2):127–132, 1998.

[26] M A Barlaz. Methane production from municipal refuse: a review of enhancement techniques and microbial dynamics. *Crit Rev Env Contr*, 19:557–584, 1990.

[27] W T M Sanders. *Anaerobic hydrolysis during digestion of complex substrates*. PhD thesis, Wageningen Universiteit, Wageningen, The Netherlands, 2001.

[28] Vavilin V A and I Angelidaki. Anaerobic degradation of solid material: Importance of initiation centers for methanogenesis, mixing intensity, and 2d distributed model. *Biotechnol Bioeng*, 89(1):113–122, 2005.

[29] G Esposito, L Frunzo, A Panico, and F Pirozzi. Modelling the effect of the olr and ofmsw particle size on the performances of an anaerobic co–digestion reactor. *Process Biochem*, 46(2):557–565, 2011a.

[30] L Neves, Oliveira R, and M M Alves. Influence of inoculum activity on the bio-methanization of a kitchen waste under different waste/inoculum ratios. *Process Biochem*, 39:2019–2024, 2004.

[31] F Raposo, M A De la Rubia, R Borja, M Alaiz, Beltran J, and C Cavinato. *An interlaboratory study as a useful tool for proficiency testing of chemical oxygen demand measurements using solid substrates and liquid samples with high suspended solid content*, volume 80. Talanta, 2009.

[32] G Liu, R Zhang, El-Mashad H M, and R Dong. Effect of feed to inoculum ratios on biogas yields of food and green wastes. *Bioresource Technol*, 100(21):5103–5108, 2009.

[33] F Concannon, P J Reynolds, Hennigan A, and E Colleran. Automated measurement of the specific methanogenic activity of anaerobic digestion biomass. *Bioch Soc Trans*, 17:425, 1988.

[34] *[ISO/DIS 14853] Determination of the ultimate anaerobic biodegradability of plastic materials in an aqueous system Method by measurement of biogas production.* Talanta, 1999.

[35] Valcke D and W Verstraete. A practical method to estimate the acetoclastic methanogenic biomass in anaerobic sludge. *J Water Poll Contr Fed*, 55:1191–1195, 1983.

[36] T L Hansen, J E Schmidt, I Angelidaki, E Marca, J C Jansen, MosbÃŠk H, and T H Christensen. Measurement of methane potentials of solid organic waste. *Waste Manage*, 24:393–400, 2004.

[37] Carrére, H Rafrafi, Y A Battimelli, M Torrijos, Delgenés J P, and G Ruysschaert. Methane potential of waste activated sludge and fatty residues: Impact of codigestion and alkaline pretreatments. *Open Environ Eng J*, 3:71–76, 2010.

[38] J Rantala and B Ahring. A two–stage thermophilic anaerobic process for the treatment of source sorted household solid waste. *Biotechnol Lett*, 16:1097–1102, 1994.

[39] F G Pohland. Landfill bioreactors: fundamentals and practice. *Water Qual Int*, pages 18–22, 1996.

[40] D Reinhart and T Townsend. *Landfill Bioreactor Design and Operation.* Lewis Publishers, Boca Raton, FL, 1998.

[41] N Hamzawi, K J Kennedy, and D D Mc Lean. Technical feasibility of anaerobic codigestion of sewage sludge and municipal solid waste. *Environ Technol*, 19:993–1003, 1998.

[42] P Sosnowski, A Wieczorek, and S Ledakowicz. Anaerobic co–digestion of sewage sludge and organic fraction of municipal solid wastes. *Adv Environ Res*, 7:609–616, 2003.

[43] D L Hawkes. Factors affecting net energy production from mesophilic anaerobic digestion. In D A Stratford, B I Wheatley, and D E Hughes, editors, *Anaerobic Digestion*, pages 131–150. Applied Science Publishers, London, 1980.

[44] G Tchobanoglous, Theisen H, and S Vigil. *Integrated Solid Waste Management.* McGraw–Hill Inc, New York, 1993.

[45] APHA/AWWA/WEF. *Standards Methods for the Examination of Water and Wastewater, 20th ed.* United Book Press, Inc., Baltimore, Maryland (USA), 1998.

[46] L M L Nollet. *Handbook of Food Analysis, second ed., revised and expanded. Marcel Dekker.* Marcel Dekker, Â©2004, New York (USA), 2004.

[47] A Galí, T Benabdallah, S Astals, and J Mata-Alvarez. Modified version of adm1 model for agro–waste application. *Bioresource Technol*, 100(11):2783–2790, 2009.

[48] *Annual book of ASTM standards*, volume 04. Waste Management, 2011.

[49] Y Chen, J J Cheng, and K S Creamer. Inhibition of anaerobic digestion process: A review. *Bioresource Technol*, 99(10):4044–4064, 2008.

[50] I Angelidaki, L Ellegaard, and B K Ahring. A mathematical model for dynamic simulation of anaerobic digestion of complex substrates: focusing on ammonia inhibition. *Biotechnol Bioeng*, 42(2):159–166, 1993.

[51] BE Rittman. Opportunities for renewable bioenergy using microorganisms. *Biotechnol Bioeng*, 100(2):203–212, 2008.

[52] J B Van Lier. High-rate anaerobic wastewater treatment: diversifying from end-of-the-pipe treatment to resourceoriented conversion techniques. *Water Sci Technol*, 57(8):1137–1148, 2008.

[53] D T Hill and C Barth. A dynamical model for simulation of animal waste digestion. *J of Water Pol Control Fed*, 10:2129–2143, 1977.

[54] C Kleinstreuer and T Poweigha. Dynamic simulator for anaerobic digestion processes. *Biotechnol Bioeng*, 24(9):1941–1951, 1982.

[55] D T Hill. A comprehensive dynamic model for animal waste methanogenesis. *Transactions of the ASAE*, 25(5):1374–1380, 1982.

[56] J D Bryers. Structured modeling of the anaerobic digestion of biomass particulates. *Biotechnol Bioeng*, 27(5):638–649, 1985.

[57] H N Gavala, I V Skiadas, N A Bozinis, and G Lyberatos. Anaerobic co–digestion of agricultural industries wastewaters. *Water Sci Technol*, 34(11):67–75, 1996.

[58] S V Kalyuzhnyi. Batch anaerobic digestion of glucose and its mathematical modeling. ii. description, verification and application of model. *Biotechnol Bioeng*, 59(2–3):249–258, 1997.

[59] F E Mosey. Mathematical modelling of the anaerobic digestion process: Regulatory mechanisms for the formation of short-chain volatile acids from glucose. *Water Sci Technol*, 15(8–9):209–232, 1983.

[60] P Pullammanapallil, J M Owens, S A Svoronos, G Lyberatos, and D P Chynoweth. Dynamic model for conventionally mixed anaerobic digestion reactors. *AIChE Annual Meeting*, paper277c:43–53, 1991.

[61] D J Costello, P F Greenfield, and P L Lee. Dynamic modelling of a single-stage high-rate anaerobic reactor–i. model derivation. *Water Res*, 25(7):847–858, 1991.

[62] D J Costello, P F Greenfield, and P L Lee. Dynamic modelling of a single-stage high-rate anaerobic reactor–ii. model verification. *Water Res*, 25(7):859–871, 1991.

[63] M Ruzicka. The effect of hydrogen on acidogenic glucose cleavage. *Water Res*, 30(10):2447–2451, 1996.

[64] M Ruzicka. An extension of the mosey model. *Water Res*, 30(10):2440–2446, 1996.

[65] D Batstone, J Keller, R Newell, and M Newland. Modelling anaerobic degradation of complex wastewater. i: model development. *Bioresource Technol*, 75(1):67–74, 2000.

[66] H N Gavala, I Angelidaki, N A, and B K Ahring. kinetics and modeling of anaerobic digestion process. In T Scheper, editor, *Biomethanation I*, pages 57–94. Springer, New York, 2003. Scheper T (Series Editor): Advances in biochemical/biotechnology, vol 81.

[67] I Angelidaki, L Ellegaard, and B K Ahring. A comprehensive model of anaerobic bioconversion of complex substrates to biogas. *Biotechnol Bioeng*, 63(3):363–372, 1999.

[68] V A Vavilin, V B Vasiliev, A V Ponomarev, and S V Rytow. Simulation-model methane as a tool for effective biogas production during anaerobic conversion of complex organicmatter. *Bioresource Technol*, 48(1):1–8, 1994.

[69] M Fuentes, N J Scenna, P A Aguirre, and MC Mussati. Application of two anaerobic digestion models to biofilm systems. *Biochem Eng J*, 38(3):259–269, 2008.

[70] D J Batstone and J Keller. Industrial applications of the iwa anaerobic digestion model no 1 (adm1). *Water Sci Technol*, 47(12):199–206, 2003.

[71] V Fedorovich, P Lens, and S Kalyuzhnyi. Extension of anaerobic digestion model no 1 with process of sulphate reduction. *Appl Biochem Biotech*, 109(1–3):33–45, 2003.

[72] I Ramirez, A Mottet, Carrere, H S Deleris, Vedrenne F, and J P Steyer. Modified adm1 disintegration/hydrolysis structures for modeling batch thermophilic anaerobic digestion of thermally pretreated waste activated sludge. *Water Research*, 43(14):3479–3492, 2009.

[73] N A Bozinis, I E Alexiou, and E N Pistikopoulos. A mathematical model for the optimal design and operation of an anaerobic co–digestion plant. *Water Sci Technol*, 34:383–391, 1996.

[74] G Kiely, G Tayfur, C Dolan, and K Tanji. Physical and mathematical modelling of anaerobic digestion of organic wastes. *Water Res*, 31(3):534–540, 1997.

[75] S Jeyaseelan. A simple mathematical model for anaerobic digestion process. *Water Sci Technol*, 35(8):185–191, 1997.

[76] R M Dinsdale, G C Premier, F R Hawkes, and D L Hawkes. Two–stage anaerobic co–digestion of waste activated sludge and fruit/vegetable waste using inclined tubular digesters. *Bioresource Technol*, 72(2):159–168, 2000.

[77] J A Eastman and J F Ferguson. Solubilization of particulate organic carbon during the acid phase of anaerobic digestion. *J Water Pollut Contr Fed*, 53(3):352–366, 1981.

[78] S Ghosh. Pilot–scale demonstration of 2–phase anaerobic digestion of activated–sludge. *Water Sci Technol*, 23(3):1179–1188, 1991.

[79] J Mata-Alvarez, S Mace, P Llabres, and S Astlas. Codigestion of solid wastes: a review of its uses and perspectives including modeling. *Crit Rev Biotechnol*, 31(2):99–111, 2011.

[80] M Lübken, M Wichern, F Bischof, S Prechtl, and H Horn. Development of an empirical mathematical model for describing and optimizing the hygiene potential of a thermophilic anaerobic bioreactor treating faeces. *Water Sci Technol*, 55(7):95–102, 2007.

[81] B Fezzani and R B Cheikh. Extension of the anaerobic digestion model no. 1 (adm1) to include phenolic compounds biodegradation processes for simulating of anaerobic co–digestion of olive mill wastes at mesophilic temperature. *j hazard mater*, 162(2–3):1563–1570, 2009.

[82] U Zaher, R Li, U Jeppsson, J P Steyer, and S Chen. Giscod: General integrated solid waste co–digestion model. *Water Res*, 43(10):2717–2727, 2009.

[83] G Esposito, L Frunzo, A Panico, and F Pirozzi. Model calibration and validation for ofmsw and sewage sludge co–digestion reactors. *Waste Manage.* in press, doi:10.1016/j.wasman.2011.07.024.

[84] F J Buendía, IM andFernández, J Villaseñor, and L Rodríguez. Feasibility of anaerobic co–digestion as a treatment option of meat industry wastes. *Bioresource Technol*, 100(6):1903–1909, 2009.

[85] P Sosnowski, A Klepacz-Smolka, K Kaczorek, and S Ledakowicz. Kinetic investigations of methane co–fermentation of sewage sludge and organic fraction of municipal solid wastes. *Bioresource Technol*, 99(13):5731–5737, 2011.

[86] S Ponsá, T Gea, and A Sánchez. Anaerobic co–digestion of the organic fraction of municipal solid waste with several pure organic co–substrates. *Biosystems Eng*, 108(4):352–360, 2011.

[87] K Derbal, M Bencheikh-Lehocine, F Cecchi, A H Meniai, and P Pavan. Application of the iwa adm1 model to simulate anaerobic co–digestion of organic waste with waste activated sludge in mesophilic condition. *Bioresource Technol*, 100(4):1539–1543, 2009.

[88] H Spanjers and P Vanrolleghem. Respirometry as a tool for rapid characterization of wastewater and activated sludge. *Water Sci Technol*, 31:105–114, 2007.

[89] A De Lucas, L Rodríguez, J Villaseñor, and F J Fernández. Fermentation of agro food wastewaters by activated sludge. *Water Res*, 41:1635–1644, 2007.

[90] L Rodríguez, J Villaseñor, F J Fernández, and I M Buendía. Respirometry as a tool for rapid characterization of wastewater and activated sludge. *Water Sci Technol*, 56:49–54, 2007.

[91] P Sosnowski, A Wieczorek, and S Ledakowicz. Anaerobic co–digestion of sewage sludge and organic fraction of municipal solid wastes. *Adv Environ Res*, 7:609–616, 2003.

[92] I Tosun, M T Gonullu, E Arslankaya, and A Gunay. Cocomposting kinetics of rose processing waste with ofmsw. *Bioresour Technol*, 99:6143–6149, 2008.

[93] W T M Sanders, M Geerink, G Zeeman, and G Lettinga. Anaerobic hydrolysis kinetics of particulate substrates. *Water Sci Technol*, 41(3):17–24, 2000.

[94] AF McDonagh, A Phimister, SE Boiadjiev, and DA Lightner. Dissociation constants of carboxylic acids by 13c–nmr in dmso. *Water Tetrahedron Lett*, 40(49):8515–8518, 1999.

[95] A Pauss, G Andre, M Perrier, and SR Guiot. Liquid–to–gas mass transfer in anaerobic processes: Inevitable transfer limitations of methane and hydrogen in the biomethanation process. *Appl Environ Microb*, 56(6):1636–1644, 1990.

[96] W Merkel and K Krauth. Mass transfer of carbon dioxide in anaerobic reactors under dynamic substrate loading conditions. *Water Res*, 33(6):2011–2020, 1999.

[97] P H M Janssen and P S C Heuberger. Calibration of process-oriented models. *Ecol Model*, 83(1–2):55–66, 1993.

[98] D I Page, A.L. Main K.L. Hickey, R. Narula, and S.J. Grimberg. Modeling anaerobic digestion of dairy manure using the iwa anaerobic digestion model n1. *Water Sci Technol*, 58(1–2):689–695, 2008.

[99] P N L Lens, A Visser, A Janssen, L W Hulstoff Pol, and G Lettinga. Biotechnological treatment of sulfate rich wastewaters. *Crit Rev Environ Sci Technol*, 28(1):41–88, 1998.

[100] R T Van Houten, L W Hulstoff Pol, and G Lettinga. Biological sulfate reduction using gas-lift reactors fed with hydrogen and carbon dioxide as energy and carbon source. *Biotechnol Bioeng*, 44:586–594, 1994.

[101] P A Alphenaar, A Visser, and G Lettinga. The effect of liquid upward velocity and hydraulic retention time on granulation in uasb reactors treating waste water with a high sulfate content. *Biores Technol*, 43:249–258, 1993.

[102] F Omil, P Lens, LW Hulstoff Pol, and G Lettinga. Effect of upward velocity and sulphide concentration on volatile fatty acid degradation in a sulphidogenic granular sludge reactor. *Proc Biochem*, 31:699–710, 1996.

[103] F Omil, P Lens, LW Hulstoff Pol, and G Lettinga. Characterization of biomass from a sulphidogenic volate fatty acid-degrading granular sludge reactor. *Enzyme Microb Technol*, 20:229–236, 1997.

[104] A Visser, I Beeksma, F Van der Zee, A J M Stams, and G Lettinga. Anaerobic degradation of volatile fatty acids at different sulfate concentration. *Appl Microb Biotechnol*, 40:529–556, 1993.

[105] F Widdel. Microbiology and ecology of sulfate- and sulphur reducing bacteria. In A.J.B. (Eds.) Zehnder, editor, *Biology of Anaerobic Microorganisms*, pages 469–586. John Wiley and Sons, New York, 1988.

[106] A Gupta, J R V Flora, M Gupta, G D Sayles, and M T Suidan. Methanogenesis and sulfate reduction in chemostats - i. kinetic studies and experiments. *Wat Res*, 28:781–793, 1994.

[107] S J W H Oude Elferink, R N Maas, H J M Harmsen, and A J M Stams. Desulforhabdus amnigenus gen.nov. sp.nov., a sulfate reducer isolated from anaerobic granular sludge. *Arch Microbiol*, 164:119–124, 1995.

[108] S J W H Oude Elferink, W M Akkermans Van Vliet, J J Bogte, and A J M Stams. Desulfobacca acetoxidans gen. nov. sp. nov., a novel acetate-degrading sulfate reducer isolated from sulfidogenic sludge. *Int. J. Syst. Bacteriol*, 49:345–350, 1998.

[109] S B I Oude Elferink, S J W H Luppens, C L M Marcelis, and A J M Stams. Kinetics of acetate utilization by two sulfate reducers isolated from anaerobic granular sludge. *Appl Environ Microbiol*, 64:2301–2303, 1998.

[110] F W J M M Hoeks, H J G Ten Hoopen, J A Roels, and J G Kuenen. Anaerobic treatment of acid water (methane production in a sulfate rich environment). *Progr Ind Microbiol*, 20:113–119, 1984.

[111] A Mulder. The effects of high sulfate concentrations on the methane fermentation of waste water. *Progr Ind Microbiol*, 20:133–143, 1984.

[112] L Herrera, J Hernandez, L Bravo, L Romo, and L Vera. Biological process for sulfate and metals abatement from mine effluents. *Environ Toxic Water*, 12:101–107, 1996.

[113] W Liamleam and A P Annachhatre. Electron donors for biological sulfate reduction. *Biotechnol Adv*, 25:452–463, 2007.

[114] G Esposito, M Fabbricino, and F Pirozzi. Four-substrate design model for single sludge predenitrification system. *J Environ Eng*, 129:394–401, 2003.

[115] Y Argaman. A steady-state model for the single sludge activated sludge system - i. model description. *Water Res*, 29:137–145, 1995.

[116] M Henze, W Gujer, and M T Van Loosdrecht. *Activated Sludge Models ASM1, ASM2, ASM2d and ASM3*. Scientific and technical Report No. 9, IWA, London, 2000.

[117] M J Wejma, F Gubbels, L W Hulshoff Pol, Stams A J M, P N L Lens, and G Lettinga. Competition for h_2 between sulfate reducers, methanogens and homoacetogens in a gas-lift reactor. *Water Sci Tecnol*, 45:75–80, 2002.

[118] R H Perry and D W Green. *Perry's Chemical Engineers Handbook*. McGraw-Hill, New York, 7th edition, 1997.

[119] P A Wilderer and W G Characklis. Structure and function of biofilms. In *Structure and function of biofilms*, pages 5–17. John Wiley & Sons, New York, 1989.

[120] B E Rittman and P L McCarty. Model of steady–state biofilm kinetics. *Biotechnol Bioeng*, 22(11):2343–2357, 1980.

[121] B E Rittman. The effect of shear stress on biofilm loss rate. *Biotechnol Bioeng*, 24(2):501–506, 1982.

[122] Wanner O and W Gujer. Competition in biofims. *Wat Sci Technol*, 17(2–3):27–44, 1984.

[123] Wanner O and W Gujer. A multispecies biofilm model. *Biotechnol Bioeng*, 28(2–3):314–328, 1986.

[124] Wanner O and W Gujer. Mathematical modelling of mixed–culture biofilms. *Biotechnol Bioeng*, 48(2–3):172–184, 1996.

[125] Wimpenny J W T and R Colasanti. A unifying hypothesis for the structure of microbial biofilms based on cellular automaton models. *FEMS Microbiol. Ecol*, 22(1):1–16, 1997.

[126] C Picioreanu, M C M Van Loosdrecht, and J J Heijnen. Mathematical modeling of biofilm structure with a hybrid differential–discrete cellular automaton approach. *Biotechnol Bioeng*, 58(1):101–116, 1998.

[127] C Picioreanu, M C M Van Loosdrecht, and J J Heijnen. A new combined differential–discrete cellular automaton approach for biofilm modeling: Application for growth in gel beads. *Biotechnol Bioeng*, 57(6):718–731, 1998.

[128] D R Noguera, G Pizarro, D A Stahl, and B E Rittmann. Simulation of multispecies biofilm development in three dimensions. *Wat Sci Technol*, 39(7):123–130, 1999.

[129] S W Hermanowicz. A simple 2d biofilm model yields a variety of morphological features. *Math Biosci*, 169(1):1–14, 2001.

[130] Bellomo, A N Bellouquid, Nieto J, and J Soler. Multiscale biological tissue models and flux–limited chemotaxis from binary mixture of multicellular growing system. *Math Models Methods Appl Sci*, Suppl. 20(7):1179–1207, 2010.

[131] B Szomolay. Analysis of moving boundary value problem arising in biofilm modelling. *Math Methods Appl Sci*, 31(15):1835–1859, 2008.

[132] C Overgaard. Application of variational inequalities to the moving–boundary problem in a fluid model for biofilm growth. *Nonlinear Analysis*, 70(10):3658–3664, 2009.

[133] M A Efendiev, S V Zelik, and S J Eberl. Existence and longtime behaviour of a biofilm model. *Commun Pure Appl Anal*, 8(2):509–531, 2009.

[134] Klapper I and J Dockery. Mathematical description of microbial biofilms. *SIAM Rev*, 52(2):221–265, 2010.

[135] L I Rubinstein. The stefan problem. *AMS Translation of Mathematical Monographs*, 27, 1971.

[136] B D'Acunto and L Frunzo. Qualitative analysis and simulations of a free boundary problem for multispecies biofilm models. *Math Comp Modelling*, 53(9–10):1596–1606, 2011.

[137] C Picioreanu, J.U. Kreft, and M C M Van Loosdrecht. Particle-based multidimensional multispecies biofilm model. *Appl. Environ. Microbiol*, 70(5):3024–3040, 2004.

[138] E Alpkvist, C Picioreanu, M C M Van Loosdrecht, and A Heyden. Three-dimensional biofilm model with individual cells and continuum eps matrix. *Biotechnol Bioeng*, 94(5):961–979, 2006.

[139] A Lens, P N L anf Visser, A Janssen, L W Hulstoff Pol, and G Lettinga. Biotechnological treatment of sulfate rich wastewaters. *Crit Rev Environ Sci Technol*, 28(1):41–88, 1998.

[140] A Grobicki and D C Stuckey. Hydrodynamic characteristics of the anaerobic baffled reactor. *Wat Res*, 26(3):371–378, 1992.

[141] G Esposito, J Wejma, F Pirozzi, and P N L Lens. Effect of the sludge retention time on h_2 utilization in a sulfate reducing gas-lift reactor. *Process Biochem*, 39(4):491–498, 2003.

[142] G Esposito, P N L Lens, and F Pirozzi. User-friendly mathematical model for the design of sulfate reducing h_2/co_2 fed bioreactors. *j environ eng ASCE*, 135(3):167–175, 2009.

[143] L B Celis-Garcia, G Gonzalez-Blanco, and M J Meraz. Chemical removal of sulfur inorganic compounds by a biofilm of sulfate reducing and sulfide oxidizing bacteria in a down-flow fluidized bed reactor. *Technol Biotechnol*, 83(3):260–268, 2008.

[144] S J W H Oude Elferink, A Visser, P L W Hulshoff, and A J M Stams. Sulfate reduction in methanogenic bioreactors. *FEMS microbiol Rev*, 15(2–3):119–136, 1994.

[145] F Widdel. Microbiology and ecology of sulfate and sulphur reducing bacteria. In A J B Zehnder, editor, *Biology of Anaerobic Microorganisms*, pages 53–76. John Wiley & Sons, New York, 1988.

[146] L B Celis, D Villa-Gomez, A G Alpuche Solis, B O Ortega Morales, and E Razo Flores. Characterization of sulfate-reducing bacteria dominated surface communities during start-up of a down-flow fluidized bed reactor. *J Ind Microbiol Biotechnol*, 36(1):111–121, 2008.

[147] M Gallegos-Garcia, L B Celis, R Rangel-MÃ©ndez, and E Razo Flores. Precipitation and recovery of metal sulfides from metal containing acidic wastewater in a sulfidogenic down-flow fluidized bed reactor. *Biotechnol Bioeng*, 102(1):91–99, 2009.

[148] B D'Acunto. *Computational Methods for PDE in Mechanics*. World Scientific, Singapore, 2004.

[149] F Brezzi, K Lipnikov, and M Shashkov. Convegergence of mimetic finite difference method for diffusion problems on polyhedral meshes with curved faces. *Math Models Methods Appl Sci*, 16(2):275–297, 2006.

[150] K Lipnikov, G Manzini, F Brezzi, and A Buffa. The mimetic finite difference methodfor the 3d magnetostatic field problems on polyhedral meshes. *J Comput Phys*, 230(2):305–328, 2011.

[151] P S Stewart. Diffusion in biofilms. *j bacteriol*, 185(5):1485–1491, 2003.

[152] H Lin Yen and K Lee Kwang. Verification of anaerobic biofilm model for phenol degradation with sulfate reduction. *J Envir Engrg*, 127(2):119–125, 2001.

[153] C E Wilke and P Chang. Correlation of diffusion coefficients in dilute solutions. *AIChE J*, 1:264–270, 1955.

[154] K Williamson and P L McCarty. Verification studies of the biofilm model for bacterial substrate utilization. *J Water Pollution Control Fedn*, 48:281–296, 1976.